NBSIR 76-1136

Failure Analysis of Fiberglass Insulator Rods

Leonard Mordfin and Nixon Halsey

Engineering Mechanics Section
Mechanics Division
Institute for Basic Standards
National Bureau of Standards
Washington, D. C. 20234

July 1976

Final Report

NBSIR 76-1136

FAILURE ANALYSIS OF FIBERGLASS INSULATOR RODS

Leonard Mordfin and Nixon Halsey

Engineering Mechanics Section
Mechanics Division
Institute for Basic Standards
National Bureau of Standards
Washington, D. C. 20234

July 1976

Final Report

U.S. DEPARTMENT OF COMMERCE, Elliot L. Richardson, *Secretary*

Edward O. Vetter, *Under Secretary*

Dr. Betsy Ancker-Johnson, *Assistant Secretary for Science and Technology*

NATIONAL BUREAU OF STANDARDS, Ernest Ambler, *Acting Director*

CONTENTS

LIST OF TABLES

LIST OF FIGURES

LIST OF FIGURES

FAILURE ANALYSIS OF FIBERGLASS INSULATOR RODS

by

Leonard Mordfin and Nixon Halsey

ABSTRACT

Failure analyses were carried out on a group
of coated fiberglass-reinforced-plastic insulator
rods that had sustained burn damage and loss of
coating in service on a Loran-C tower. The investiga-
tion included chemical, flammability, electrical
and mechanical tests as well as a variety of measure-
ments and inspections. The burn damage, consisting
chiefly of carbonaceous tracking and charring, was
attributed primarily to the occurrence of electrical
discharges, from the energized end fittings to the
rods, under conditions in which the electrical leak-
age path resistances had been reduced by moisture
from rain, fog and ocean spray. The effects of this
damage on the structural integrity of the rods were
evaluated. Recommendations were made for reducing
the incidence of such damage in the future, based
on the use of skirted insulator rods or more ef-
fective coating materials. The principal cause
of the coating loss was not positively identified.
This form of damage was not found to have serious
consequences except as a secondary factor which
may have contributed to the occurrence of some
partial electrical discharges.

Key Words: Breakdown, electrical; failure analysis;
fiberglass-reinforced plastics; flammability; guy
insulators; high-voltage tests; insulators, tower
guy; Loran C; pultruded rods; rods, insulator.

1. INTRODUCTION

Seventeen glass-reinforced-plastic (GRP) rod insulators were re-moved from a 625-ft (190-m) tower at the U.S. Coast Guard's Loran-C station in Angissoq, Greenland, and were shipped to the National Bureau of Standards (NBS) for study. The rods had originally been installed on the lower ends of the tower's top-loading elements in 1964, and burning damage of the rods was discovered in December 1973. NBS was requested to perform inspections, tests, measurements, and analyses in an attempt to determine the cause of the burning; to speculate on the conditions which may have led to the burning; and to provide recommendations for avoiding burning in the future. This report presents the results of this investigation.

The work was administered by the Engineering Mechanics Section of NBS under the sponsorship and with the financial assistance of the U.S. Coast Guard. High-voltage tests were carried out by A. L. Gabriel, C. M. Keating, and J. E. Brown of the Bonneville Power Administration (BPA) of the U.S. Department of the Interior, and flammability tests by Dr. G. D. Mitchell of the NBS Fire Science Division. Acknowledgements are also due to W. J. Pummer and Dr. R. W. Burke of the NBS Polymers and Analytical Chemistry Divisions, respectively, for providing chemical analyses; to H. Eisenstadt of the Defense Mapping Agency Topographic Center for furnishing topographic information; and to O. O. Owens of the Engineering Mechanics Section for assistance in mechanical testing.

2. THE ANGISSOQ INSTALLATION

The Angissoq installation is located on a small island near the southern tip of Greenland, approximately 500 miles (800 km) south of the Arctic Circle. The Loran tower is a one-megawatt, 100-kHz, top-loaded monopole antenna. The power is pulsed at a rate of 160 per second with a pulse duration of 40 to 50 microseconds. At the peak of the pulse the voltage is 270 kV rms.

The guying arrangement for the tower is shown schematically in Figure 1. The top-loading elements, fabricated from aluminum-conductor, steel-reinforced cable, are electrically conducting and an integral part of the antenna's radiating field. Twenty-four such elements, each 600 ft (183 m) long, are uniformly dispersed around the periphery of the tower. Each element is guyed with galvanized cable anchored to the ground, with an insulator assembly separating the top-loading element from the guy wire. The insulator assembly, shown schematically in Figure 2, consists of two GRP insulator rods in parallel with a corona ring at the upper end. (Similar assemblies serve to insulate the struc-tural guys from the tower but these are not of concern in the present study.)

3. THE SPECIMENS

Seventeen GRP rods with end fittings were furnished for this study, all of which had been removed from service in the insulator assemblies of the top-loading elements. As received, each rod carried one or more numerical designations and four of the rods were also marked to indicate which end had been oriented toward the top or the bottom of its insulator assembly. In the case of rods which had served as a companion pair in the same insulator assembly, both carried the same numerical designation. To avoid confusion, therefore, all of the rods were renumbered for the purposes of this study. The first column of Table 1 shows the NBS designation for each rod and the second column lists the designations and other markings which were attached to the rods as they were received at NBS.

The rods had been manufactured by a process similar to pultrusion and consist of unidirectional, continuous, fiberglass roving in an epoxy matrix. The resin content of the rods was nominally 24 ± 3 percent. The rods were coated with epoxy resin that was loaded with a titanium dioxide pigment. The specified diameter of the rods before coating was 0.775 (+0.010, -0.005) in [19.69 (+0.25, -0.13) mm], and the specified thickness of the coating was 0.005 to 0.010 in (0.13 to 0.25 mm). The rated tensile strength of the rods was 35 000 lbf (156 kN).

The end fittings were conventional open spelter sockets designed for 3/4-in (19-mm) diameter wire rope. They were forged from steel and galvanized.

In fabricating an insulator assembly, small holes, 1 in (25 mm) deep, were drilled concentrically into each end of an insulator rod having a length of 14.5 ft (4.42 m). The end fittings were slipped over the rods and a conical metal wedge, nominally 1-3/4 in (44 mm) long and 0.860 in (21.8 mm) in diameter*, was driven into each small hole. This split the rod ends and wedged them into a roughly conical shape. The end fittings then were alined concentrically with the rod, and the openings in the sockets where the rods emerged were sealed with a plastic compound. Finally, the sockets were potted with an epoxy-polyamide-grit mixture, and the mixture was cured.

All of the rods, except for X12, had been put into service in 1964 and were removed some nine or ten years later. Rod X12, which had been manufactured with the others, was first installed toward the end of this period as a replacement for Rod X10, and was subsequently removed about one month later. Thus, while the coatings on sixteen of the rods had weathered to a pale yellow, the coating on Rod X12 was still white.

---

*Actual dimensions of one wedge (see Section 5) were 1.79 and 0.88 in (45 and 22 mm), respectively.

TABLE 1. Rod Designations and Descriptions

NBS No.	As-received markings	Nature of coating	Visible helix
X1	1, C1, 9 of 18	brittle	yes
X2	2, C2, bottom, top	brittle	no
X3	C8	tough; not well-adhered	yes
X4	C8	very flaky	yes
X5	9, bottom, top	flaky	yes
X6	10, 6 of 18	brittle	no
X7	12	brittle	no
X8	C13, 16 of 18	very brittle	no
X9	C13, 4 of 18	brittle	yes
X10	15, C15	tough; well-adhered	no
X11	15, 12 of 18	well-adhered	no
X12	15A	well-adhered	no
X13	18, 11 of 18	well-adhered	no
X14	18, 13 of 18	well-adhered	no
X15	19, 17 of 18	well-adhered	no
X16	20, 7 of 18, bottom	well-adhered	no
X17	22, 2 of 18, bottom	flaky	no

The end fitting on the upper end of Rod X16 was somewhat smaller than, although of the same general type as, the other end fittings.

Photographs of portions of fifteen rods, showing damage sustained in service, are reproduced in Figures 3 through 19 and are discussed below. These figures are arranged in order of the rod designation numbers. Rods X12 and X14 are not included; these rods sustained only slight, if any, damage.

In general, the rods exhibited two different kinds of damage. The first was burn damage, which appeared as scorched surface areas (not visible in the photographs), as carbonaceous tracks (see, for example, Figs. 9 and 17), or as charred regions (see, for example , Fig. 14), depending upon the severity of the damage. The second kind of damage was loss of coating (see, for example, Figs. 7 and 8). Closer examination of the rods revealed that the coatings were not all the same. Instead, there appeared to be at least two different kinds. One was relatively tough and usually tended to be rather well-adhered to the GRP substrate. The second was relatively brittle and generally tended to flake off more or less easily with the point of a penknife. The general nature of the coating on each rod is described in the third column of Table 1.

During the manufacturing process, before final curing, the rods were wrapped with a special tape which was later removed before the coating was applied. This produced a helical track on the surfaces of most rods (see, for example, Fig. 6) which was visible through some of the coatings. The last column in Table 1 indicates those rods on which the helical track was clearly visible through the coatings.

4. INSPECTIONS AND MEASUREMENTS

4.1 Dimensional Measurements

Measurements were made on the rods and are reported in Table 2. The lengths of the rods, between end fittings, were quite uniform and averaged 13.91 ft (4.24 m). The outer diameter of each rod was measured at five locations and averaged. The coating thickness on most of the rods was also measured by peeling off a small piece of it. On four rods, however, the coating was so well-adhered that this could not be accomplished.

In all but one case (Rod X8) the coating thickness was within the specified limits (Section 3). The uncoated diameters, calculated by subtracting two coating thicknesses from the respective outer diameters, also fall within the specified limits, with one exception (Rod X4).

TABLE 2. Dimensions of Rods

NBS No.	Length between fittings		Average outer diameter		Average coating thickness	
	ft	(m)	in	(mm)	in	(mm)
X1	13.91	(4.24)	0.789	(20.0)	0.007	(0.2)
X2	13.92	(4.24)	.796	(20.2)	.006	(.2)
X3	13.91	(4.24)	.785	(19.9)	.007	(.2)
X4	13.91	(4.24)	.780	(19.8)	.009	(.2)
X5	13.91	(4.24)	.788	(20.0)	.006	(.2)
X6	13.92	(4.24)	.794	(20.2)	.005	(.1)
X7	13.91	(4.24)	.794	(20.2)	.006	(.1)
X8	13.90	(4.24)	.791	(20.1)	.004	(.1)
X9	13.91	(4.24)	.792	(20.1)	.006	(.1)
X10	13.92	(4.24)	.790	(20.1)	.010	(.2)
X11	13.93	(4.24)	.795	(20.2)	.008	(.2)
X12	13.93	(4.24)	.787	(20.0)	a	a
X13	13.91	(4.24)	.789	(20.0)	a	a
X14	13.90	(4.24)	.805	(20.5)	a	a
X15	13.92	(4.24)	.790	(20.1)	.005	(.1)
X16	13.92	(4.24)	.792	(20.1)	a	a
X17	13.91	(4.24)	.789	(20.0)	.006	(.2)

a. Not measured

4.2 Coating Loss

Coating loss ranged from zero, or nearly zero, on seven rods which had well-adhered coatings, to major losses on six rods which had flaky or poorly adhered coatings. Four rods with brittle coatings fell into an intermediate category which experienced only the loss of a chip here or there. Table 3 shows, for each rod, the amount of coating loss in square inches (and square centimeters) and the amount of the loss as a percentage of the total surface area. With one trivial exception, on every rod which experienced some loss of coating more than two-thirds (and frequently more than 90 percent) of the loss occurred in the upper one-third of the rod length. (The manner in which the upper ends of the rods were identified is described later.)

It is interesting that of those rods which had served as companion pairs in single insulator assemblies (X3 and X4, X8 and X9, X10 and X11, X11 and X12, X13 and X14) both exhibited major coating loss or both exhibited negligible coating loss. In other words, in none of the five companion pairs did one rod show major coating loss while its companion showed negligible coating loss.

Of the six rods which experienced major coating loss, four (Table 1) had visible helices. Only one rod with a helix visible through its coating did not experience major coating loss.

4.3 Burn Damage

In this report the expression "burn damage" is used to describe all damage which apparently resulted from electric arcing, flashover and/or lightning, whether or not a true ignition ever took place. It thus includes minor scorching and carbonaceous tracking as well as heavy charring.

Upon receipt at NBS four of the seventeen rods carried markings to indicate which ends of the rods had been attached to the upper and/or lower ends of their respective insulator assemblies (Table 1). On three of these (i.e., all except Rod X2) most of the burn damage was toward the upper end. This is consistent with the physical arrangement of the tower, which ordinarily places the greatest electrical stress on the upper ends of the insulator rods. On this basis, and strictly for the purpose of identification, those ends which exhibited the most severe burn damage were arbitrarily designated as the upper ends.

Table 4 lists the total area of burn damage for each rod. In making this measurement, surface scorching which produced only a dis-coloration of the coating and no measurable loss of material was not included. The figures referenced in the table are those that show the most severe burn damage for each rod. From the table and the figures it is evident that five rods suffered severe burn damage, two of them having burned virtually all the way through near their upper end fittings. (The upper end fittings from these two rods are shown in Figs. 20 and 21).

7

TABLE 3. Coating Loss

Rod No.	Fig. No.(a)	Surface area of lost coating		Pct of total surface area	Pct of total loss in upper 1/3 of rod
		in^2	(cm^2)	pct	pct
X1	--	1	(6)	0.2	0
X2	--	2	(13)	.5	75
X3	5	35	(226)	8.5	100
X4	6	55	(355)	13.3	95
X5	7	33	(213)	8.0	76
X6	8	3	(19)	.7	67
X7	--	2	(13)	.5	100
X8	--	20	(129)	4.8	90
X9	11	39	(252)	9.4	98
X10	--	0	(0)	0	-
X11	13	~0	(1)	~0	100
X12	--	0	(0)	0	-
X13	--	0	(0)	0	-
X14	--	0	(0)	0	-
X15	--	0	(0)	0	-
X16	--	0	(0)	0	-
X17	19	16	(103)	3.9	81

a. Only those figures which depict the
   principal area of coating loss are
   listed.

TABLE 4. Burn Damage

Rod No.	Fig. No.(a)	Surface area of burn damage in^2	(cm^2)	Minimum cross-sectional area pct	Angular location of most severe burn deg
X1	3	0.2	(1.)	--	-15
X2	4	0.5	(3.)	--	+45
X3	--	0.03	(0.2)	--	-60
X4	--	0.5	(3.)	--	-90 to 0
X5	--	1.1	(7.)	--	-90 to +60
X6	--	0.01	(0.1)	--	+75
X7	9	0.2	(1.)	--	+75
X8	10	22.9	(148.)	3	-45
X9	11	1.8	(12.)	--	-75 to -30
X10	12	27.6	(178.)	3	-90 to +30
X11	13	0.03	(0.2)	--	-75
X12	--	0.2	(1.)	--	-30 to 0
X13	14	20.8	(134.)	58	+90
X14	--	0.00	(0.0).	--	-
X15	15	26.0	(168.)	79	-60
X16	16	26.2	(169.)	67	+30
X17	19	0.6	(4.)	--	+75

a. Only those figures which clearly depict
the principal area of burn damage are
listed.

For the five rods which experienced severe burning, Table 4 lists the minimum remaining cross-sectional area of each rod as a percentage of the original cross-sectional area. These percentages are only approximate, since it was impossible to determine the depth of the char on these rods without introducing additional damage.

It had been suggested that much of the burning damage may have been caused by arcing from the corona ring to a rod, or by arcing between rods. In order to examine this possibility consider Figure 22 which shows, schematically, an end view of the end fitting at the upper end of a rod. In the physical arrangement of the insulator assemblies, the two companion rods are closest to each other along axis X-X; the shortest path between a corona ring and a rod is also along this axis. The location of the most severe burning damage on each rod was tabulated, in Table 4, in terms of its angular departure from the X-X axis. The angle Θ was used for this purpose. Since the end fittings are symmetrical about their Y-Y axes, all of the tabulated angles were arbitrarily chosen to fall within the semicircle ranging from -90 to +90 degrees. The fact that the preponderance of angles is not concentrated at 0 degrees suggests that the burn damage was not caused by arcing between companion rods or between rods and corona rings.

This finding was confirmed by examination of those pairs of rods that had served as companions in the same insulator assemblies (X3 and X4, X8 and X9, X10 and X11, X11 and X12, X13 and X14). In no instance was the burn damage on both rods of a pair located in such a way that it could have resulted from arcing between the rods.

An interesting observation resulted from comparison of Rods X10 and X12. (X10 was a severely burned rod and X12 was its replacement.) While the burn damage on X12 was extremely slight, it appeared to be in essentially the same location as the burn damage on X10.

As pointed out earlier, most of the burn damage on most of the rods which experienced it was concentrated near one end of each rod. However, four rods (X2, X7, X16, X17) also experienced some burn damage near their other ends. This is depicted, for example, in Figures 4 and 18. Fortunately, three of these rods (X2, X16, and X17) were received with markings designating their upper and/or lower ends.

4.4 Relationship between Coating Loss and Burn Damage

On the basis of the examinations of coating loss and burn damage, certain characteristics of the relationship between the two are evident.

Six rods experienced major coating loss (Table 3), and five rods experienced severe burn damage (Table 4), but only one rod (X8) experienced both.

10

Seven rods experienced virtually no coating loss (Table 3), and four rods experienced negligible burn damage (Table 4), but only two rods (X11 and X14) experienced neither type of damage to a substantial extent.

Of the five rods which experienced severe burn damage four had well-adhered coatings with no coating loss.

On each of the six rods which experienced major coating loss, most of the burn damage occurred in the uncoated regions of the rods.

4.5 End Fittings

During preliminary examinations of the insulators, before the formal investigation was started, the upper end fitting from Rod X10 was cut in half to permit examination of the potted end of the rod. As shown in Figure 21 a rather large void was found in the center of the rod, extending from the tip of the conical wedge. The void appeared to have resulted from entrapment of an air pocket during the potting process. Since this end fitting was adjacent to that part of the rod which had burned severely, it was suspected that the void may have been a contributing factor. It was hypothesized that the void may have promoted the development of electrical corona or, alternatively, that it may have accumulated moisture due to rain or ocean spray and thereby created a conductive path for electrical leakage current.

With a view toward the possible development of a useful quality-control tool, the feasibility of detecting voids inside the end fittings by nondestructive inspection techniques was explored. Several ultrasonic and radiographic techniques were used but none was adequate for the task [1]*. The interface between the end fitting and the potting compound could be detected using fast-neutron radiography, but, because of the number of material interfaces and the different attenuation characteristics of the different materials, none of the techniques was capable of showing the conical wedge with adequate detail.

Subsequently, six end fittings were selected for dissection to permit visual examination for internal voids. Two of these fittings were adjacent to severely burned sections of rod and one was near a deep carbonaceous track. The dissections revealed no voids in any of the six fittings and showed, in the case of the severely burned rods, that the burns did not extend more than a centimeter or so into the fittings. See Figure 23. These observations suggest that the void in the upper end fitting of Rod X10 was found purely by coincidence, and that such voids are probably unrelated to the principal cause of burning damage in the Angissoq insulators.

---

*Numerals in square brackets refer to similarly numbered references cited in Section 12.

11

5.   CHEMICAL AND MATERIAL-IDENTIFICATION TESTS

The wedge was removed from the lower end fitting of Rod X15. Mass and volume measurements on this wedge showed it to have a density of 0.103 lb/in^3 (2.85 Mg/m^3), and hardness tests indicated a hardness of 64 on the Rockwell B scale. These measurements, together with the appearance and the non-magnetic nature of the wedge, suggest that it was fabricated from a moderately high-strength aluminum alloy.

A small piece of Rod X9 was ground up and formed into a pellet, and its infrared transmission spectrum was determined using a spectrophotometer. This determination revealed that the resin used in manufacturing the rods was, indeed, epoxy and not polyester, which is more commonly used in pultrusions.

In view of the marine atmosphere to which the insulators had been exposed, some indication of the salt contamination of the insulator surfaces was considered desirable. A relatively sensitive indicator of the presence of sodium chloride, the "taste test", was dutifully applied to all seventeen of the insulator rods with negative results in every instance. In order to arrive at a more quantitative measure, four short lengths of rod with intact coatings were then cut from Rod X9. Each was immersed in a 10-percent hydrochloric acid solution for fifteen minutes and removed, and then the sodium content in the solution was determined by flame emission spectrometry with repetitive optical scanning. The results for the four samples, expressed as the quantity of sodium per unit of surface area of the rod samples, were 1.30, 0.385, 0.910 and 1.56 g/m^2. The significance of these measurements is discussed in Section 9.1.

6.   FLAMMABILITY TESTS

A series of tests was conducted to evaluate the flammability of the rod material and to explore the influences of the coating and of salt contamination on the flammability. An adaptation of the Limiting Oxygen Index (LOI) test [2] was selected for this purpose. This test method provides a means for studying the effect of changes in a material on its flammability. While the results do not necessarily correlate with actual use conditions, the method has been described as the most reproducible test available for fire-retardant materials [3]. In the basic method a thin flat specimen is vertically supported in a column containing a slowly rising mixture of oxygen and nitrogen, the top of the specimen is ignited, and the minimum concentration of oxygen (the LOI) that will just support combustion under conditions of candle-like burning is measured.

Since the insulator rods are cylindrical in shape rather than flat, preliminary tests were performed to see whether cylindrical specimens could be used. Undamaged lengths of Rod X16 were employed for this purpose. A thin flat specimen machined from one length of rod was tested first. It produced an LOI of 24 percent. Next, a length of full cross

12

section was tested. Again, an LOI of 24 percent was obtained, suggesting that either (a) the shape of the specimen was not a significant factor, or (b) the shape effect was effectively canceled by an opposite effect resulting from the removal of the coating on the flat specimen. Finally, a test was conducted on a thin disk of full cross section, supported vertically. While an accurate determination of the LOI was not possible with this configuration, this test revealed that the coating material by itself was far more flammable than the basic GRP rod material, although this was not obvious in tests of full-sized specimens. Presumably, the mass of the full-sized specimens acts as a heat sink under candle-like burning conditions, preventing separate combustion of the coatings.

In the main series of tests, in which a similar but different test apparatus was used, eight full-sized specimens were tested after having been preconditioned as follows:

two specimens were tested in the as-received condition;

two specimens were washed with a small amount of warm water and detergent and wiped dry;

two specimens were immersed in a five-percent saltwater solution for seven days, then removed and wiped dry; and

the coatings were carefully peeled from the last two specimens.

The first six of these specimens were cut from an undamaged part of Rod X10 which had a well-adhered coating. The last two specimens were cut from an unburned part of Rod X8 which had an easily removable coating.

The results of the flammability tests are given in Table 5. The standard deviation of the mean LOIs from the first three sets of tests is less than one percentage point; this is within the range obtained with nominally identical specimens [2]. This suggests that the flammabilities of the specimens from Rod X10 were not significantly affected by the three preconditioning treatments that were applied to them. On the other hand, the specimens from Rod X8, which had their coatings removed, appeared to be somewhat less flammable than the specimens from Rod X10. It is not immediately obvious whether this difference is due to the relatively high flammability of the coating or whether it results from more basic differences in the material characteristics of the two rods.

7. ELECTRICAL TESTS

In order to explore the possibility that burning was caused by leakage currents in the insulator rods, an attempt was made to measure the electrical resistances of the rods. For this purpose a megohmmeter having a range of 10^{14} ohms (100 TΩ) and an applied voltage of 1 kV dc was used with the leads spaced 1 in (25 mm) apart on the rod. A meter

TABLE 5.   Flammability Tests

Test No.	Rod No.	Condition	Limiting Oxygen Index volume pct
F1	X10	as received	30
F2	X10	as received	27
Avg			28.5
F3	X10	washed	28
F4	X10	washed	27
Avg			27.5
F5	X10	saltwater immersed	30
F6	X10	saltwater immersed	27
Avg			28.5
F7	X8	coating removed	28
F8	X8	coating removed	35
Avg			31.5

reading of infinity was consistently obtained. The test was repeated on
lengths of rod that had been immersed in saltwater for several days and
then dried. The same result was obtained, suggesting that substantially
higher voltages or high frequencies, or both, would be required to
produce measurable leakage currents. Subsequently, eight insulators were
preconditioned and submitted to the Bonneville Power Administration for
a series of high-voltage tests.

The unavailability of high-voltage, high-frequency testing apparatus
necessitated that these tests be conducted with 60-Hz voltages, although
it is recognized that this leaves some question as to the applicability
of the test results to the problem at hand.

7.1 Specimens

The eight insulator rods selected for this purpose had all experi-
enced only minor burn damage. They were preconditioned in the same
manner as the flammability specimens (Section 6). In order to possibly
gain some additional information from the high-voltage tests, seven of
the insulator rods chosen had brittle or flaky coatings while the eighth
(X11) had a well-adhered coating. The two insulator rods which were
preconditioned by having their coatings removed had already suffered
major coating loss. Of the other six rods, five were chosen with only
minor loss, while the sixth (X17) had major coating loss. The rod
designations and their preconditioning treatments were as follows:

X6 and X17	as received
X2 and X11	washed
X1 and X7	immersed in saltwater
X4 and X5	coatings removed.

Except as noted hereafter, all of the high-voltage tests were performed
with pairs of similarly conditioned rods mounted in insulator assemblies
(see Fig. 2) with corona rings at the upper (energized) ends. The
results of the tests [4] are summarized and discussed below.

7.2 RIV and Visual Corona Tests

A radio influence voltage (RIV) is a high-frequency voltage gener-
ated as a result of ionization and may be propagated by conduction,
induction, radiation or a combination of all three. The RIV of an
insulator is the radio-frequency voltage produced, under specified
conditions, by the application of a 60-Hz voltage. In certain situations
increased RIV levels are believed to indicate a degradation of dielectric
quality. Results of RIV tests on the four insulator pairs are shown
graphically in Figure 24. The results for the insulators in the three
coated conditions all plot within a band that is relatively narrow in
comparison with the probable test-to-test variability on nominally
identical insulators. The insulators which had their coatings removed
showed higher RIVs up to applied voltages of approximately 200 kV.
Above this voltage level the results for the uncoated rods plot within
the same band as those for the coated rods.

15

Using the same power supply, visual corona tests were performed on the four insulator assemblies to assist in locating the sources of the radio-influence voltages. As the applied voltage was increased, the first visual corona on each insulator assembly appeared at the junction of an insulator rod with its upper end fitting. The inception voltages for these visual coronas are listed in Table 6. Note that these voltages are different for the two insulators in each assembly. Note, also, the low inception voltages for the two rods which had their coatings removed. This observation correlates with the higher RIVs measured with the insulator assembly that was fitted with these rods.

As the applied voltage was further increased, corona appeared around the corona rings of the insulator assemblies. The onset voltages for these coronas were all in the narrow range of 189 to 207 kV rms, which is consistent with the relatively uniform RIV response of the four assemblies above 200 kV.

None of the insulator rods experienced any visible damage as a result of these tests.

7.3 Withstand Voltage Tests

Following the RIV and visual corona tests the applied voltage on each insulator assembly was quickly raised to 500 kV and maintained for one minute. Again none of the rods experienced any visible damage.

The applied voltage was then removed and the assemblies were exposed to a simulated rainfall. After being thoroughly wetted the assemblies were subjected to a voltage of 100 kV, with the following results:

The insulator assembly containing the rods which had been immersed in saltwater (X1 and X7) failed immediately. Heavy corona appeared at the junctions of the rods and their upper end fittings and Rod X7 developed a carbonaceous track over a length of about 12 in (300 mm) from its upper end fitting. This track penetrated the coating and passed directly through a 1-in (25-mm) long track (Fig. 9) that existed prior to the test. The GRP substrate did not appear to have been damaged significantly. Both sides of the track were covered with soot. Rod X1 suffered little, if any, burn damage.

The insulator assembly containing the rods which were tested in the as-received condition (X6 and X17) failed approximately 15 seconds after energization. Scintillation developed along the upper part of Rod X6 and produced a carbonaceous track, approximately 2 in (50 mm) long, near the upper end. Interestingly, this track developed on a previously undamaged portion of the rod's surface, although prior damage, in the form of short carbonaceous tracks and lost coating, existed nearby (Fig. 8). Rod X17 (which had major coating loss) was undamaged.

TABLE 6.   Visual Corona Tests

Rod No.	Condition	Inception voltage kV
X6	as received	141
X17	as received	186
Avg		164
X2	washed	185
X11	washed	192
Avg		188
X1	saltwater immersed	147
X7	saltwater immersed	>205
Avg		>176
X4	coating removed	65
X5	coating removed	58
Avg		62

The other two insulator assemblies survived one minute at the 100-kV level without burning and the voltages on these were then increased to 200 kV.

The insulator assembly containing the washed rods (X2 and X11) failed after approximately 30 seconds at this voltage. Heavy corona appeared at the junctions of the rods and the upper end fittings and scintillation developed along the upper portions of the rods. A 1 1/2-in (38-mm) long carbonaceous track near the upper end of Rod X2, which existed prior to this test, was extended for another 2 1/2 in (64 mm) with considerable soot formation. The new damage penetrated the coating at intermittent points but did not appear to have damaged the substrate. Rod X11 suffered some localized scorching of the surface which did not look like anything more severe than a permanent discoloration of the coating.

The insulator assembly containing the rods which had their coatings removed (X4 and X5) survived one minute at the 200-kV level without failure. Scintillation developed along the upper part of Rod X5 and aggravated a 3-in (76-mm) long carbonaceous track near the upper end that existed prior to the test. Rod X4 was not damaged in this test.

7.4 Flashover Voltage Tests

Two insulator assemblies were then subjected to both dry and wet flashover tests, one with coated rods and one with the rods which had their coatings removed. Because of the damage to the coated rods in the previous tests, a matched pair was not available and, accordingly, Rods X1 (saltwater immersed) and X11 (washed) were tested together.

In the dry tests a voltage of 400 kV was applied and was then increased at a rate of 10 kV/s until the insulators flashed over. In the wet tests 50 kV were applied and then increased at the same rate until flashover occurred. The observed flashover voltages were as follows:

Rod Nos.	Dry flashover voltage kV	Wet flashover voltage kV
X1 & X11	943	486
X4 & X5	883	530

These tests caused only minor burn damage in regions of the rods where damage from previous tests already existed. Rod X11 experienced further scorching of its surface over a length of approximately 24 in (600 mm)

from its upper end fitting. The 3-in (76-mm) long track on Rod X5, mentioned above (Section 7.3), was widened from about 1/8 in (3 mm) to about 3/16 in (5 mm) at some points.

7.5 Fog Atmosphere Test

The insulator assembly with Rods X1 and X11 was then installed in a fog chamber and a voltage of 280 kV was applied and thereafter maintained constant. Fog generation was initiated and allowed to accumulate. As the surfaces of the rods became wetted, leakage current increased and burning spots began appearing near the ends of the rods. Eventually, scintillation developed over the full lengths of the rods and smoke and steam were observed rising from the surfaces. As the fog became denser, long arcing paths appeared and after 87 minutes severe burning and flashover developed on Rod X1.

As a result of this test, Rods X1 and X11 suffered carbonaceous tracking over most of their lengths, with the worst damage occurring near their lower ends. Rod X1 was the more severely burned of the two, with tracks up to 1/2 in (13 mm) wide. Most of the tracking on Rod X11 had the appearance of fine black lace, consisting of thousands of disconnected hairline tracks generally oriented in the transverse direction. The more severe tracks on both rods were surrounded by considerable soot.

7.6 Damage Comparisons

Comparisons of the burn damage experienced in service at Angissoq with that suffered in the above electrical tests provided some interesting observations.

The carbonaceous tracks produced in the electrical tests tended to be wider but not as deep as those sustained in service. The tracks produced in the tests were accompanied by considerable soot, on both sides of the tracks, whereas the rods as received from Angissoq were clean. It is considered unlikely that soot had accumulated at Angissoq and had subsequently been washed away by rain. NBS attempts to remove the soot from the rods used in the electrical tests met with only limited success when plain water was used. A mildly abrasive cleanser had to be used to remove all of it.

In situations where burning was experienced, whether in service or in the tests, all or most of the damage to an insulator assembly tended to be concentrated in only one of the two companion insulator rods.

8. MECHANICAL TESTS

8.1 Tensile Tests

A series of tensile tests was performed to investigate the effects of service-incurred burn damage on the structural integrity of the rod insulators. Except as noted, all of these tests were carried out in a 100 000-lbf (445-kN) capacity, horizontal, hydraulically powered testing machine [5] at a crosshead speed of 0.75 in/min (0.32 mm/s).

The first two tests were conducted full-scale on complete insulators. To mount the insulators in the machine, lugs which were clamped in the machine's wedge-type jaws were used to grip the clevis pins in the insulator end fittings. Rod X14, which had experienced no visible damage of any kind in service, was tested first in order to establish baseline data for comparison purposes. At a load of 44 000 lbf (196 kN) a thin sliver of the rod material, about 3/8 in (10 mm) wide, split off at the lower end fitting. The remainder of the rod continued to carry load and attained a maximum load of 53 200 lbf (237 kN), at which point it disintegrated explosively. This value exceeds the 35 000-lbf (156-kN) rated capacity of the rods by a comfortable margin.

The second full-scale test was performed on Rod X15, which had been severely damaged in service. This rod had burned about a fourth of the way through at about an inch from its upper end fitting (Fig. 15). Measurements indicated that about 79 percent of the original cross-sectional area remained, but it was impossible to determine how much of this remaining cross section was structurally functional and how much of it was char. The rod sustained a maximum tensile load of only 16 000 lbf (71 kN). At this point the rod sheared in two longitudinally, the split emanating from the base of the burn. The remainder of the rod broke off from the charred region just inside the upper end fitting. The low value of maximum load suggests that relatively little of the remaining cross section of the rod was undamaged by the burning.

In order to establish the degree of damage which rods can withstand without a degradation of structural performance, three lengths of rod were then tested to determine the full strength of the product. These were cut from undamaged sections of rod insulators. Since commercial end fittings, including those used in the Angissoq system, generally introduce geometric discontinuities and stress concentrations which prevent the full strengths of pultruded rods from being attained [6], special end fittings had to be used for these tests. Three such end fittings have been developed at NBS; the aluminum-block end fitting [7], the H3M end fitting [8], and the Mod 4 end fitting [8]. It is usually impossible to determine beforehand which of these three end fittings will work best on a given type of pultruded rod. Consequently, it was decided to use all three. The three had originally been developed for 1/2-in (13-mm) diameter rod; scaled-up versions (Figs. 25-27) were there-fore fabricated for the present tests. The end fittings were mounted on their respective rod specimens with NBS C2W3 potting compound [8].

20

The results of the tests are given in Table 7. It may be seen that the Mod 4 end fitting worked best with this rod material, and that the rods have full strengths of at least 65 700 lbf (292 kN).* By contrast, the full-scale test of undamaged Rod X14, with the manufacturer's end fittings, attained only 53 200 lbf (237 kN), which is 19 percent less. It would seem, therefore, that an insulator rod, of the type under consideration here could sustain a 19 percent loss of cross-sectional area without any loss of load-carrying capacity because the strength of the insulator would still be determined by the limitations of the end fittings. (This, of course, does not apply to losses of cross-sectional area that are produced by sharp notches, which introduce high stress concentrations of their own, but rather to more gradual losses such as would be expected from burn damage.) This conclusion is supported by the results of other studies which showed that, depending upon the efficiency of the end fittings, losses of cross-sectional area of 10 to 30 percent could be sustained without any loss of tensile load-carrying capacity [7,9].

Considering that the insulators have undamaged strengths which far exceed their 35 000 lbf (156-kN) rated strengths it would appear that even greater losses of cross-sectional area -- up to 47 percent -- could be sustained without reducing their load-carrying capacities below the rated value.** The significance of this is that insulator rods which have experienced minor burn damage do not pose a threat to the structural integrity of the antenna system and do not have to be replaced for this purpose. On the other hand, rods which have suffered major burn damage should be replaced even if the loss of cross-sectional area appears to be less than 47 percent because charring may have rendered part of the remaining cross section unsound.

8.2 Hardness Tests

Hardness tests were made on the cylindrical surfaces of several of the insulator rods to obtain some indication of the degree of cure of the material. In general, these tests were unrewarding. The measurements exhibited abnormally high scatter, even from one location to another on the same rod. It is surmised that this scatter may have resulted from differences in the coating thickness and in the degree of adhesion of the coating to the substrate from one point to the next. To eliminate these variables, the tests were then repeated on transverse cross sections of short lengths of the rods. In this case, hardness numbers of 69 or 70 on the Rockwell E scale were consistently obtained. This exceeds the hardnesses of uncoated, post-cured, polyester pultrusions [10]. Since polyester and epoxy laminates generally exhibit

---

*This suggests a tensile strength of approximately 140 000 lbf/in^2 (970 kPa) on the basis of the cross-sectional area of the uncoated rod.

**Note that on the only two rods which actually sustained complete failure in service (X8 and X10), the tensile fractures were not incurred until about 97 percent of the cross-sectional areas had been burned away. This suggests that the tensile loads on the rods, at the instants of failure, were of the order of only 2000 lbf (9 kN).

21

TABLE 7. Tensile Tests of Insulator Lengths

Rod No.[a]	Average diameter[b] in	(mm)	End fittings	Free length in	(m)	Maximum load lbf	(kN)	Mode of failure
X16[c]	0.792	(20.1)	Al block	72	(1.8)	40 800	(181)	Tensile failure inside fitting plus longitudinal splitting.
X13	0.789	(20.0)	H3M	96	(2.4)	33 900	(151)	Tensile failure inside fitting plus longitudinal splitting.
X3	0.782	(19.9)	Mod 4	84	(2.1)	65 700	(292)	Tensile failure in free length plus pullout from one fitting.

a. Indicates insulator rods from which specimens were cut.

b. Does not necessarily agree with average diameter of entire insulator rod.

c. Tested in 400,000-lbf (1.78-MN) capacity, vertical, screw-powered testing machine [5].

22

hardnesses within the same range [11], it is reasonable to conclude that the epoxy-based insulator rods from the Angissoq installation were, in fact, fully cured. There is no way of determining, however, whether the rods were in this condition at the time they were installed or whether the curing process gradually proceeded to completion under the ambient service conditions over the years since installation.

8.3 Diametral Compression Tests

A previous study [12] showed that changes in the wet dielectric strength of a pultruded rod product, resulting from changes in the material constituents or the manufacturing conditions, could be correlated with changes in the transverse tensile strength of the product. Accordingly, diametral compression tests were performed on 0.2-in (5-mm) thick disks cut from undamaged portions of several of the insulator rods in order to measure their transverse tensile strengths. The procedure developed in previous investigations on other pultruded rod products [8,13] was followed. Although reasonably good consistency was obtained with disks from the same rod, Table 8 shows rather large differences between rods.

These differences are not immediately explainable. The range of transverse tensile strength values falls within the range of values measured on a variety of commercially available pultruded rod products; but variations of this magnitude have not previously been observed with any single product, except when comparing virgin material with that which had been weathered outdoors for several months or years.

9. ON THE CAUSES OF THE DAMAGE

9.1 Limitations of the Investigation

The design of this investigation, like most, was based upon certain reasonable assumptions. In this case, however, there is evidence that some of these assumptions were invalid and, as a consequence, the interpretation of the test results is less than straightforward. It is important to recognize this limitation before proceeding to a discussion of the central questions addressed by the investigation.

Table 8 indicates a major difference between the transverse tensile strengths of three of the insulator rods as compared with the strengths of three other rods. It is unlikely that the lower strength values resulted from a degradation of the fiber/matrix bonds due to solar radiation or moisture absorption, or that the higher values are indicative of a more complete cure of the matrix having been attained in service, since all of the insulator rods (except Rod X12) were exposed to essentially the same environment. Similarly, it is unlikely that the lower values resulted from damage incurred by electrical discharges within the rods (punctures), since there was no evidence of internal tracking damage or voids in any of the rods. On the other hand, it is significant that the three insulator rods which had low transverse

23

TABLE 8. Diametral Compression Tests

Rod No.	Average transverse tensile strength	
	lbf/in^2	(MPa)
X3	1800	(12)
X8	2000	(14)
X9	2000	(14)
X10	3400	(23)
X13	3500	(24)
X16	3600	(25)

strengths also had poorly adhered coatings, while those rods that ex-
hibited high transverse strengths also had well-adhered coatings. This
observation suggests a reasonable likelihood that all of the insulator
rods were not manufactured identically; and that there were, in fact, at
least two distinct batches of rods involved in the group which was
received for study. (Consideration of the helices observed on certain
rods (Table 1), and comparison of those data with Table 8, suggest that
there may have been even more than two batches involved.) Thus, the
various tests which were designed to detect differences attributable to
service-induced damage or to laboratory-imposed conditions may actually
have yielded results which are clouded by unexpected, inherent, manufac-
turing differences.

In a similar vein, the preconditioning treatments applied to the
rods for some of the test series were based upon the assumption that the
rods, as received, were highly contaminated with salt as a result of
prolonged exposure to a marine environment. It appears that this may
not actually have been the case. Consider the sodium contamination
measured on the surface of one of the rods (Section 5). If it is assumed
that this sodium was present principally as sodium chloride, and that it
was deposited on the rod by airborne ocean spray, then it may be shown
by calculations that the quantity of sodium present represents the
residue from the evaporation of a film of seawater only about 0.1 mm
thick. This is an extremely small quantity of salt in comparison with
the extensive depositions which were observed on GRP rods that had been
exposed to a simulated marine environment in the laboratory for only
2000 hours [13]. Consider, also, the differences in appearance between
the burn damage on the as-received rods and that experienced in the
electrical tests. While the latter tests produced considerable soot on
the rod surfaces, the as-received rods were totally devoid of it. It
seems unlikely that the salt and the soot had been washed away by rain,
since the soot could not be removed by simple rinsing (Section 7.6), and
since rain would be expected to foster additional arcing and soot forma-
tion (Section 9.2) -- unless the power to the antenna system had been
turned off some time prior to the removal of the rods. The cleanliness
of the as-received rods remains unexplained but, nonetheless, these
observations indicate that the washing treatment, which was subsequently
applied to some of these rods at NBS, was largely ineffectual.

Another factor which inhibits the proper interpretation of the test
results is the difference in the voltage characteristics between the
Angissoq installation (100-kHz pulsed) and the electrical tests (60-Hz
continuous wave (CW)). A cursory review of the literature suggests that
the effects of this difference on the burning behavior of rods is largely
unknown. Early work [14] showed that the threshold voltages for corona
inception and for sparkover in air were relatively independent of fre-
quency up to 1 kHz, while at 40-kHz CW the threshold voltages appeared
to be somewhat less than at 60-Hz CW, except for highly polished surfaces.
On the other hand, with pulsed voltages the threshold for sparkover was
higher than with continuous waves. Recent work has added little to the
characterization of high-frequency effects on the inception voltages for

corona [15], but the reduction in sparkover voltage at high frequency
has been confirmed [16]. Regarding the effects of pulsed voltages, the
sponsor reported that an insulator rod was burned up in only two minutes
at 150 kV and 100-kHz CW, even though the rods at Angissoq survived for
years at 270 kV and 100-kHz pulsed. It appears, in summary, that
measurements of voltage levels for corona inception, arcing and flash-
over, made at 60-Hz CW, provide little more than general indications of
behavior under 100-kHz pulsed voltages.

9.2 Burn Damage

The possibility that the burn damage on the Angissoq insulators was
caused by lightning cannot be ruled out categorically. While the extent
of the damage appeared to be greater and more dispersed than that which
might be attributable to a single stroke, it is not beyond reason that
it was the cumulative result of numerous strokes over a period of months
or years. Certainly, the terrain and the climate at Angissoq would tend
to favor the possibility. On the other hand, if the tower had been
struck by lightning on a series of occasions, one would not expect all
of the damage to have been restricted to the insulators on the top-
loading elements. Local blackening of the metal structure and burning
of the insulators on the structural guys (Fig. 1) would also have oc-
curred. Since only minor coating losses on some structural guy insula-
tors were reported, it is assumed, for the purposes of this report, that
lightning was not, in fact, the principal cause of the observed burning
damage.

This leaves corona, arcing, flashover, and similar phenomena re-
lated to the operating voltage of the system as the probable causes of
the burning damage. Several factors and mechanisms, which had origin-
ally been considered as having possibly contributed to the development
of burn damage, were ruled out by the tests and measurements performed
in this study: (1) It was found that most of the end fittings on the
most severely burned rods did not contain voids. (2) It was shown that
there was no simple correlation between coating loss and the incidence
of burn damage. If anything, rods with well-adhered coatings tended to
experience more burn damage. However, the burn damage on rods which
experienced major coating loss usually occurred where the coating had
been lost. (3) It was also shown that the burn damage was probably not
due, in general, to arcing between companion rods or between rods and
their respective corona rings.

The electrical tests showed that the corona inception voltages for
the junctions between the rods and their upper end fittings, and for the
corona rings, are less than the operating voltage of the Angissoq instal-
lation. Thus, corona may have been present as a normal operating condi-
tion on rod ends and corona rings at Angissoq, although this was not
reported. The presence of corona facilitates electrical breakdown by
increasing the electrical surface of the conductor, and by degrading the
dielectric quality of insulation over a long period of time. But corona,

by itself, does not produce carbonaceous tracking and charring; this was substantiated by tests on other GRP rods which were subjected to violent corona for 17 hours at 400 kV (60 Hz) without corona rings and sustained no visible damage [17].

The withstand and flashover tests showed that the voltages required to cause burning damage on dry insulators were sufficiently high, in comparison with the Angissoq operating voltage, to effectively rule out this mechanism as an explanation of the observed burning damage. The situation with wet insulators was entirely different, however. The electrical tests showed that insulators which had been wetted by rain or dense fog could sustain burn damage under voltages which are significantly less than, or equal to, that used at Angissoq.

With these observations in hand it is not difficult to postulate a realistic damage mechanism which is consistent with the bulk of the data available. Tiny droplets or rivulets of water are electrically conductive when they contain even the minutest amount of salt or other contaminant. The presence of such a droplet on the rod, immediately adjacent to or near the upper end fitting, can provide a terminal for a partial discharge from the fitting, either by direct conduction or by means of an arc from the fitting to the nearby droplet. The leakage currents thus produced cause a localized heating of the rod surface which, in time, would oxidize the polymeric surface leaving a thin carbonaceous track. The track, being electrically conductive even after it had dried, would provide a jumping-off point for an arc to the next water droplet slightly further down the rod, extending the track or starting a new one. At the same time, since it continued to carry current each time an arc developed, the original track would grow deeper and wider. In a heavy fog or a rainfall of such duration as to produce long rivulets of water on the rod, the process could continue until complete flashover of the rod would result. This would explain why four of the rods received from Angissoq had sustained burn damage at their lower, as well as their upper, ends.

This damage mechanism also serves to explain why no more than one rod, out of each companion pair, tended to experience severe burning. The two rods in each insulator assembly are not constrained to remain at exactly the same elevation above the ground. Rather, the assembly can rotate about its longitudinal axis, due to twisting and untwisting of the wire rope guys, thus placing one rod somewhat above the other in the general case. During a heavy rainfall, with water rivulets coursing down the top-loading elements from the tower, nearly all of this water would run down the lower of each pair of rods, with the upper one being wetted solely by the raindrops directly incident upon it. This, in turn, would tend to produce far more arcing and tracking on the lower rod than on the upper one.

27

The postulated damage mechanism can also be used, with some elaboration, to explain why the worst burn damage was sustained by rods having negligible coating loss, while on those rods which had experienced major coating loss most of the burn damage occurred in the uncoated regions. Where coating loss had occurred, the rod surfaces were rougher and more porous than the coating and, therefore, tended to be wetted and to retain moisture more easily than the coating. As a result, these uncoated regions were more likely to provide termination points for arcs from the upper end fitting or from a nearby carbonaceous track. (Incidentally, the greater roughness of the uncoated regions also explains why the corona inception voltages were less for the rods which had their coatings removed than for the coated rods.) On the other hand, it was found that the coating is more flammable than the GRP substrate material so that it would tend to carbonize and track more readily than uncoated rod in the presence of leakage currents. This explains why the uncoated rods experienced less damage than the coated rods in the electrical tests. Since, as pointed out earlier, there is reason to believe that there were at least two different coating materials used in the manufacture of the rods, it is entirely possible that the well-adhered coating had a higher flammability than the flaky coating and was, therefore, more susceptible to carbonaceous tracking in the presence of surface leakage currents. If so, this would explain why the worst burn damage was sustained primarily on rods which had experienced little, if any, coating loss.

The principal thrust of the above paragraph is, simply, that arcing was more prone to occur where coating loss had been experienced, but the worst burn damage was still apt to take place on a rod having a relatively flammable coating even if coating loss had not occurred and the incidence of arcing was less.

The flammability tests showed that the rods have LOIs in excess of 21 percent and it follows, therefore, that they are basically self-extinguishing in air. This explains why the rods, once ignited, did not invariably burn to destruction. Instead, the proposed damage mechanism suggests that burn damage was only incurred while surface leakage currents were present, i.e., while there was actual arcing from the upper end fitting or from an established carbonaceous track to the next water droplet on the rod, or while there was complete flashover. Once a rain had ceased to fall, or a fog had dispersed, the moisture on the surface of a rod would quickly vaporize, due to the leakage current, to the point where further arcing would cease.

(An alternative, though similar, damage mechanism has also been proposed, which also merits presentation here. According to this theory, the electrical failure of the Angissoq insulators

28

"... is attributed to the intrusion of salt into
the weather-deteriorated polymeric coating. These
salt deposits are probably limited to the immediate
area of any crack, chip, or other surface damage and
do not extend into the interface area. When wetted,
these deposits create many small, highly conductive
paths for current flow and places high electrical
stresses on the undamaged surface areas. This, in
turn, causes arcing across the undamaged areas and
once the polymeric material is burned, it remains
conductive. In addition, this new surface damage
creates additional areas for salt entrapment."[4]

This damage mechanism may, indeed, have been responsible for the failures
observed in the electrical tests, since, in those tests, the rods which
had been preconditioned by washing and by having their coatings removed
performed significantly better than those rods which had been preconditioned
by immersion in saltwater. On the other hand, it does not appear likely
that this mechanism was principally responsible for the failures at
Angissoq since the worst burn damage, on the as-received rods, was con-
fined primarily to rods that had experienced no coating damage.

(Research has shown that epoxy films are relatively permeable to
chloride ions [18] and this suggests the possibility that the salt may
have been able to penetrate the coatings by diffusion even where the
coatings were intact. However, the permeability of epoxy resins de-
creases rapidly with temperature [19]so it is improbable that salt
diffusion was a significant factor at Angissoq.)

9.3 Coating Loss

It has been pointed out that of those rods which had served as com-
panion pairs in single insulator assemblies both exhibited major coating
loss or both exhibited negligible coating loss. At first, this suggests
the possibility that the loss of coating may have resulted from companion
rods striking or rubbing against each other due to wind-induced vibration;
or that the rods may have become twisted together due to the twisting or
untwisting of the wire rope guys. However, if either of these were the
case, then most of the coating loss would probably have occurred near
the midlengths of the rods rather than in their upper thirds.

Another possibility is that the coating loss was caused by icing
and repeated freeze-thaw cycles. Icing is most commonly formed when the
air and the affected surface temperatures are slightly above, at, or
below 0 °C (32 °F), and supercooled moisture is present. The average
0 °C (32 °F) isotherm passes very close to Angissoq during six months of
the year (Dec-May) and, similarly, the southern part of Greenland experi-
ences a relatively high frequency of occurrence of supercooled fog,
throughout the year. Also, Angissoq is near a region that has a high
frequency of occurrence of supercooled clouds for six months of the year

(Dec-May), a condition which is conducive to the development of glaze storms [20]. The deficiency in this explanation is also that it would appear to affect all parts of the insulator rods equally rather than their upper portions preferentially.

The fact that most of the coating loss occurred in what is believed to be the upper parts of the insulator rods suggests that corona may somehow have been responsible. It is known that ozone is invariably generated whenever corona is present and that most organic compounds are readily oxidized by ozone. But this does not explain why the incidence of major coating loss was apparently confined to companion pairs of rods.

10. ON REDUCING THE INCIDENCE OF DAMAGE

10.1 Coating Loss

Although the principal cause of the coating loss on the Angissoq insulator rods is unknown, the remedy is obvious. It is abundantly evident, from seven of the seventeen rods which were examined, that well-adhered coatings which are resistant to peeling and flaking can be manufactured. Unfortunately, it appears that the formulation of the well-adhered coating may have compromised its flammability qualities, so that the use of the coating may have avoided coating loss at the expense of a greater susceptibility to burn damage. The formulation of a suitable coating with high resistance to combustion and/or carbonaceous tracking is discussed later.

10.2 Burn Damage

In accordance with the postulated damage mechanism, there are three general approaches that can be considered, either singly or in combination, for reducing the incidence of burn damage in GRP insulators for top-loading elements:

1. Reduce the electrical stress at the top of the insulator rods, where burn damage apparently begins.

2. Raise the leakage path resistance of the insulator rods to reduce the tendency for electrical discharges to occur.

3. Enhance the flame-retarding and anti-tracking qualities of the insulator rods to reduce the burn damage incurred in the presence of arcing and leakage currents.

Each of these approaches are discussed here.

While there is no evidence that corona, in itself, was a direct cause of the observed burn damage, it could have been a contributing factor. It has been pointed out that corona could lead to coating loss; but more important, the presence of corona at the junction of a rod and its upper

end fitting can effectively increase the distance over which an electrical
arc from the fitting can strike in order to reach some receptive terminal
point on the rod. The inception of corona at the rod/fitting junctions
can be eliminated by suitable redesign of the corona rings [17]. However,
given the 270-kV operating voltage of the Angissoq system, it does not
seem likely that a corona ring -- even a very effective one -- could
avert partial discharges from the energized end fittings in the presence
of water droplets or rivulets on adjacent portions of rod. Furthermore,
the voltages required to produce complete flashover do not appear to be
influenced by the design of the corona rings [17].

(In this connection, and with relevance to lightning protection, it
was shown by means of high-voltage impulse tests on other GRP rods, that
flashover could be diverted from the rod surfaces when corona rings were
used on both ends of the rods [7]. Flashover occurred in the air between
the rings, and the rods were not damaged thereby. However, these tests
were conducted under dry conditions and, again, it seems likely that if
the rods had been sufficiently wet the rod surfaces would have provided
a preferential path for the flashover.)

The tendency for arcing to occur along the surface of a rod could
be reduced by avoiding the development of sites on the rod surfaces
where water droplets can momentarily accumulate. This can be achieved,
to some extent at least, by keeping the rod surfaces clean of contamina-
tion particles, and by using rods with extremely smooth, nonporous
surfaces to reduce wettability.

While some users clean their GRP insulator rod surfaces regularly,
this does not seem to be a feasible practice for highly inaccessible
rods on installations situated in remote geographical locations.

With regard to the desirability of having smooth rod surfaces, it
has been observed that uncoated rods, as produced by many pultrusion
manufacturers, are substantially smoother than coated rods, at least
when they are new*. It may be noteworthy that of the four communications
systems that had burn damage problems with GRP insulators (three of them
Loran-C installations), and which are known to the authors, all involved
coated rods. This may not be a meaningful observation, however, since
it is possible that uncoated rods are not widely used in high-voltage

_____

*For the purposes of this discussion, rods manufactured with a trans-
parent, integral gel coating of the matrix material are considered
uncoated; the term "coatings" is reserved for compositions that differ
from the matrix material of the rod, being added chiefly for enhanced
weatherability.

outdoor applications. There is evidence* that uncoated rods, exposed to
sunlight for extended periods, develop a condition known as "blooming"
or fiber prominence. The outer surfaces of the matrix material deteriorate
under the sustained action of ultraviolet radiation, leaving glass
fibers exposed. In this state the surfaces are neither smooth nor
nonporous, and may be expected to be particularly susceptible to arcing
when wet.

Given, therefore, that some coating is needed on the rods for long-
term weather resistance, it would appear desirable to add a second
coating to reduce wettability. Such water-repellant coatings have been
developed and have, in fact, demonstrated significant increases in
surface electrical leakage resistance in the presence of moisture [21].

An entirely different technique for reducing the tendency for
arcing involves the use of GRP insulators fabricated with regularly
spaced, transverse skirts [22-24]. The shapes of these insulators
provide inherently longer leakage paths and, in addition, inhibit the
formation of rivulets by shedding water at the lower extremities of the
skirts. These insulators have been finding increased acceptance in
European power-transmission systems.

Arcing and leakage current, though undesirable, do not necessarily
lead to the formation of carbonaceous tracks. Most plastics, including
most epoxies, oxidize in the process of combustion or in the presence
of electric arcs, leaving elemental carbon from the polymeric structure
as a solid residue. By adding a strong oxidizing agent such as aluminum
hydrate to the polymer formulation, the decomposition process is changed
so that the carbon is carried away in the form of carbon monoxide and
volatile hydrocarbons. Effectively, then, the material erodes; but the
tracks are not carbonaceous and, therefore, non-conducting. In the case
of insulator rods, this would inhibit the growth and the spread of
tracks and virtually avoid surface flashover.

Some thermoplastics also offer anti-tracking qualities by virtue of
their chemical constitutions. Polytetrafluoroethylene (PTFE) is particu-
larly notable in this regard, since it is also exceptionally weather-
resistant. Numerous commercial formulations, suitable for use as coatings
or jacketing materials, have also been developed in recent years and,
reportedly, offer exceptionally high resistance to fire [25].

Unfortunately, the aluminum hydrate additive, in the proportions in
which it must be used, reduces the mechanical properties of GRP. Simi-
larly, PTFE is not a suitable matrix material for pultruded rod. Thus,

---

*Unpublished results of real-time weathering tests conducted by a
pultrusion manufacturer, and of a survey, by another manufacturer, of
pultrusions in outdoor service.

while these materials can be used to provide anti-tracking or flame-resistant coatings, a different approach would be required for the GRP substrates. It has been reported that aramid-reinforced epoxy offers flammability and electrical properties which are equal or superior to those of glass-reinforced epoxy [26], while NBS research has shown that the wet dielectric strength of aramid-reinforced polyester is less than that of glass-reinforced polyester [12]. Considerable work has been done, in recent years, on the development of fire-retarding agents for glass-reinforced polyester [27].

11. SUMMARY

A group of damaged GRP insulator rods, which had been removed from service on a Loran tower in Angissoq, Greenland, were submitted to NBS for failure analyses. The rods, which had sustained both burn damage and loss of coating, were subjected to a variety of inspections, tests and measurements. There was evidence that the rods may not all have been manufactured identically; this complicated the failure analyses.

The burn damage, which had led to complete failure of some rods, was attributed primarily to the occurrence of electrical discharges from the energized end fittings. It appeared that most of the discharges had been only partial but there was also evidence that complete flashover probably had occurred on some rods. The principal factor which contributed to the occurrence of the discharges was the presence of moisture from rain, fog and/or airborne ocean spray, which significantly lowered the leakage path resistances of the rods. Other factors which may have contributed include salt contamination, electrical corona at the junctions of the rods with the energized end fittings, and the loss of coating on some of the rods. The poor flammability and tracking resistances of the rods and their coatings contributed to the severity, if not the incidence, of the burn damage.

The principal cause of the coating loss, which was extensive on some rods, could not be identified, but climatic conditions and the presence of electrical corona are believed to have been contributing factors. The coating loss did not impair the structural integrity of the rods; but as mentioned above, it may have been a secondary factor contributing to the occurrence of electrical discharges.

One approach toward reducing the incidence of burn damage would be to use skirted insulator rods, which effectively increase the leakage path resistances in moist environments. A second approach, which might be less expensive in the long run, would be to select or develop an improved coating material for the rods. Ideally, such a coating should be tough and well-adhered, weather resistant and water repellant, arc resistant, track resistant and fire resistant. Regardless of which of these approaches is used, the basic GRP rod material should also be made more fire resistant if this can be accomplished without serious compromise of its mechanical properties. The design of more effective

33

corona rings and the use of such rings on the lower, as well as the upper, ends of the insulator rods, might also provide some protection against damage due to lightning.

The insulator rods can tolerate moderate carbonaceous tracking without any loss of tensile load-carrying capacity. Even burns that consume rather substantial percentages of a rod's cross-sectional area do not pose an immediate threat to the structural integrity of the system. However, rods that sustain major burn damage should always be replaced because burned rods are more susceptible to further burn damage and because undetected charring beneath the burned surface may have rendered some of the remaining material unsound.

12. REFERENCES

1. Sushinsky, G. F. and Mordfin, L., Nondestructive Examination of Glass-Reinforced-Plastic Rod End Fittings, NBSIR 76-1084 (April 1976).

2. American Society for Testing and Materials, Standard Method of Test for Flammability of Plastics Using the Oxygen Index Method, ASTM Designation D2863, 1975 Annual Book of ASTM Standards, Part 35 (1975).

3. Parvin, K., Polyester Resins of Reduced Fire Hazard, Proc. Reinforced Plastics/Composites Institute, 30th Anniversary Conf., Washington, Feb. 4-7, 1975, paper 2-F (Society of the Plastics Industry, N.Y., 1975).

4. Gabriel, A. L. and Brown, J. E., Electrical Tests on Fiber Glass Guy Insulators, Technical Report No. ERF-75-128, Bonneville Power Administration (Vancouver, Wash., July 10, 1975).

5. Chwirut, D. J., coordinator, Research and Testing Facilities of the Engineering Mechanics Section, National Bureau of Standards, Washington, D. C., NBS Spec. Publ. 370 (1973).

6. Halsey, N., Mitchell, R. A. and Mordfin, L., Evaluation of GRP Rod and Rope Materials and Associated End Fittings, NBSIR 73-129 (Dec. 1972).

7. Halsey, N., Properties of Glass Fiber-Reinforced Polymers for Application to Guy-Insulator Systems of Communication Towers, Phase 2, Test Methods and Evaluations of Glass Fiber-Reinforced Polymer Rods for Use in Guy-Insulator Systems of Loran C Towers, NBS Report 10261 (June 1970).

8. Marlowe, D. E., Halsey, N., Mitchell, R. A. and Mordfin, L., Non-Metallic Antenna-Support Materials, First Annual Interim Report, NBSIR 73-233 (April 1973).

9. Halsey, N., Glass Reinforced Plastic Rod Insulators, NBS Report of Test on U.S. Coast Guard MIPR No. Z-7099-1-13072 (Feb. 18, 1971).

10. Halsey, N., Marlowe, D. E. and Mordfin, L., Non-Metallic Antenna-Support Materials, Second Annual Interim Report, NBSIR 74-557 (June 1974).

11. Gross, S. (editor), Modern Plastics Encyclopedia 1973-1974, (McGraw-Hill, N.Y., Oct. 1973).

12. Halsey, N., Marlowe, D. E., Mitchell, R. A. and Mordfin, L., Non-Metallic Antenna-Support Materials, Final Report, AFML-TR-76-42, Air Force Materials Lab (Wright-Patterson AFB, Ohio, May 1976).

13. Halsey, N. and Mordfin, L., Environmental Effects on the Strength of a Glass Fiber-Reinforced-Plastic Rod Material, NBSIR 76-1069 (March 1976).

14. Peek, F. W. Jr., Dielectric Phenomena in High Voltage Engineering, 2nd edit., pp 65-66 and 106-111 (McGraw-Hill, N. Y., 1920).

15. Loeb, L. B., Electrical Coronas, Their Basic Physical Mechanisms, pp 569-586 (Univ. of Calif. Press, Berkeley, 1965).

16. Kotter, F. R., A Study of Air-Gap Breakdown at 28.5 Kilohertz, NBSIR 75-731 (June 1975).

17. Gabriel, A. L. and Brown, J. E., Electrical Tests on U.S.C.G. Designed Grading Ring Assemblies, Technical Report No. ERD-75-235, Bonneville Power Administration (Vancouver, Wash., Dec. 4, 1975).

18.. Matsui, E. S., Permeation of Chloride and Sodium Ions through Protective Coating for Naval Shore Structures, Report No. TN-1373, Civil Engineering Laboratory, Naval Construction Battalion Center (Port Hueneme, Calif., Feb. 1975).

19.. Parham, J. L., Specific Permeability of Epoxy Resin Systems, Report No. RL-TR-71-5, U.S. Army Missile Command (Redstone Arsenal, Ala., June 14, 1971).

20.. Sanderson, J. I., Occurrence of Ice in the Form of Glaze, Rime and Hoarfrost with Respect to the Operation and Storage of V/STOL Aircraft, Report No. ETL-SR-73-1, U.S. Army Engineer Topographic Laboratories (Fort Belvoir, Va., Jan. 1973).

21. Baker, H. R. and Bolster, R. N., The Prevention of Surface Electrical Leakage in the Presence of Moisture, NRL Report 7326, Naval Research Laboratory (Washington, Oct. 26, 1971).

22. Polvara, A., Plastics as Insulating Materials for Traction and High Voltage Lines [in Italian], Materie Plastiche ed Elastomeri (June 1969). Also English translation, PTFE/Polyester Glass Fibre Insulators for Power Transmission, Imperial Chemical Industries Ltd. (Welwyn Garden City, Hertfordshire, England, March 1970).

23. Anon., Rodurflex Plastics Insulators for Overhead Transmission Lines, Rosenthal Technik AG (Selb, W. Germany, June 1973).

24. Anon., Second Generation of High-Voltage Insulator, Publication No. 2554-H, Ohio Brass Co. (Mansfield, Ohio).

25. Hughes Aircraft Co., Improved Cable Fire Protection, report to
    Naval Ship Engineering Center on Contract No. N0024-74-C-5083
    (Fullerton, Calif., Jan. 1974).

26. Sturgeon, D. L. G. and Venkatachalem, T. K., Potential Contribution
    of High Strength, High Modulus Aramid Fibers to the Commercial
    Feasibility of Lighter than Air Craft, Proc. Interagency Workshop
    on Lighter than Air Vehicles, edited by J. F. Vittek, Jr., FTL
    Report R75-2, MIT Flight Transportation Laboratory, pp 243-255
    (Jan. 1975).

27. See annual Proc. Reinforced Plastics/Composites Institute (Society
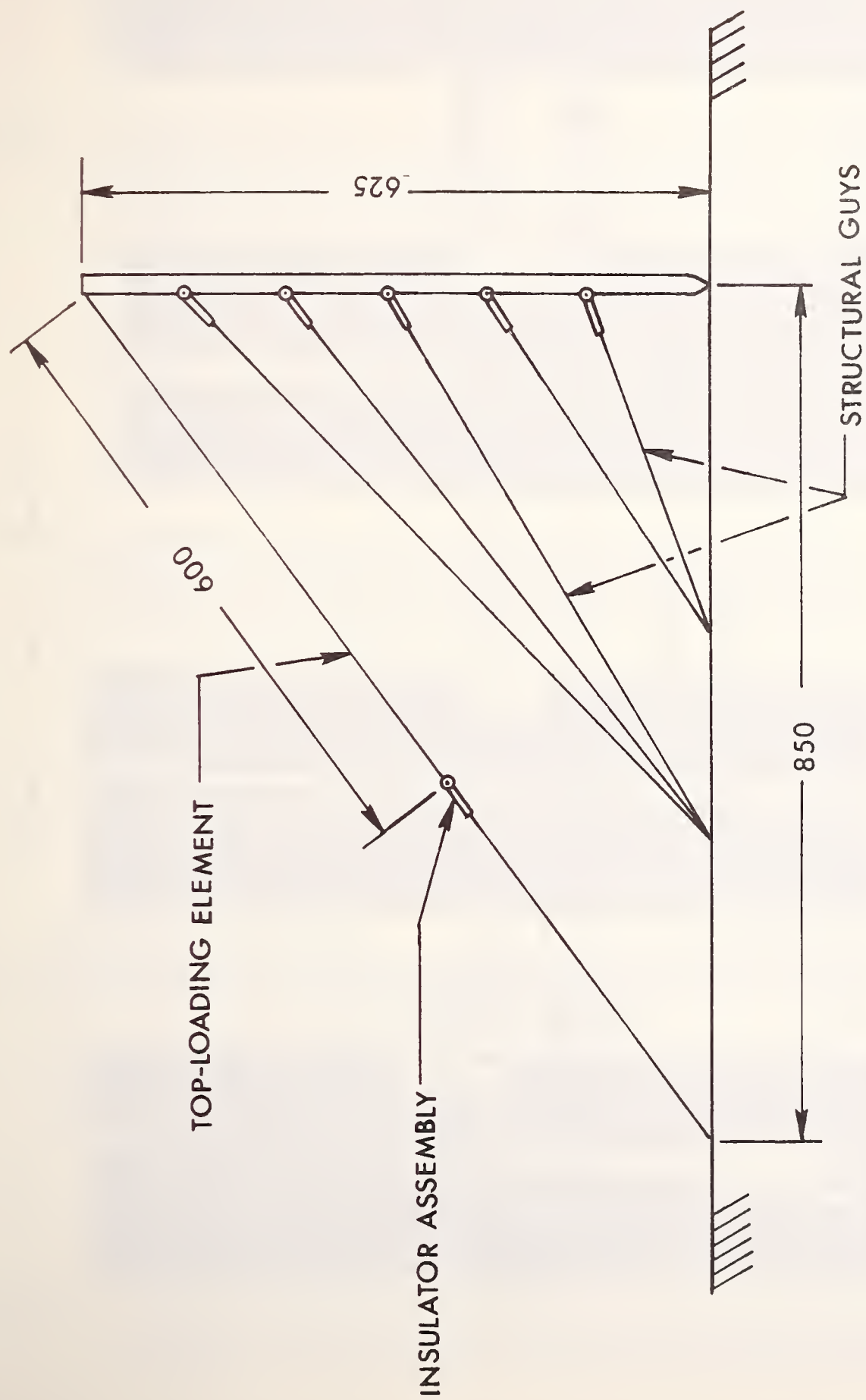   of the Plastics Industry, N.Y.).

Figure 1. Guying arrangement for Angissoq tower, not to scale. All dimensions in feet (1 ft = 0.3048 m).
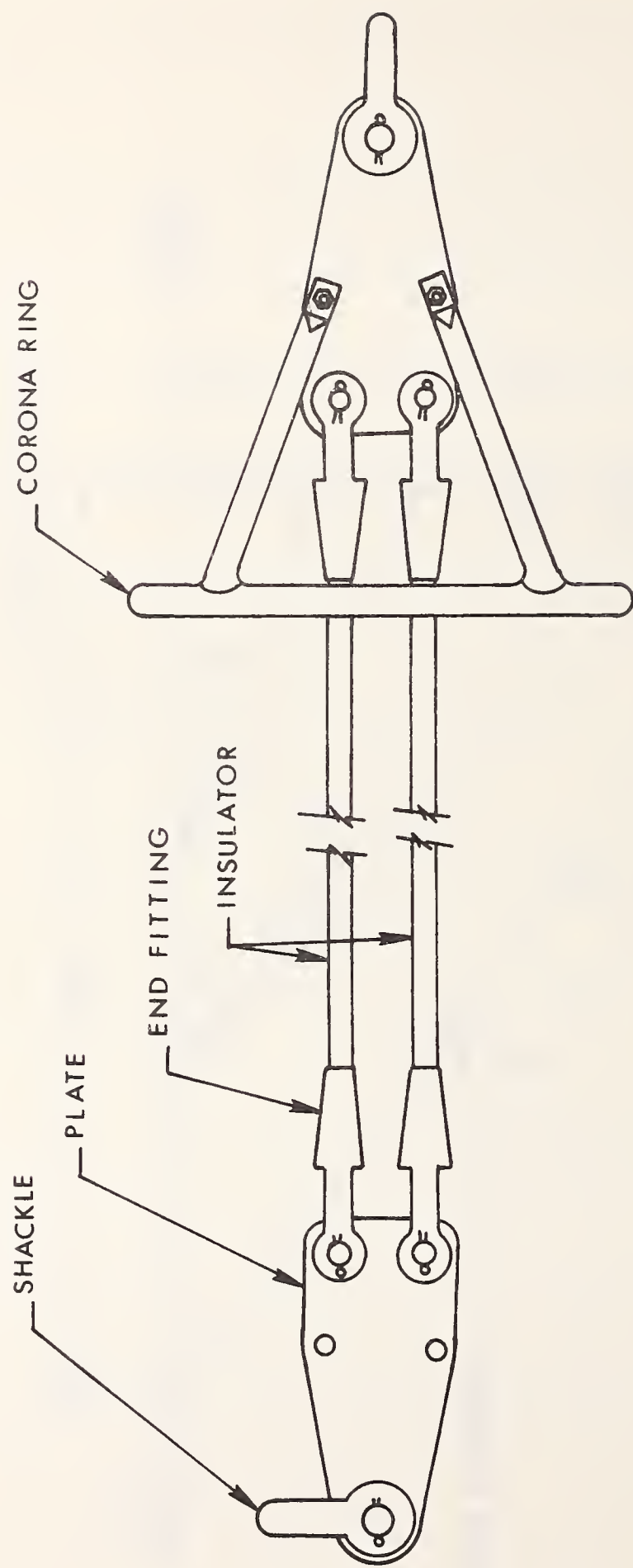
Figure 2. Insulator assembly.
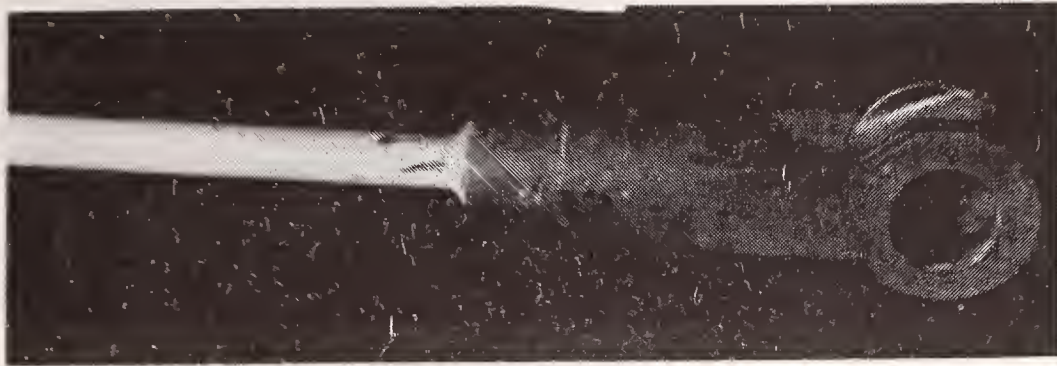
Figure 3. Upper end of Rod X1 showing two short carbonaceous tracks adjacent to the end fitting.

Figure 4. Lower end of Rod X2 showing two short carbonaceous tracks adjacent to the end fitting. The upper track is the less severe of the two, and is situated in a small area in which the coating is gone.

Figure 5. Upper end of Rod X3 showing substantial loss of coating. Helical markings are faintly visible on the uncoated surface.

Figure 6. Upper end of Rod X4 showing substantial loss of coating. The helical markings on the uncoated surface are clearly visible.
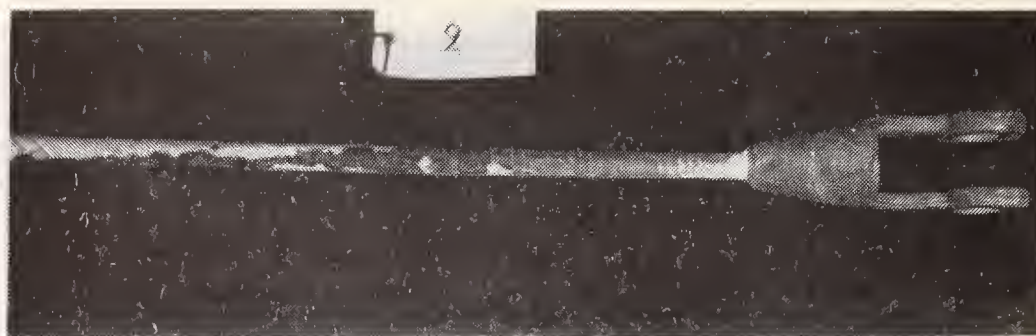
Figure 7.   Upper end of Rod X5 showing substantial loss of coating.

Figure 8.   Upper end of Rod X6 showing minor losses of coating.
Shallow carbonaceous tracks are faintly visible in the
uncoated areas.

Figure 9.   Upper end of Rod X7 showing a 1-in (25-mm) long carbonaceous
track.   The longer streak on the left is a scuff mark.

Figure 10.   Upper end of Rod X8 showing severe carbonaceous tracking
and charring.   The rod appeared to have burned almost
completely through, with the last 3 percent of its cross
section having failed in tension.   Some small areas of
coating loss are evident along the upper edge of the burn
damage.   The fitting from this end of the rod is shown in
Figure 20.
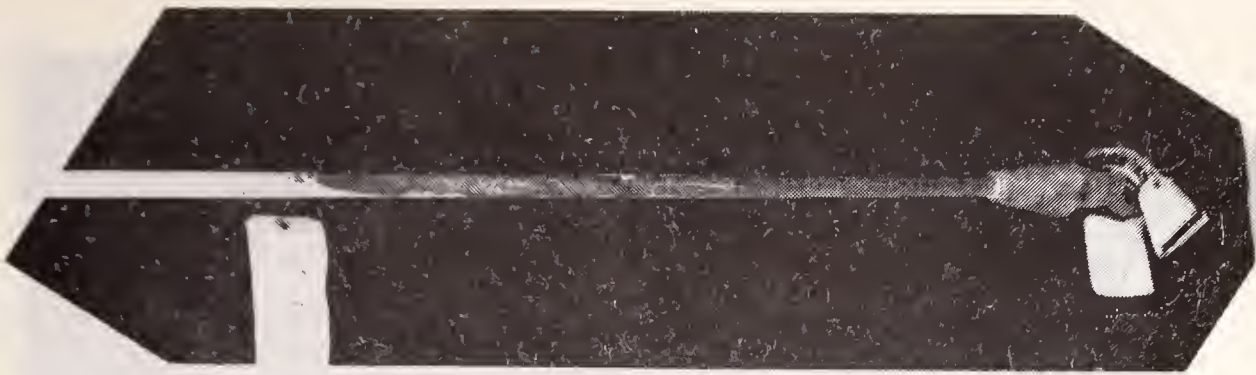
Figure 11. Upper end of Rod X9 showing substantial loss of coating.
A carbonaceous track is evident near the middle of the
uncoated area.
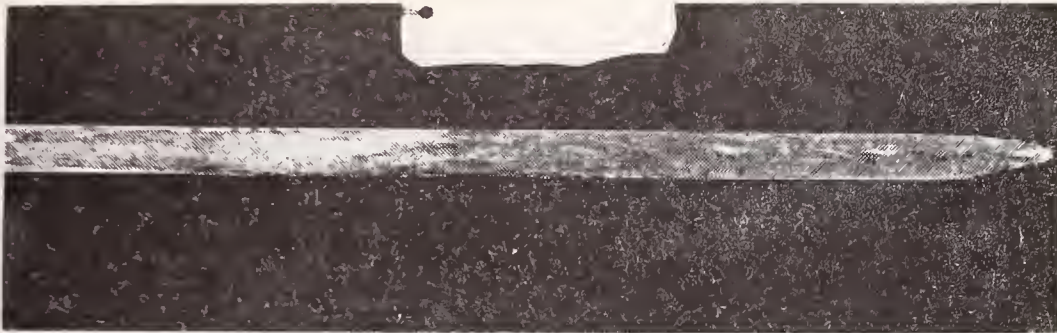
Figure 12. Upper end of Rod X10 showing severe carbonaceous tracking
and charring. The rod appeared to have burned almost
completely through, with the last 3 percent of its cross
section having failed in tension. The fitting from this
end of the rod is shown in Figure 21.
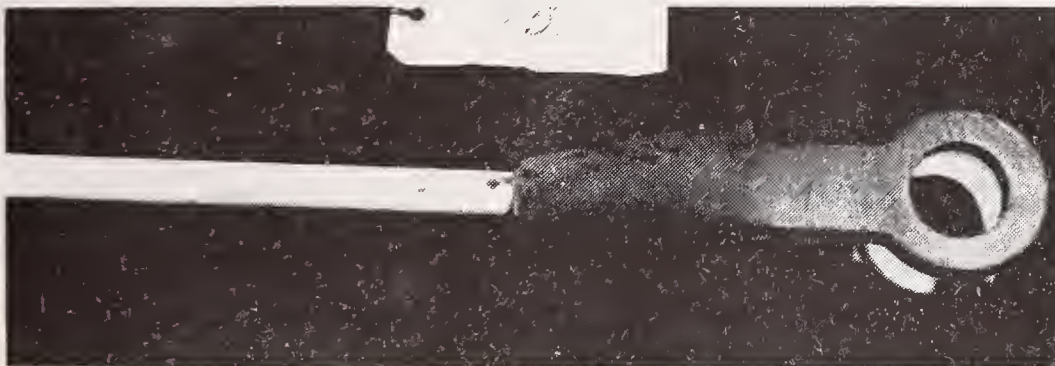
Figure 13. Upper end of Rod X11 showing a small area adjacent to the
end fitting where the coating had been lost, and a thin
carbonaceous track extending from this area onto the coating.

Figure 14. Upper end of Rod X13 showing severe carbonaceous tracking
and charring.
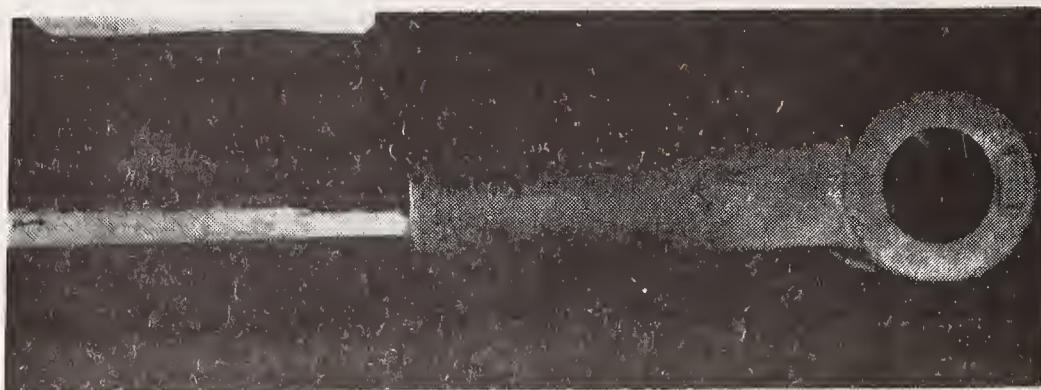
Figure 15.   Upper end of Rod X15 showing severe carbonaceous tracking and charring.
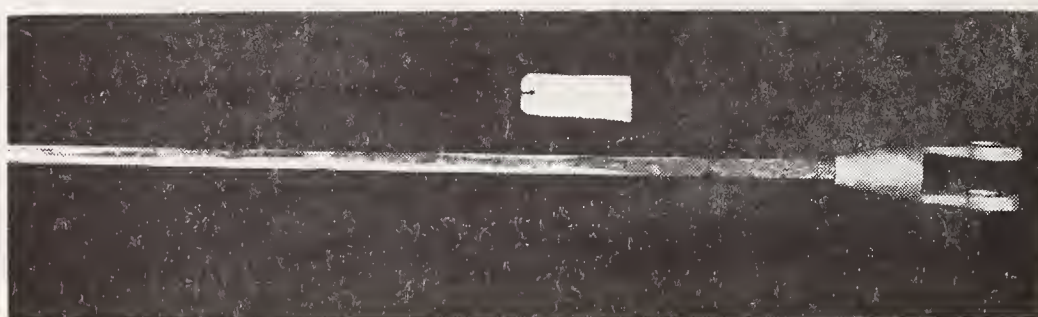
Figure 16.   Upper end of Rod X16 showing severe carbonaceous tracking and charring.   See, also, Figures 17 and 18.

Figure 17.   Upper end of Rod X16 showing long carbonaceous track on the surface opposite to that depicted in Figure 16.

Figure 18.   Lower end of Rod X16 showing carbonaceous track.

Figure 19. Upper end of Rod X17 showing substantial coating loss and intermittent carbonaceous tracking both inside and outside of the uncoated area.
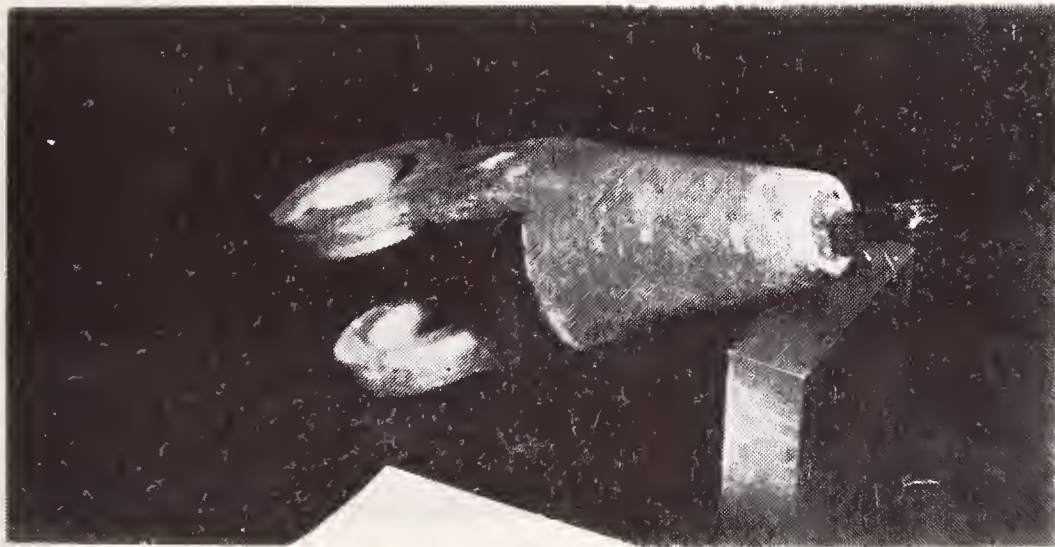
Figure 20. Upper end fitting from Rod X8. See, also, Figure 10.
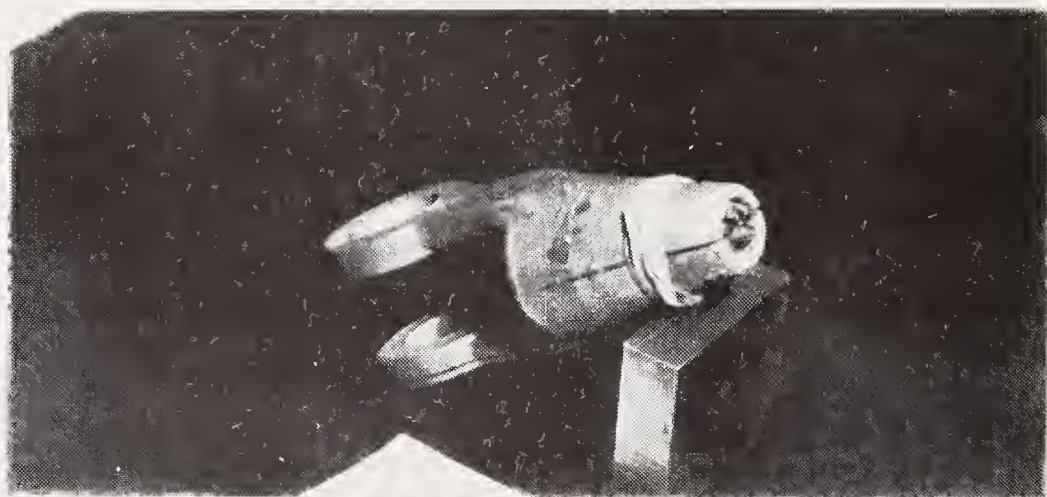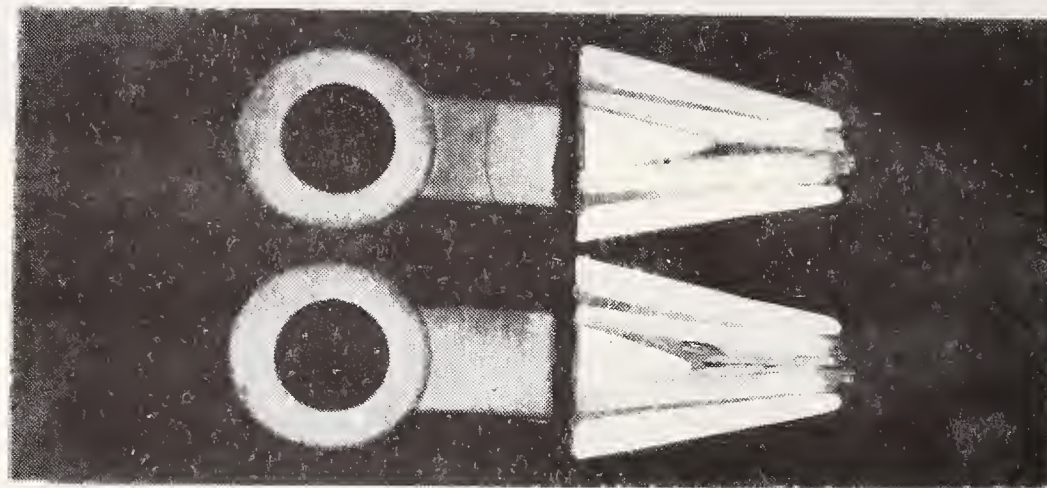
Figure 21. Sectioned (above) and reassembled (below) views of the upper end fitting from Rod X10. Note the large void in the potting compound near the tip of the conical wedge. The void does not appear to have been open to the atmosphere. See, also, Figure 12.
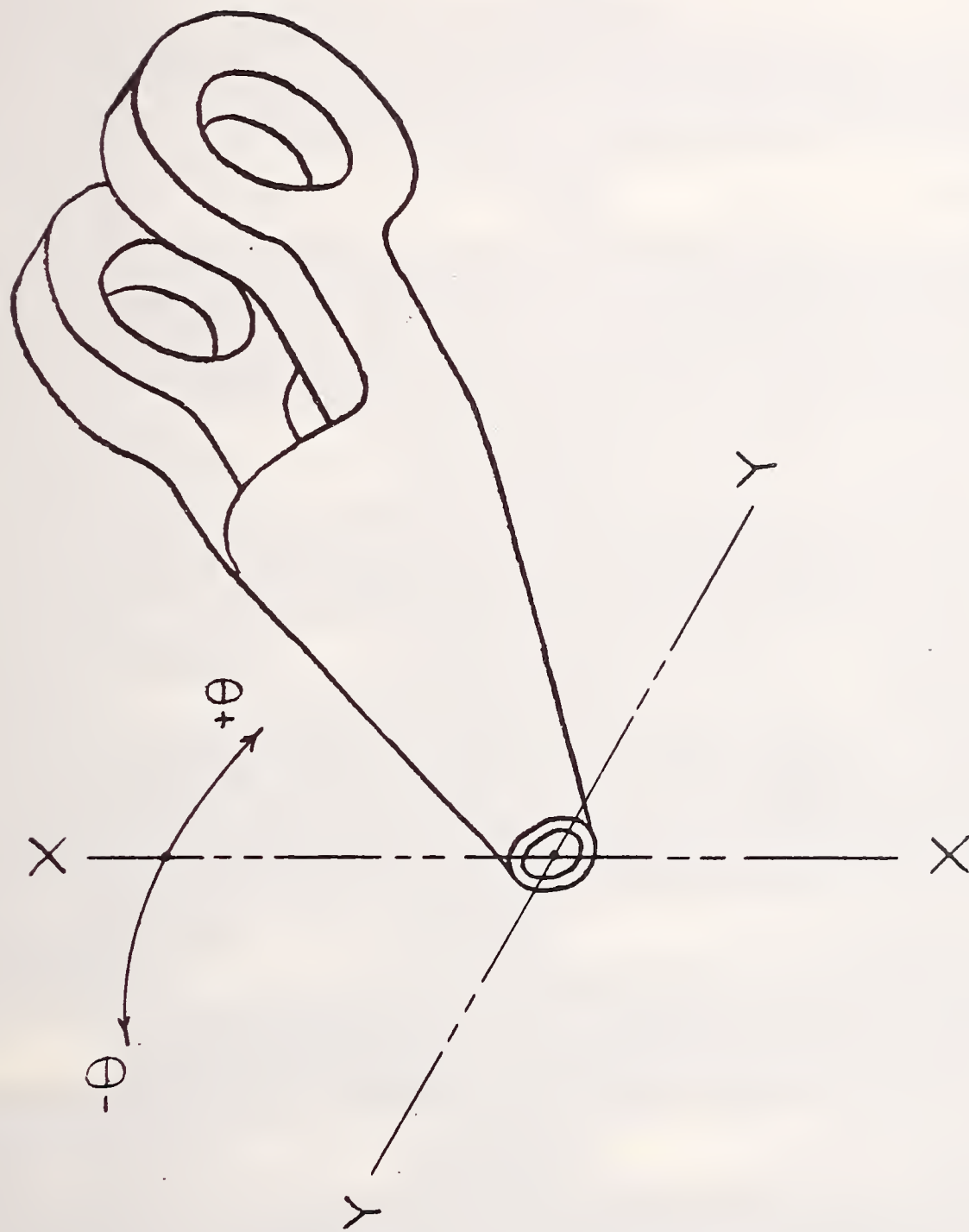
Figure 22. Sketch of end fitting showing coordinate system used for identifying the angular locations of damage.
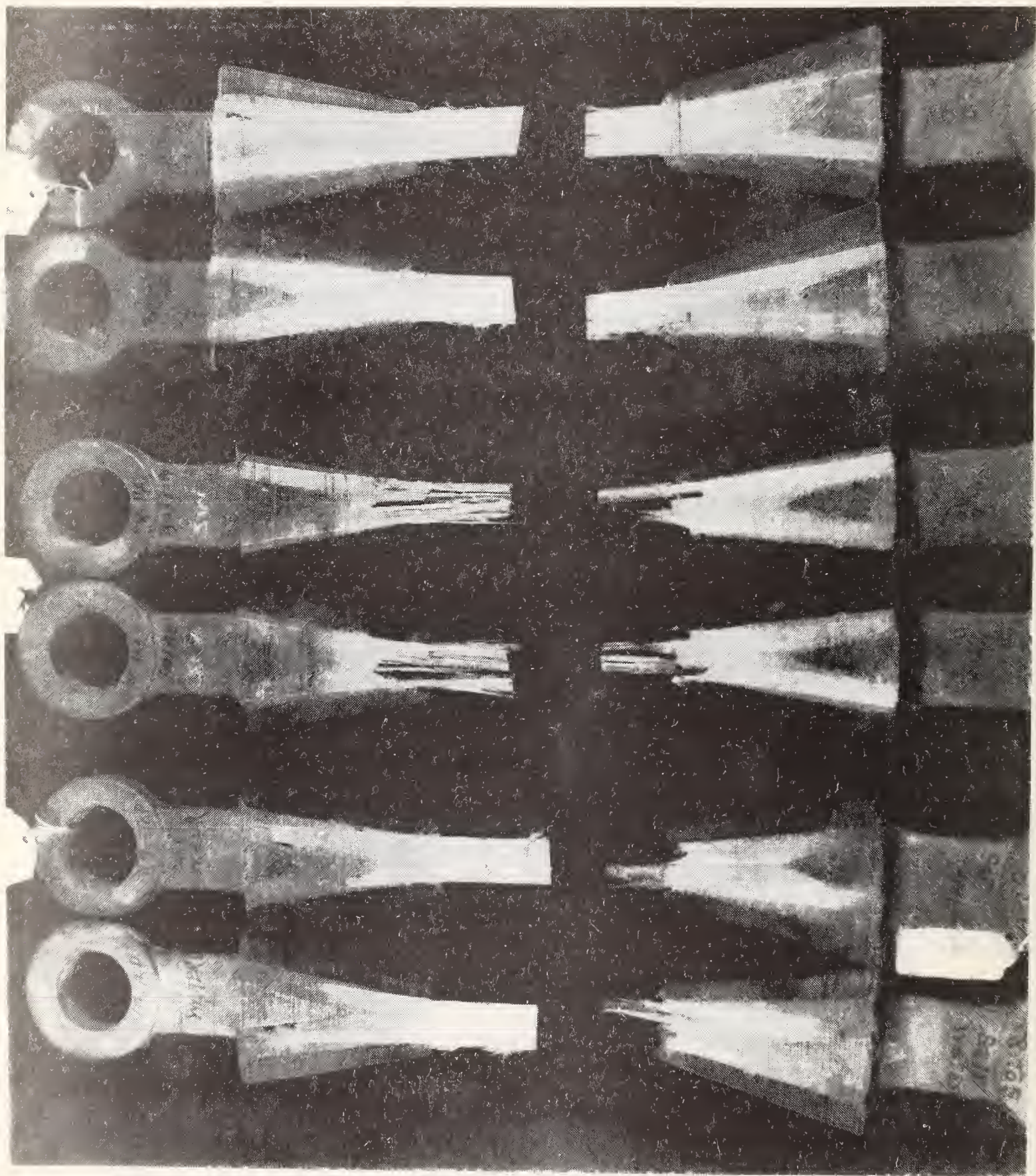
Figure 23. Dissected end fittings. Top row, left to right: X9 upper, X14 lower, X9 lower. Bottom row, left to right: X8 upper, X15 upper, X14 upper.
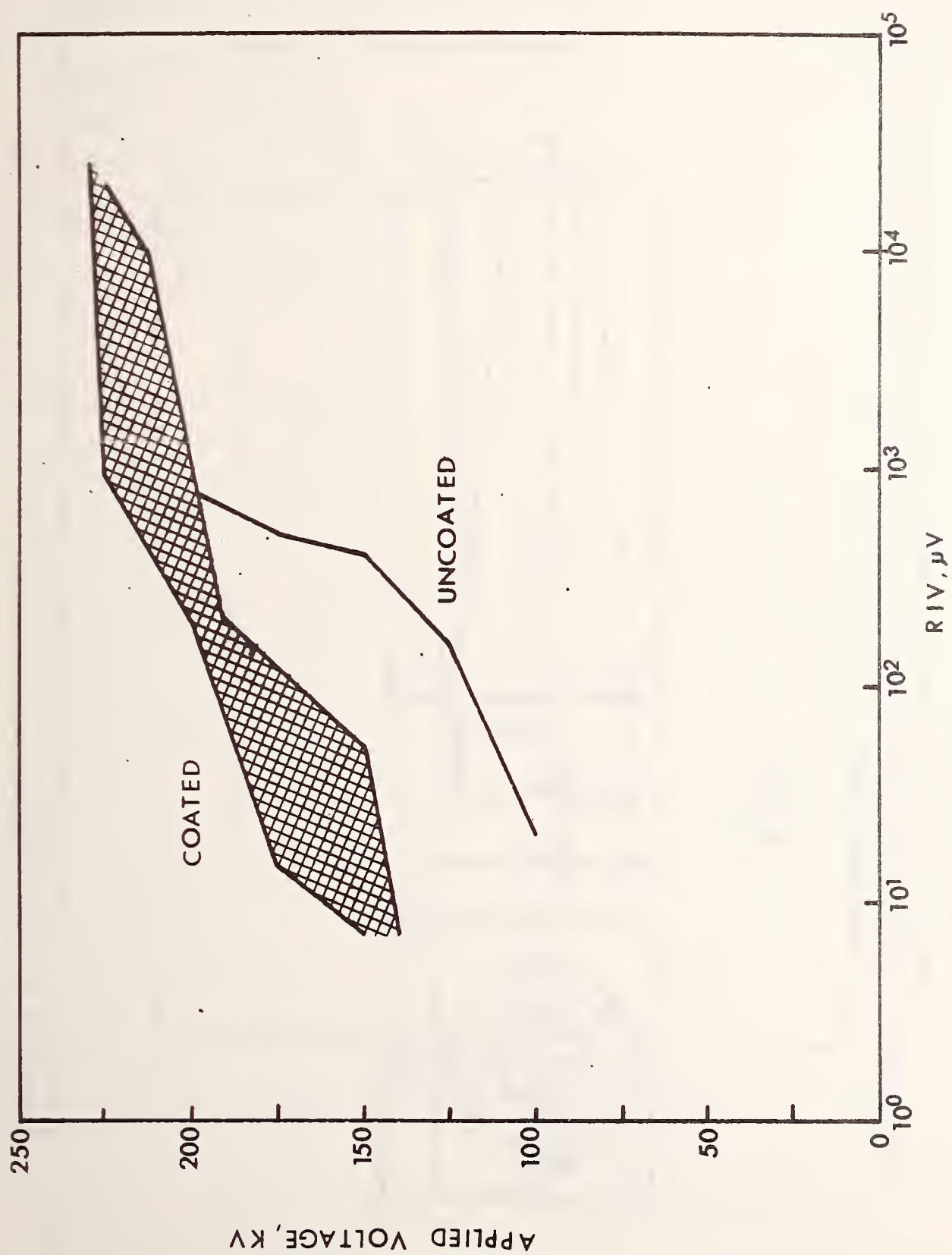
Figure 24. Results of RIV tests.
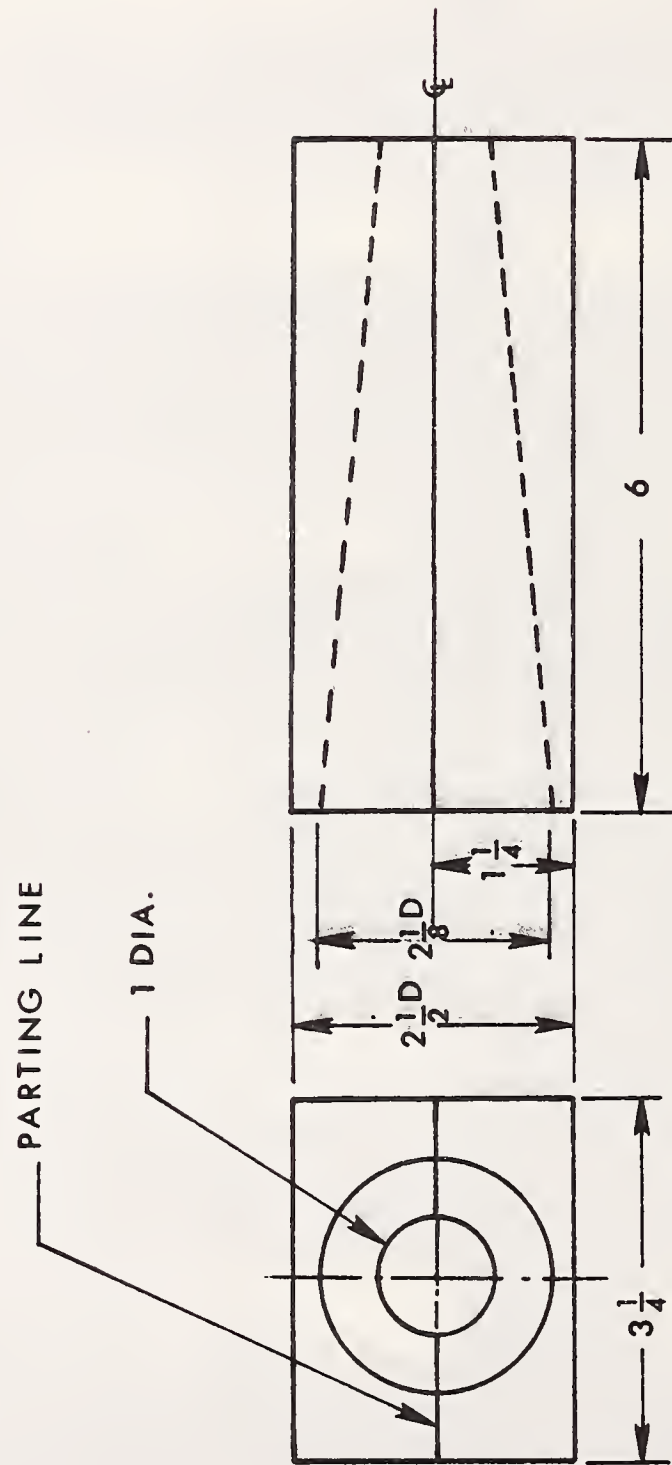
Figure 25. Aluminum-block end fitting for 0.79-in (20-mm) diameter rods. All dimensions in inches (1 in = 25.4 mm).
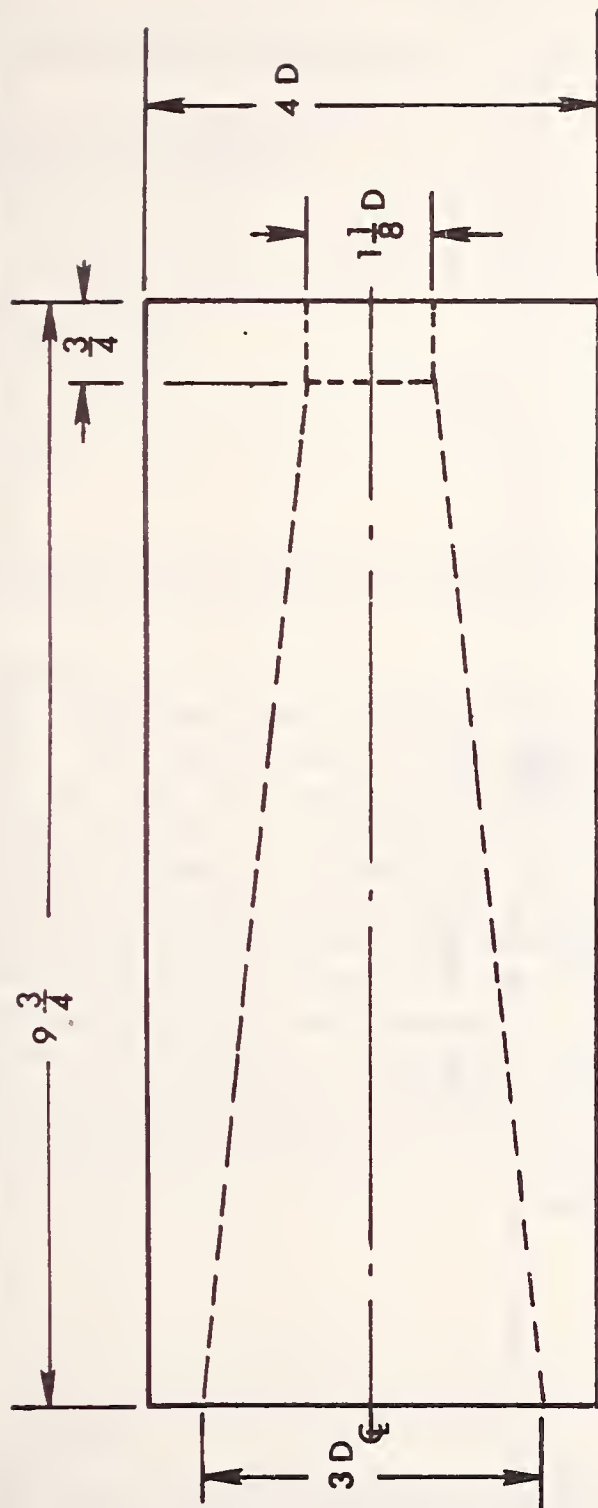
Figure 26. H3M end fitting for 0.79-in (20-mm) diameter rods. Fitting is rotationally symmetric about longitudinal center line. All dimensions in inches (1 in = 25.4 mm).
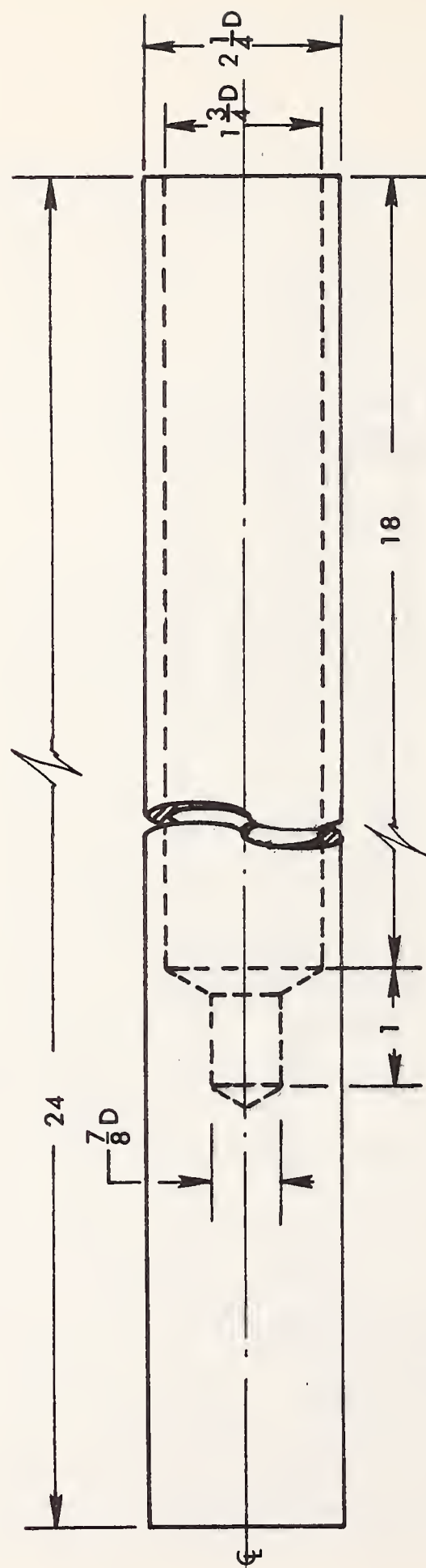
Figure 27. Mod 4 end fitting for 0.79-in (20-mm) diameter rods. Fitting is rotationally symmetric about longitudinal center line. All dimensions in inches (1 in = 25.4 mm).

U.S. DEPT. OF COMM. BIBLIOGRAPHIC DATA SHEET	1. PUBLICATION OR REPORT NO. NBSIR 76-1136	2. Gov't Accession No.	3. Recipient's Accession No.

4. TITLE AND SUBTITLE	5. Publication Date July 1976
Failure Analysis of Fiberglass Insulator Rods	6. Performing Organization Code

7. AUTHOR(S) Leonard Mordfin and Nixon Halsey	8. Performing Organ. Report No. NBSIR 76-1136
9. PERFORMING ORGANIZATION NAME AND ADDRESS	10. Project/Task/Work Unit No. 2130445
NATIONAL BUREAU OF STANDARDS DEPARTMENT OF COMMERCE WASHINGTON, D.C. 20234	11. Contract/Grant No. MIPR Z-70099-5-51020

12. Sponsoring Organization Name and Complete Address (Street, City, State, ZIP)	13. Type of Report & Period Covered Final
U. S. Coast Guard Headquarters 400 Seventh Street, S.W. Washington, D. C. 20590	14. Sponsoring Agency Code

15. SUPPLEMENTARY NOTES

16. ABSTRACT (A 200-word or less factual summary of most significant information. If document includes a significant bibliography or literature survey, mention it here.)

Failure analyses were carried out on a group of coated fiberglass-reinforced-plastic insulator rods that had sustained burn damage and loss of coating in service on a radar tower. The investigation included chemical, flammability, electrical and mechanical tests as well as a variety of measurements and inspections. The burn damage, consisting chiefly of carbonaceous tracking and charring, was attributed primarily to the occurrence of electrical discharges, from the energized end fittings to the rods, under conditions in which the electrical leakage path resistances had been reduced by moisture from rain, fog and ocean spray. The effects of this damage on the structural integrity of the rods were evaluated. Recommendations were made for reducing the incidence of such damage in the future, based on the use of skirted insulator rods or more effective coating materials. The principal cause of the coating loss was not positively identified. This form of damage was not found to have serious consequences except as a secondary factor which may have contributed to the occurrence of some partial electrical discharges.

17. KEY WORDS (six to twelve entries; alphabetical order; capitalize only the first letter of the first key word unless a proper name; separated by semicolons)

Breakdown, electrical; failure analysis; fiberglass-reinforced plastics; flammability; guy insulators; high-voltage tests; insulators, tower guy; Loran C; pultruded rods; rods, insulator.

18. AVAILABILITY [X] Unlimited	19. SECURITY CLASS (THIS REPORT)	21. NO. OF PAGES
☐ For Official Distribution. Do Not Release to NTIS	UNCLASSIFIED	57
☐ Order From Sup. of Doc., U.S. Government Printing Office Washington, D.C. 20402, SD Cat. No. C13	20. SECURITY CLASS (THIS PAGE)	22. Price
[X] Order From National Technical Information Service (NTIS) Springfield, Virginia 22151	UNCLASSIFIED	$4.50

NBSIR 76-1137

Thermal Data Requirements and Performance Evaluation Procedures for the National Solar Heating and Cooling Demonstration Program

E. Streed
M. McCabe
D. Waksman
J. Hebrank
T. Richtmyer

Office of Housing and Building Technology
 and Thermal Engineering Section
Center for Building Technology
Institute for Applied Technology
National Bureau of Standards
Washington, D.C. 20234

August 1976

NBSIR 76-1137

THERMAL DATA REQUIREMENTS AND PERFORMANCE EVALUATION PROCEDURES FOR THE NATIONAL SOLAR HEATING AND COOLING DEMONSTRATION PROGRAM

Office of Housing and Building Technology
 and Thermal Engineering Section
Center for Building Technology
Institute for Applied Technology
National Bureau of Standards
Washington, D.C. 20234

August 1976

PREFACE

The overall goal of the National Solar Heating and Cooling Demonstration Program is "to stimulate industrial and commercial capability, including that of small businesses, to produce and distribute solar heating and cooling systems, and through widespread applications, reduce the demand on present fuel supplies." To help achieve this goal, the Demonstration Act further provides that solar heating and combined heating and cooling systems will be installed in a substantial number of buildings in the climatic regions existing in the different United States geographic areas. Evaluation of the performance and reliability of the current technology can be expedited by testing under carefully controlled conditions and by demonstration in the field.

The purpose of this document is to provide the rationale and description of the data requirements, instrumentation types and data analysis methods used to monitor and evaluate the field demonstration systems. It is recognized that complete instrumentation and subsequent technical evaluation of each system/building/climate combination cannot be performed because of the cost and data analysis limitations. Therefore, only selected unique installations will be completely instrumented and as the exact design and location of all sites becomes available, optional measurements will be made to evaluate significant features.

The report has been prepared at the National Bureau of Standards under the general guidance and review of the Solar Heating and Cooling Performance Evaluation Committee, Mr. H. J. Hale, Solar Division, Energy Research and Development Administration (ERDA), Chairman. Members of the committee include:

M. McCabe	National Bureau of Standards (NBS)
W. Christensen	Department of Defense
W. Freeborne	Department of Housing and Urban Development
A. Kromis	NASA - Marshall Space Flight Center (MSFC)
W. Littles	NASA - MSFC
F. Morse	ERDA
E. Streed (Secretary)	NBS

Specific acknowledgments are extended to Dr. Dan Ward, Colorado State University, for providing operational data and technical inputs and to David E. Galehouse, Consulting Engineer, for sensitivity and error analysis calculations. The consultation and technical reviews of Dr. J. Wayne Littles, NASA-MSFC, Dr. Mike Nash and Mr. John Bartlett, International Business Machines, and Dr. James E. Hill, NBS, have contributed significantly to this document. Thanks are also expressed to Mr. Frank Bridgers, Dr. Jack Duffie, Dr. Gerald Lowery, Prof. John Yellott, and Dr. George O. G. Löf for general review and comments regarding organization, completeness, and terminology. The encouragement and support of Mr. Jack Hale, ERDA, and Mr. Robert Dikkers, NBS/CBT, Solar Program Manager, to prepare the document in final form, is gratefully appreciated.

i

This report was prepared as a reference document to prescribe a standard list of thermal performance factors and data analysis methods that can be used to evaluate solar heating and cooling systems for the National Demonstration Program. In describing these factors and the associated measurements, specific solar energy system designs have been identified and their features characterized to illustrate the type and location of sensors. Inclusion of a particular design in this report in no case implies a recommendation or endorsement by the Federal government, and the presentation should not be construed as a certification that any component, subsystem, or system is preferred at the current state of technology development. Similarly, the omission of a component, subsystem, or system does not imply that the capabilities are less than those that are included. The designs presented were obtained primarily from the open literature and are intended to be used for illustration purposes only.

The thermal performance data obtained from the Demonstration Program are intended to serve a variety of users including architects, engineers, manufacturers, developers and homeowners, code officials, standards writing organizations, and government planners for energy conservation, economic and building technology applications. An attempt has been made to identify and determine the many factors needed to satisfy the interest and needs of these diversified disciplines. However, recognizing that requirements or technology will change during the course of a five-year program, the evaluation factors and measurements can be modified.

Comments and suggestions are welcome and should be sent to:

> Manager, Solar Energy Program
> National Bureau of Standards
> Building 225, Room A-114
> Washington, D.C. 20234

NOMENCLATURE

A_c	Collector gross area
C_p	Specific heat
COP	Coefficient of Performance
F_R	Collector panel heat removal factor
h_{FG}	Latent heat of vaporization
K	Sampling interval factor
I_T	Total incident solar radiation in plane of array
M	Mass
$\dot{M}$	Mass flow rate
N	Performance index, number of samples
Q	Cummulative thermal energy
Q_u	Rate of useful energy extraction from collector
T	Temperature
TI or τ	Time
UA	Overall heat transfer coefficient
U_L	Collector heat loss coefficient

GREEK LETTERS

$\propto$	Collector panel solar absorptance
$(\propto\tau)_e$	Effective product of solar absorptance and transmittance of cover and absorber panel
Δ	Difference
η	Efficiency
σ	Sensor or measurement uncertainty, standard deviation
τ_1	Integration time 1, etc.
τ	Collector cover transmittance at air mass 2 or time

SUBSCRIPTS

a	Air, ambient
f	Mass flow
f,i	Fluid inlet
I	Insolation
in	Inlet
out	Exit
ΔT, TD	Temperature difference
S	Sampling rate
W	Water, Flow

SI CONVERSION UNITS

In view of the present accepted practice in this country for building technology, common U.S. units of measurement have been used throughout this document. In recognition of the position of the United States as a signatory to the General Conference of Weights and Measures, which gave official status to the metric SI system of units in 1960, assistance is given to the reader interested in making use of the coherent system of SI units by giving conversion factors applicable to U.S. units used in this document.

Length
1 in = 0.0254 meter (exactly)
1 ft = 0.3048 meter (exactly)

Area
$1 \text{ in}^2 = 6.45 \times 10^{-4} \text{ meter}^2$
$1 \text{ ft}^2 = 0.09290 \text{ meter}^2$

Volume
$1 \text{ in}^3 = 1.639 \times 10^{-5} \text{ meter}^3$
$1 \text{ gal (U.S. liquid)} = 3.785 \times 10^{-3} \text{ meter}^3$

Mass
$1 \text{ ounce-mass (avoirdupois)} = 2.834 \times 10^{-2} \text{ kilogram}$
1 pound-mass (avoirdupois) = 0.4536 kilogram

Pressure or Stress (Force/Area)
$1 \text{ inch of mercury (60°F)} = 3.377 \times 10^{3} \text{ pascal}$
$1 \text{ pound-force/inch (psi)} = 6.895 \times 10^{3} \text{ pascal}$

Energy
1 foot-pound-force (ft-lbf) = 1.356 joule
$1 \text{ Btü (International Table)} = 1.055 \times 10^{3} \text{ joule}$

Power
$1 \text{ watt} = 1 \times 10^{7} \text{ erg/second}$
1 btu/hr = 0.2929 watt

Temperature
$t_{°C} = 5/9 \ (t_{°F} - 32)$

Heat
$1 \text{ Btu-in/h-ft}^2\text{-°F} = 1.442 \times 10^{-1} \text{ W/m-K}$ (thermal conductivity)
$1 \text{ Btu/lbm} - °F = 4.184 \times 10^{3} \text{ J/kg-K}$ (heat capacity)
$1 \text{ langley} = 4.184 \times 10^{4} \text{ J/m}^2 = 1 \text{ cal/cm}^2 = 3.69 \text{ Btu/ft}^2$

TABLE OF CONTENTS

TABLES AND FIGURES

DATA REQUIREMENTS AND THERMAL PERFORMANCE EVALUATION PROCEDURES FOR THE
NATIONAL SOLAR HEATING AND COOLING DEMONSTRATION PROGRAM

1.0   INTRODUCTION

A major objective of the Solar Heating and Cooling Demonstration Program, described
in ERDA-23A [1], is to provide data on the technical performance of solar heating
and cooling systems.* This data, following its collection, analysis, and evaluation
will be used to provide the information and data base needed to evaluate subsystem
and system performance, to develop definitive performance criteria and to formulate
analytical models for use as design guidelines for solar heating and cooling systems.
This report is intended to provide a description and rationale for the instrumentation
selection and resultant data required to monitor and evaluate the thermal effective-
ness and reliability of solar heating, cooling and hot water systems in meeting
building thermal loads and in conserving conventional fuels or energy.

A basic assumption utilized in the preparation of this report concerns the purpose
of the data to be acquired by the described instrumentation. Because of the demon-
stration nature of the program, the data acquired must be sufficient to allow for
the evaluation of the thermal effectiveness of the solar components and system, but
is not intended to be utilized directly in the development of specific components.

Because nationally accepted test procedures for building heating and cooling systems
do not exist at the present time and because of the relatively large number of combina-
tions possible for solar and conventional HVAC systems, the data requirements,
measurement procedures and equations used to determine the performance factors
dicussed in this report will require modifications dictated by the characteristics
of the specific system being evaluated.

The approach and methodology employed to obtain, evaluate and compare thermal
performance data is shown in Figure 1. Measurements from the on-site sensors are
used to determine the solar system energy contribution, the auxiliary energy require-
ments, the building heating or cooling load, the climatic conditions and the comfort
level maintained by the system. Selected buildings and certain type solar systems will
be analytically modeled to predict system performance and building thermal response
as a function of the measured climatic conditions. The resulting predictions will
then be compared with the experimental data and the analytical modeling procedures
validated. Validated analytical models will be used to predict performance on
similar solar system/building types having either reduced levels of instrumentation
or none at all.

---

*Solar heating and cooling systems are referred to as Solar Energy Systems in this
report.
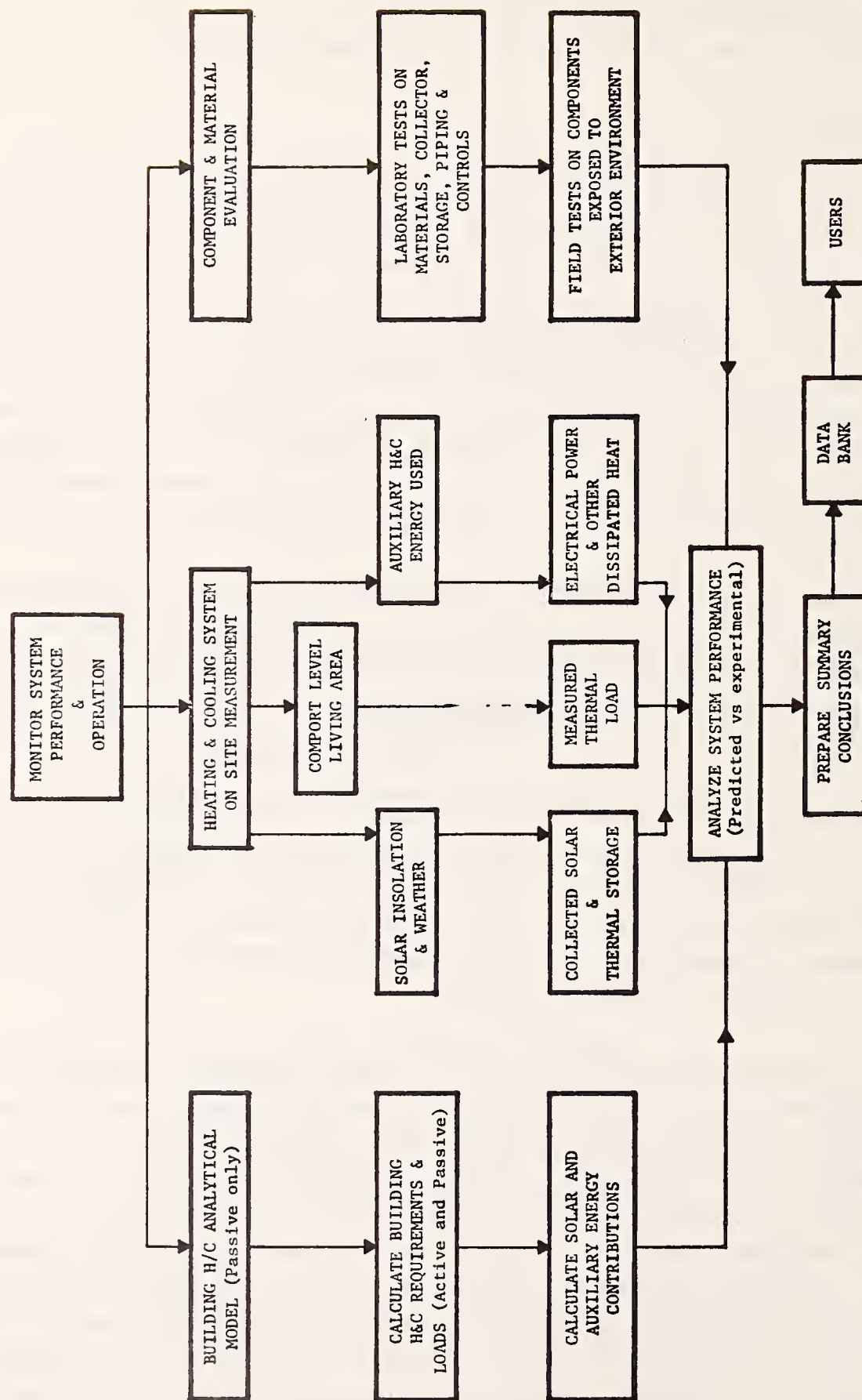
Figure 1 Flow Chart of Elements Comprising Monitoring of System Performance and Operation

Additional laboratory or field test data on critical components as a function of time and operating conditions should also be made to the extent necessary to characterize their performance and resolve differences between predicted and measured system performance.

2.0   PROGRAM OBJECTIVES

Technical performance evaluation of each solar energy system/building/climatic region demonstration will be based upon the following factors:

1. Determining the savings in fossil fuel and electrical energy resulting from the use of solar energy for space heating, space cooling and/or hot water.*

2. Determining the total heating, cooling and/or HW thermal energy loads and the fraction of each load supplied by solar energy for monthly, seasonal and/or annual periods.

3. Measuring the solar energy system efficiency for converting solar radiation into useful thermal energy for monthly and seasonal or annual periods.

4. Measuring the thermal performance of major subsystems or components and the thermal interactions between collector array, storage and energy conversion equipment

5. Measuring the occupants use of the system by means of parameters such as the temperature level maintained and hot water demand.

6. Determining the major system operational characteristics and degradation over the life of the demonstration (1 to 5 years).

7. Obtaining records of the incident solar radiation and other pertinent site environmental nparameters that could affect the performance of the system over the life of the demonstration.

---

* The term hot water (HW) as used in this report includes both residential domestic hot water (DHW) and commercial service hot water (SHW). The commercial service hot water may either be potable or nonpotable depending on its intended use.

3.0   PERFORMANCE EVALUATION PROCEDURE

Performance factors and associated data requirements have been classified into
three categories. Category one (primary) items are required for a data summary
that is considered essential to adequately measure the solar energy system or sub-
system thermal effectiveness and determine the energy saved by the solar energy
system in comparison with the energy that would have been used by a conventional
hot water, space heating, or space cooling systems. Without this data, comparative
evaluations of different solar energy subsystems and systems would be incomplete
or impossible. These primary performance evaluation factors are shown in Table 1
and described in detail in Section 6.0.

Category two (secondary) requirements are for data deemed important and useful in
evaluating different subsystems or components. Such data make it easier to
understand the component interactions that occur in system operation and serve
as an aid in comparative analysis or simulation but are not essential. In general
second category data can be determined by appropriate calculations or approxi-
mations using category one measurements however in some cases the data can only be
direct measurements.

An example of a secondary performance factor is the storage efficiency. The
average storage medium temperature is the significant parameter in determining the
amount of stored energy available. The change of storage medium temperature during
a time period with no addition or withdrawal of energy can provide a measure of the
storage efficiency. The storage medium temperature is thus very useful but is not
unique to the system thermal evaluation.

Category three data are obtained from special measurements which are not particularly
essential for current analysis needs, but which serve to define system operational
conditions. Wind direction and velocity are examples of such measurements.
The building load, particularly infiltration, and collector losses are related to
wind effects. However, most analyses to data have not incorporated corrections
or used detailed calculations to correlate performance with wind data.

3.1   Standard Designations for Sensors and Subsystems

In order to standardize the performance calculations and identify sensors
according to type and location, an alpha-numeric name is provided for each per-
formance factor and sensor. A five character name is used consisting of one or
two letters which designate either the sensor type or the measured or calculated
quantity and a three digit number which identifies the subsystem or data group as
follows:

4

Letter Designations

C = Specific Heat

D = Direction or Position

EE = Electric Energy
EP = Electric Power

F = Fuel Flow Rate

I = Incident Solar Flux (Insolation)

N = Performance Parameter

P = Pressure

PD = Differential Pressure

Q = Thermal Energy

T = Temperature

TD = Differential Temperature

V = Velocity

W = Heat Transport Medium Mass Flow Rate

TI = Time

Subsystem Designations

Number Sequence	Subsystem/Data Group
001 to 099	Climatological
100 to 199	Collector and Heat Transport
200 to 299	Thermal Storage
300 to 399	Hot Water
400 to 499	Space Heating
500 to 599	Space Cooling
600 to 699	Building/Load

Thus the sensor designation T101 defines an absolute temperature measurement in the collector subsystem and the variable name Q600 defines a heat flow measurement or calculation for a building load grouping.

3.2   General Solar System Description and Energy Balance

Prior to discussing the performance evaluation and measurement requirements of solar energy systems, it is useful to describe in general terms the equipment and subsystems that comprise a solar energy system and to describe the flow of thermal energy from the solar equipment, through the energy conversion and distribution equipment to the building. As shown in Figure 2, the basic elements of a solar hot water, space heating and space cooling system include a solar energy collection and storage subsystem (ECSS), an energy conversion and distribution subsystem (ECDS) and the building.

5

SUBSYSTEM	VARIABLE	DESCRIPTION	DEFINING EQUATION FOR ACTIVE SYSTEM
CLIMATIC	Q001	TOTAL SOLAR INCIDENT	$\int I001 d\tau$
	N113	AVG. AMBIENT DB TEMPERATURE	$(1/TI)\int T001 d\tau$
ENERGY COLLECT. AND STORAGE (ECSS)	Q100	SOLAR ENERGY COLLECTED	$(1/Ac)\int W100 \cdot C100 \cdot TD100 d\tau$
	Q203	TOTAL SOLAR ENERGY UTILIZED	$Q300+Q400+Q500$ or $\int W400 \cdot C400 \cdot TD401 d\tau$
	N111	ECSS CONVERSION EFFICIENCY	$\int Q203 d\tau / Ac \cdot \int Q001 d\tau$
HOT WATER (HWS)	Q302	HOT WATER LOAD	$\int W301 \cdot C301 \cdot (TD301+TD302) d\tau$
	N300	SOLAR FRACTION OF HW LOAD	$(1/TI) \cdot [TD301/(TD301+TD302) d\tau$
	Q311	ELECTRIC ENERGY SAVED	$Q310-Q309$
	Q313	FOSSIL ENERGY SAVED	$Q312-Q306$
SPACE HEATING (SHS)	Q402	SPACE HEATING LOAD	$\int W600 \cdot C600 \cdot TD600 d\tau$
	N400	SOLAR FRACTION OF HEATING LOAD	$\int (Q405+Q406) d\tau / \int Q402 d\tau$ or $\int Q400 d\tau / \int Q402 d\tau$
	Q415	ELECTRIC ENERGY SAVED	$Q414-Q413$
	Q417	FOSSIL ENERGY SAVED	$Q416-Q410$
SPACE COOLING (SCS)	Q502	SPACE COOLING LOAD	$\int [W600 \cdot C600 \cdot TD600 + W601 \cdot h_{FG}] d\tau$
	N500	SOLAR FRACTION OF COOLING LOAD	$\int Q500 d\tau / \int Q506 d\tau$
	Q512	ELECTRIC ENERGY SAVED	$Q511-Q510$
	Q514	FOSSIL ENERGY SAVED	$Q513-Q508$
BUILDING/ SYSTEM SUMMARY	N406	AVG. BLDG. DB TEMPERATURE	$(1/TI)\int T600 d\tau$
	Q600	TOTAL AUXILIARY ENERGY	$Q301+Q401+Q501$
	Q601	TOTAL OPERATING ENERGY	$Q102+Q303+Q403+Q404+Q503$
	Q602	TOTAL ENERGY DELIVERED TO BLDG. LOAD	$Q302+Q402+Q502$
	Q603	TOTAL ENERGY CONSUMED	$Q102+Q307+Q411+Q515$
	Q604	TOTAL ELECTRIC ENERGY SAVED	$Q311+Q415+Q512$
	Q605	TOTAL FOSSIL ENERGY SAVED	$Q313+Q417+Q514$
	N601	SOLAR FRACTION OF TOTAL LOAD	$\dfrac{\int [N300;Q302+N400;Q402+N500;Q502] d\tau}{\int (Q302+Q402+Q502) d\tau}$
	N602	SYSTEM PERFORMANCE FACTOR	$\dfrac{\int Q602 d\tau}{\int [Q306+Q410+Q508+(Q601+Q305+Q409)/NELEC] d\tau}$

TABLE 1 PRIMARY PERFORMANCE EVALUATION FACTORS

6
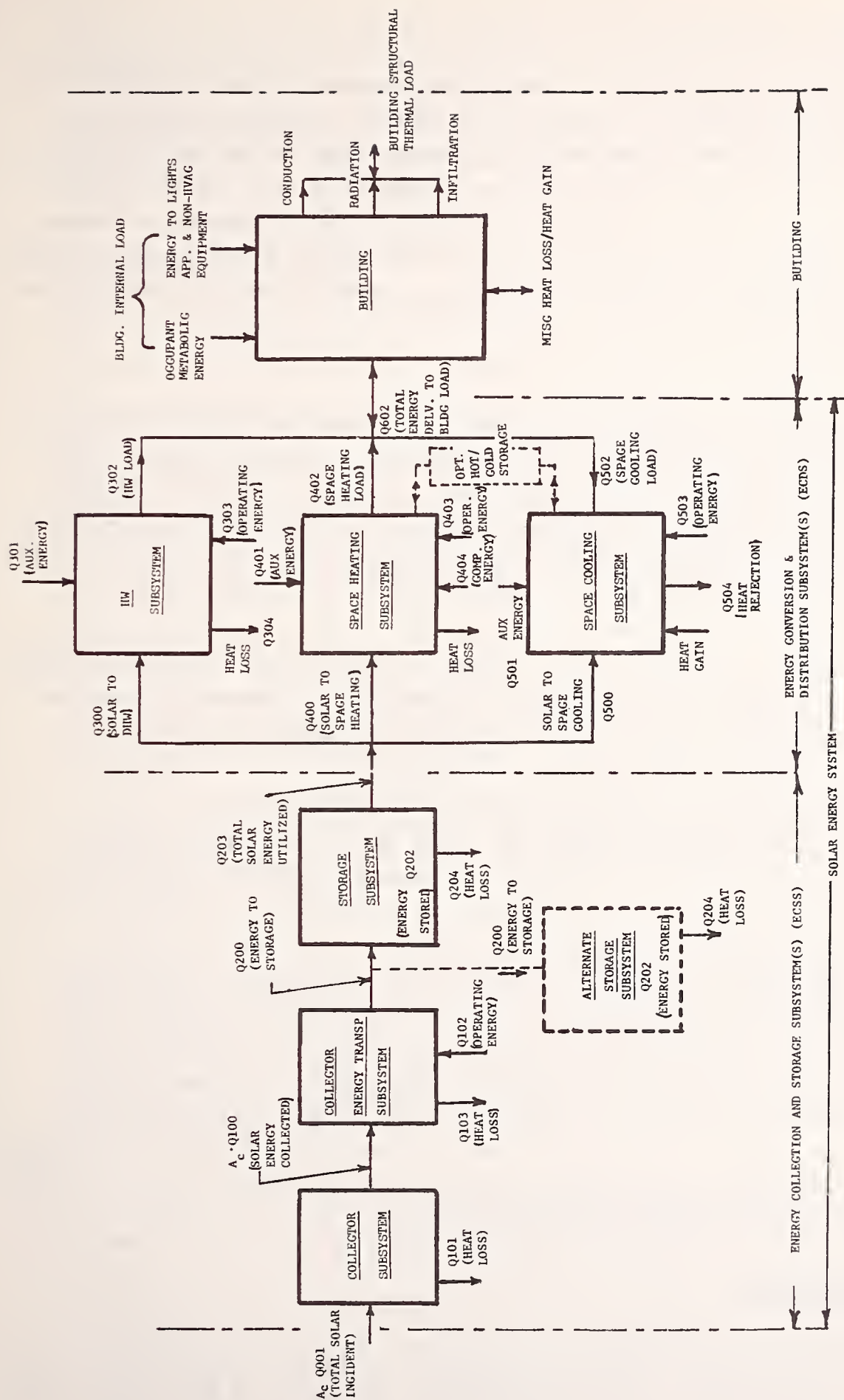
FIGURE 2 ENERGY FLOW DIAGRAM FOR A GENERAL SOLAR HEATING, COOLING HOT WATER SYSTEM

7

3.2.1 Functions

The function of the collector subsystem, collector energy transport subsystem, and storage subsystem (ECSS) is to convert the relatively variable incident solar radiation to a relatively steady source of thermal energy in the form of elevated temperature heat transport fluid or storage medium. This solar source acts as a significant thermal energy source for the building's energy conversion equipment. The major purpose of the ECSS is to reduce the consumption of non-renewable energy sources such as natural gas, oil, and electricity normally used to provide the hot water, heating, and cooling for the building.

The energy conversion and distribution subsystem is comprised of three subsystems to provide the distinct functions of HW heating, space heating and space cooling and utilizes conventional HVAC equipment such as electric or fuel fired heating furnaces, hot water heaters, heat pumps, absorption chillers and their associated pumps, fans, heat exchangers, controls, piping and ductwork. The function of this equipment is to combine the energy available from the solar subsystem with the auxiliary energy available from the conventional energy sources when the supply of solar energy is inadequate, and to convert the solar energy to a useful energy form for the building. To accomplish this conversion and distribution function, additional electrical energy is required to power the pumps, fans, and controls.

The building consists of the various structural elements in which of thermal energy between the outdoor and indoor environments occurs primarily by the process of conduction, convection, radiation, and infiltration. When the solar heat gain and the structural heat losses and gains are combined with the internal heat gains from the lights, appliances and other equipment and the metabolic heat from the occupants, and these loads are absorbed by the air in the temperature controlled spaces of the building, they comprise the building thermal load. If the HVAC equipment's rate of heat removal or addition to the building is exactly equal to the building thermal load, the air temperature is stabilized and the building is in balance. In the context of this report, hot water is also treated as a building thermal load in that the HW subsystem capability to provide the thermal energy required at the desired temperature must be balanced against the actual rate of hot water consumption.

3.2.2 Thermal Energy Flow

A primary tool which can be used in the location and choice of measurements is the concept of heat balances. For a given component, the amount of energy input must equal the energy output plus the change in stored energy within the component.

This tool can be particularly useful as a check on the installed instrumentation. By obtaining the heat balance periodically on a component or subsystem, evaluation of the losses and accuracy of the installed data instrumentation can be made. Only when the heat balance "error" is no longer within acceptable limits will selected investigation (on the particular subsystem) be required to determine the need for sensor recalibration or subsystem maintenance.

The performance evaluation factors can be defined in terms of the thermal energy quantities shown for the generalized system of Figure 2, in which an arrow leading into a box represents the net flow of a particular thermal energy quantity into a subsystem. The quantities shown represent the integrated rate of thermal energy flow over a sufficient period of time such that thermal storage in each subsystem (with the exception of the storage subsystem) is negligible. For example, in Figure 2 the quantity Q203 represents the net flow of thermal energy out of the ECSS system and into the energy conversion and distribution subsystem. The quantity Q602 represents the net flow of thermal energy between the building and the energy conversion and distribution subsystem; i.e., the total building energy load.

3.2.2.1 Subsystem Heat Loss

Examination of Figure 2 indicates a quantity called "heat loss" (or "heat gain") associated with each subsystem element. This quantity represents the difference between the total energy that originally entered the subsystem and the thermal energy delivered by the subsystem. In most cases, the subsystem heat loss represents thermal energy transferred to the subsystem environment by heat loss through the component insulation.

Depending on the physical location of the component, the subsystem environment can be outside the building either above or below ground or inside the building either in a temperature controlled or a non-controlled space. No further use is made of the heat lost by components located outside the building and above ground. However, the heat lost by components in the other locations can affect the performance of the solar energy system.

For example, with a buried non-insulated storage unit some heat lost to the environment when the storage medium temperature is relatively high may eventually be recovered when the storage medium temperature is low. In addition, for those components located within the building, some or all of the subsystem's heat loss may find its way into the temperature controlled portion of the building which is shown in Figure 2 as a miscellaneous heat loss/heat gain for the building. The entire subsystem heat loss for those components located within a temperature

controlled space will be effective in reducing the building's heat load during the heating season and in increasing the building's cooling load during the cooling season.

In the case of a subsystem having components located in a non-temperature controlled room in a building, the effects of subsystem heat loss on the solar energy system performance are difficult to assess. The heat loss from a storage unit located in an unheated basement will certainly raise the air temperature of the room, which will reduce the heat losses for the heating equipment and increase the heat gains for the cooling equipment located in that room. However, little benefit of the subsystem heat loss will be realized unless specific means are provided to utilize the heat loss to reduce the building heating requirements.

Examination of each subsystem element in Figure 2 reveals the energy quantities that must be either measured or estimated to determine the subsystem heat balance. Subsystem heat loss is probably the most difficult quantity to measure, therefore, it must be determined from the heat balance by measuring or calculating all the other quantities.

In the following description of subsystem equipment measurements and performance evaluation, the basic approach to performance measurement is to instrument all energy flow quantities except subsystem heat loss and to determine this quantity by the energy balance method. Additional instrumentation is recommended for the solar collector subsystem and storage subsystem to enable correlation of heat loss with observed temperature differentials and thus more effectively monitor these important subsystems. It is recognized that this approach to instrumentation may not always be practical, because of other constraints such as sensor cost, reliability and performance, available data channels, etc. When such reductions in measurement are considered, it will be necessary to assess the impact on over-all evaluation and accuracy of the stated objectives of performance analysis.

In the subsequent sections describing the performance evaluation of solar energy systems, the performance equations are developed on the basis that subsystem heat loss does not affect the performance of a solar energy system with respect to such primary evaluation factors as energy saved, heating and cooling load, and the solar fraction of the heating and cooling load. However, it is necessary that the heat loss for solar energy transport and storage subsystems located in temperature controlled spaces be determined. When significant losses are calculated , the pertinent equations (energy saved, heating and cooling load, and solar fraction of the heating and cooling load) must be modified to indicate heat loss effects.

10

4.0   ACTIVE SYSTEM DESCRIPTIONS AND PERFORMANCE CALCULATIONS

The following section describes the flow schematic drawings and instrumentation requirements for several typical solar energy systems, which are used for hot water, space heating and space cooling, to illustrate the methods of evaluating performance. The objectives of this section are to define the various subsystems sufficiently to enable an analyst to convert a site contractor's solar energy system mechanical drawings (showing the equipment, piping, ducting, controls etc.) into the various system, subsystems and components as shown in Figures 2, 3, 4, 5 and 6. The location and type of sensors can then be selected and the performance evaluation equations defined based on the guidelines established herein.

In order to illustrate the sensor locations and performance evaluation factors, the subsystem component configurations shown in Figures 3, 4, 5 and 6 were assumed to represent reasonable subsystems that are capable of utilizing solar energy to reduce the consumption of conventional energy. It is recognized that numerous variations on these subsystem and component configurations are possible. It is therefore re-emphasized that the schematic drawings are <u>illustrative only</u> and should <u>not</u> be interpreted as recommendations by the government as to the most efficient means to use solar energy to reduce conventional energy consumption in satisfying the hot water heating and space heating and cooling requirements of buildings.

In order to provide some flexibility in the selection of sensors, three different categories of performance evaluation have been defined; primary, secondary and special. Primary factors are deemed mandatory for each system and therefore all sensors used to calculate primary performance factors must be provided. Secondary performance factors are desireable and these data will normally be provided as a fallout of the data provided with the primary sensors, however, whenever additional non-primary sensors are required to calculate a secondary performance factor, the requirement to provide the additional sensor is optional. Special performance factors are calculated from data taken with special sensors, which are provided as determined by the needs of each particular system and site.

4.1   Energy Collection and Storage Subsystem

Figure 3 describes the flow schematics, instrumentation and performance calculations required to characterize two alternate energy collection and storage subsystems (ECSS) and to define the required sensor locations and performance evaluation factors.

Subsystem elements common to both systems include a collector subsystem, energy transport subsystem and a storage subsystem. In System A, the heat transfer medium is a liquid and the storage subsystem is in series with the collector subsystem and the energy conversion and distribution subsystem (ECDS), therefore all the

11
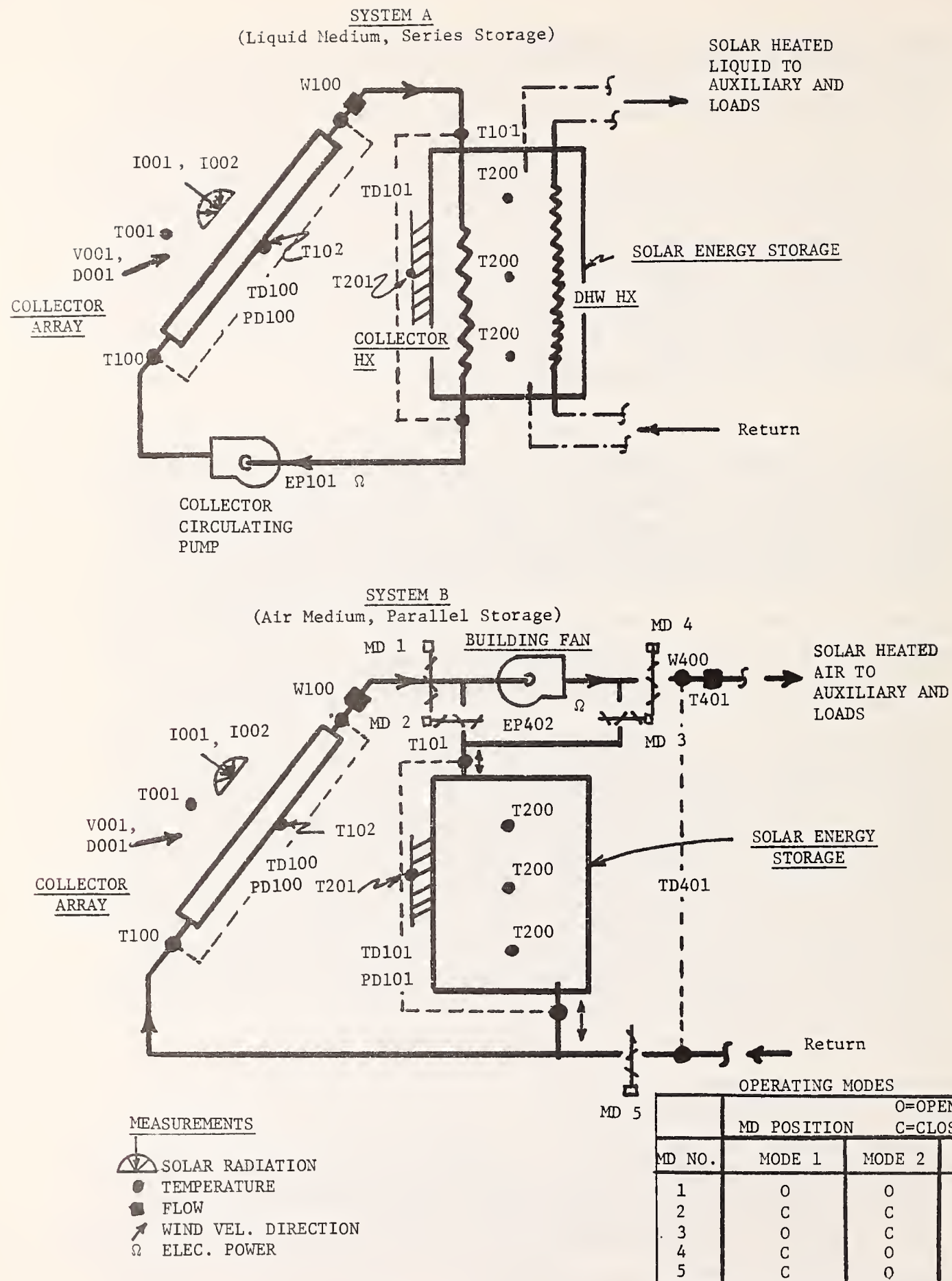
FIGURE 3   SPACE HEATING SUBSYSTEM FLOW SCHEMATICS AND SENSORS

12

CATEGORY	VARIABLE	DESCRIPTION	DEFINING EQUATION
P	Q001	Total Solar Incident	$\int I001d\tau$
SM	Q002[1]	Direct Solar Incident	$\int(I001-I002)d\tau$
P	Q100	Solar Energy Collected	$(1/Ac)\int W100 \cdot C100 \cdot TD100d\tau$
S	Q101	Collector Heat Loss	$\int[I001-(1/Ac)(W100 \cdot C100 \cdot TD100)d\tau, \ W100 \neq 0$
S	Q102	ECSS Operating Energy [2]	$\begin{cases} 3413\int EP101d\tau, & \text{SYSTEM A} \\ 3413\int\emptyset \cdot EP401d\tau, & \text{SYSTEM B} \end{cases}$
S	Q103	Collector Transp. Heat Loss [3]	$\begin{cases} A_c \cdot Q100+NPUMP \cdot Q102-Q200, & \text{SYSTEM A} \\ A_c \cdot Q100+NFAN \cdot Q102-Q200, & \text{SYSTEM B/MODE 1} \\ A_c \cdot Q100+NFAN \cdot Q102-Q203, & \text{SYSTEM B/MODE 2} \\ Q201+NFAN \cdot Q102-Q203, & \text{SYSTEM B/MODE 3} \end{cases}$
S	Q200	Energy to Storage	$\begin{cases} \int W100 \cdot C101 \cdot TD101d\tau, & \text{SYSTEM A} \\ \int W100 \cdot C101 \cdot TD101d\tau, & \text{SYSTEM B/MODE 1} \\ 0, & \text{SYSTEM B/MODES 2 \& 3} \end{cases}$
S	Q201	Energy from Storage	$\begin{cases} Q300+Q400+Q500, & \text{SYSTEM A} \\ 0, & \text{SYSTEM B/MODES 1 \& 2} \\ \int W400 \cdot C101 \cdot TD101d\tau, & \text{SYSTEM B/MODE 3} \end{cases}$
S	Q202	Hourly Increase in Stored Energy	$(MC_p)_s[T200(\tau)-T200(\tau-1)]$
P	Q203	Total Solar Energy Utilized	$\begin{cases} Q300+Q400+Q500, & \text{SYSTEM A} \\ 0, & \text{SYSTEM B/MODE 1} \\ \int W400 \cdot C401 \cdot TD401d\tau, & \text{SYSTEM B/MODES 2 \& 3} \end{cases}$
S	Q204	Storage Heat Loss	$Q200-(Q201+Q202)$
S	Q205	ECSS Total Heat Loss	$Q101+Q103+Q204$
S	N100	Daily Integrated Collector Efficiency	$\int Q100d\tau/\int Q001d\tau$
S	N101	Instant. Collector Efficiency	$W100 \cdot C100 \cdot TD100/Ac \cdot I001$, QUASI-STEADY CONDITIONS [4]
S	N102	Collector Panel Efficiency Factor	$(1/TI)\int[(T100-T001/I001]d\tau$, QUASI-STEADY CONDITIONS [4]
S	N103	Collector Panel Factor F_p $(\tau\alpha)$	COMPUTER SUBROUTINE, QUASI-STEADY CONDITONS [4]
S	N104	Collector Panel Factor $F_R U_L$	COMPUTER SUBROUTINE, QUASI-STEADY CONDITIONS [4]
S	N105	Collector Hx Effectiveness	$(1/TI\int[TD101/(T101-T200)]d\tau, \ W100 \neq 0$, SYSTEM A
S	N106	DHW Hx Effectiveness	$(1/TI)\int[TD300/(T200-T300)]d\tau, \ W300 \neq 0$, SYSTEM A
S	N107	Collector Transp. Efficiency	$(1/TI)\int[(Q100-Q103)/Q100]d\tau, \ W100 \neq 0$
S	N108	Storage Efficiency	$\int(Q201+Q202)d\tau/\int Q200d\tau$
SM	N109	Storage Heat Loss Parameter	$(1/TI)\int(T200-T201)d\tau$
S	N110	ECSS Coefficient of Performance	$\int Q203d\tau/ \ Q102d\tau$
P	N111	ECSS Conversion Efficiency	$\int Q203d\tau/Ac \cdot \int Q001d\tau$
S	N112	ECSS Utilization Efficiency	$\int Q203d\tau/Ac \cdot \int Q100d\tau$
P	N113	Avg. Ambient DB Temperature	$(1/TI)\int T001d\tau$
SM	N114	Avg. Wind Velocity	$(1/TI)\int V001d\tau$
SM	N115	Avg. Wind Direction	$(1/TI)\int D001d\tau$
SM	N116	Avg. Collector Pressure Differential	$(1/TI)\int PD100d\tau, \ W100 \neq 0$
SM	N117	Avg. Storage Pressure Differential	$(1/TI)\int PD101d\tau$, SYSTEM B/MODES 1 \& 3

(1) Provided for concentrating collectors only
(2) $\emptyset$ = Ratio of Pressure Drop in ECSS to Total Pressure Drop
(3) NPUMP, NFAN = Ratio of pump or fan shaft work to electrical energy input
(4) QUASI-STEADY Conditions occur when I001, T001, T100, W100 are essentially constant for 15 minutes.

FIGURE 3   PRIMARY AND SECONDARY PERFORMANCE FACTORS FOR SPACE HEATING SUBSYSTEMS

13

thermal energy collected is transferred through the storage tank before going to
the ECDS. In System B, the heat transport medium is air and the storage subsystem
is in parallel with the collector subsystem and the ECDS, thus permitting collected
solar energy to be transferred to either the storage subsystem or to the load.

In System A, during sunny periods the collector circulation pump circulates the
heat transport fluid through the collector array where it is heated by absorbed
solar radiation. The absorbed energy is transferred to the storage tank via the
collector heat exchanger.

In SYSTEM B a fan combined with five motorized dampers (MDS) permits operation of the
system in three different modes. In Mode 1 on a sunny day when there is no demand
for space heating, the fan circulates air between the collector and storage unit and
thereby temporarily stores thermal energy for future use. In Mode 2 when a demand
exists for space heating and there is solar radiation available, the fan circulates
air between the collector and the building load. In Mode 3 when a demand exists
for space heating and there is insufficient solar radiation available, the fan circulates
air between the storage unit and the building load and thus makes available the
previously stored thermal energy for space heating. In Modes 2 and 3, whenever
the building heating load is not satisfied by the available energy either from
the collector or from storage, a final stage of heating is provided by an auxiliary
source using conventional fossil fuel or electrical energy.

To obtain data for full evaluation of all performance factors, the sensor types and
locations shown in Figure 3 are required. These include the sensors for a local
weather station which consists of total (direct plus diffuse) solar radiation at the
solar array tilt angle and ambient dry bulb temperature. Wind velocity and
direction sensors are provided on certain selected sites as special measurements.
On solar energy systems using concentrating collectors, an additional sensor
measuring diffuse radiation is also required. The collector and heat transport
subsystems have temperature sensors at the collector array inlet, on the absorber
plate of one panel and at the collector heat exchanger inlet in addition to
differential temperature sensors across the collector array and collector heat
exchanger. The storage subsystem temperatures include the average storage
medium and exterior ambient temperatures. Storage subsystems utilizing stratifica-
tion to improve performance should measure interior temperatures at specific
locations rather than average storage medium temperature.

In SYSTEM A, a single mass flow sensor is required to determine the liquid flow rate between the collector and storage subsystems. In SYSTEM B, two mass flow sensors are required. One flow sensor measures the air flow rate through the collector and the second sensor measures the air flow rate to the load. The air flow rate to the storage system is determined by the difference in flow rate to the two sensors, assuming negligible air leakage. Operating power measurement is required for the circulating pump of SYSTEM A, or the building fan of SYSTEM B and for the operating controls of both systems. Since the building fan of SYSTEM B also provides the energy to move air through the non-solar equipment and the building, only a portion of this power is charged against the solar energy system. Pressure differential sensors are provided across the collector arrays in both systems and across the storage unit in SYSTEM B as special measurements.

Figure 3 also defines the performance calculations necessary for each type of energy system. As indicated, many of the equations are appropriate for both system types and where different equations are required, the particular system is noted. However, not all active solar system types to be considered for the demonstration program can be described by the listed equations. In that case, the equations must be rewritten as required, to define the desired performance factors for the specific systems to be evaluated. In addition to the performance calculations noted, several of the calculated quantities are considered of special significance and are categorized as primary performance evaluation factors. These variables will be discussed in greater detail in Section 6.

4.2   Hot Water Subsystem

Figure 4 shows the flow schematic, instrumentation requirements and performance calculations required for the HW subsystem. The subsystem selected for illustration consists of the HW storage tank, circulation pump, auxiliary heat exchanger, piping and controls but does not include the HW heat exchanger which is located within the solar storage tank and is therefore considered a part of the storage subsystem. (Had the HW heat exchanger been located on the outside of the solar storage tank, it would have been considered a part of the HW subsystem).

In operation, heat is transferred from the storage subsystem to the HW storage tank by circulating potable water through the HW heat exchanger which is located in the storage tank. Whenever a demand is made for hot water, solar preheated water is withdrawn from the top of the HW storage tank and replaced by cold make-up water at the bottom. If the temperature of the water leaving the HW tank is

15
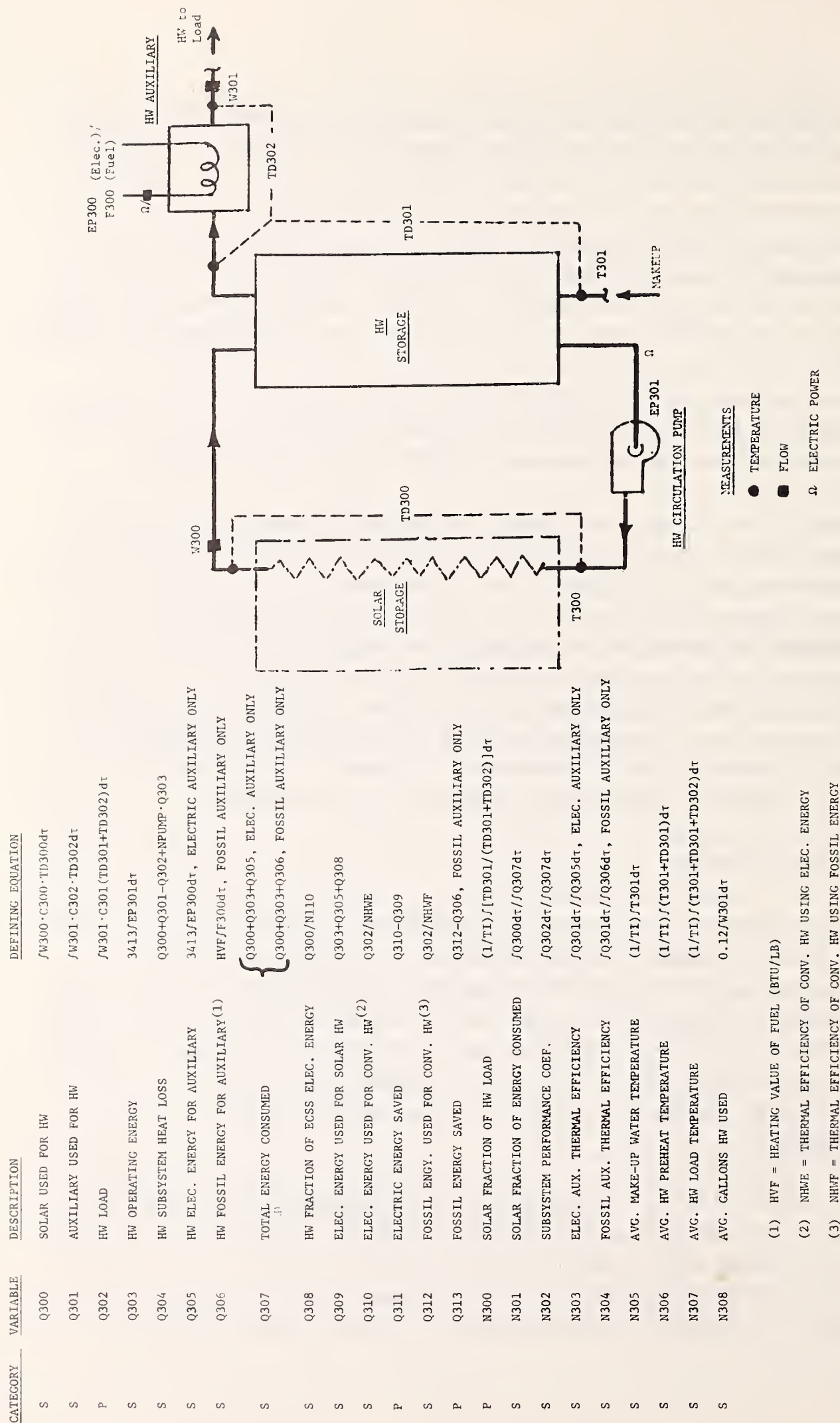
FIGURE 4   HOT WATER SUBSYSTEM FLOW SCHEMATIC, SENSORS AND PERFORMANCE CALCULATIONS

CATEGORY	VARIABLE	DESCRIPTION	DEFINING EQUATION
S	Q300	SOLAR USED FOR HW	$\int W300 \cdot C300 \cdot TD300\,d\tau$
S	Q301	AUXILIARY USED FOR HW	$\int W301 \cdot C302 \cdot TD302\,d\tau$
P	Q302	HW LOAD	$\int W301 \cdot C301(TD301+TD302)\,d\tau$
S	Q303	HW OPERATING ENERGY	$3413\int EP301\,d\tau$
S	Q304	HW SUBSYSTEM HEAT LOSS	$Q300+Q301-Q302+NPUMP \cdot Q303$
S	Q305	HW ELEC. ENERGY FOR AUXILIARY	$3413\int EP300\,d\tau$, ELECTRIC AUXILIARY ONLY
S	Q306	HW FOSSIL ENERGY FOR AUXILIARY(1)	$HVF\int F300\,d\tau$, FOSSIL AUXILIARY ONLY
S	Q307	TOTAL ENERGY CONSUMED	$\begin{cases} Q300+Q303+Q305, \text{ ELEC. AUXILIARY ONLY} \\ Q300+Q303+Q306, \text{ FOSSIL AUXILIARY ONLY} \end{cases}$
S	Q308	HW FRACTION OF ECSS ELEC. ENERGY	$Q300/N110$
S	Q309	ELEC. ENERGY USED FOR SOLAR HW	$Q303+Q305+Q308$
S	Q310	ELEC. ENERGY USED FOR CONV. HW(2)	$Q302/NHWE$
P	Q311	ELECTRIC ENERGY SAVED	$Q310-Q309$
S	Q312	FOSSIL ENGY. USED FOR CONV. HW(3)	$Q302/NHWF$
P	Q313	FOSSIL ENERGY SAVED	$Q312-Q306$, FOSSIL AUXILIARY ONLY
P	N300	SOLAR FRACTION OF HW LOAD	$(1/TI)\int[TD301/(TD301+TD302)]\,d\tau$
P	N301	SOLAR FRACTION OF ENERGY CONSUMED	$\int Q300\,d\tau//Q307\,d\tau$
S	N302	SUBSYSTEM PERFORMANCE COEF.	$\int Q302\,d\tau//Q307\,d\tau$
S	N303	ELEC. AUX. THERMAL EFFICIENCY	$\int Q301\,d\tau//Q305\,d\tau$, ELEC. AUXILIARY ONLY
S	N304	FOSSIL AUX. THERMAL EFFICIENCY	$\int Q301\,d\tau//Q306\,d\tau$, FOSSIL AUXILIARY ONLY
S	N305	AVG. MAKE-UP WATER TEMPERATURE	$(1/TI)\int T301\,d\tau$
S	N306	AVG. HW PREHEAT TEMPERATURE	$(1/TI)\int(T301+TD301)\,d\tau$
S	N307	AVG. HW LOAD TEMPERATURE	$(1/TI)\int(T301+TD301+TD302)\,d\tau$
S	N308	AVG. GALLONS HW USED	$0.12/W301\,d\tau$

(1)   HVF = HEATING VALUE OF FUEL (BTU/LB)

(2)   NHWE = THERMAL EFFICIENCY OF CONV. HW USING ELEC. ENERGY

(3)   NHWF = THERMAL EFFICIENCY OF CONV. HW USING FOSSIL ENERGY

insufficient, auxiliary energy is added either electrically or by combustion
of fuel to provide the desired HW temperature.

Temperature sensors are located at the HW heat exchanger inlet and at the
makeup to the HW storage tank and across the auxiliary heating unit.

Liquid flow measurements are required for the HW circulation loop and for
the HW flow to the load. Operating power measurements include electrical
energy consumed by the pump and controls. Electrical power or fuel flow rate
must be measured depending on the auxiliary energy source.

Figure 4 also lists the performance calculations required for the HW sub-
system. A further discussion of the primary performance factors is given in
Section 6.

4.3   Space Heating Subsystem

Figure 5 shows the flow schematic, instrumentation requirements and performance
calculations for two alternate space heating subsystems using a liquid
heat transport medium. In SYSTEM A, an all-electric heating system,
a liquid-to-air heat exchanger is located in the air duct as the primary
solar heating component, a liquid-to-air heat pump is the secondary
solar-heating component and an electric resistance heating coil is the
backup auxiliary component which is used when the solar energy storage is
depleted. In SYSTEM B, an all fossil fuel heating system, solar heated
liquid is passed through a liquid-to-air heat exchanger located in a con-
ventional fan-coil heating unit. Auxiliary energy is provided in the heat
transport loop by a conventional gas or oil fired furnace to supplement
the solar energy source during peak demand periods or when insufficient
solar energy is available. In both systems the building supply
air is heated as it flows across the various heat exchangers located in
the air duct and this increase in sensible energy represents the amount
of heat provided to the space heating load.

In SYSTEM A, four distinct modes of operation are considered, which are
numbered in order of increasing electrical energy consumption and therefore
decreasing preference. In Mode 1, when the temperature of the storage
medium is sufficiently high to carry the building heating load, the two-way

17
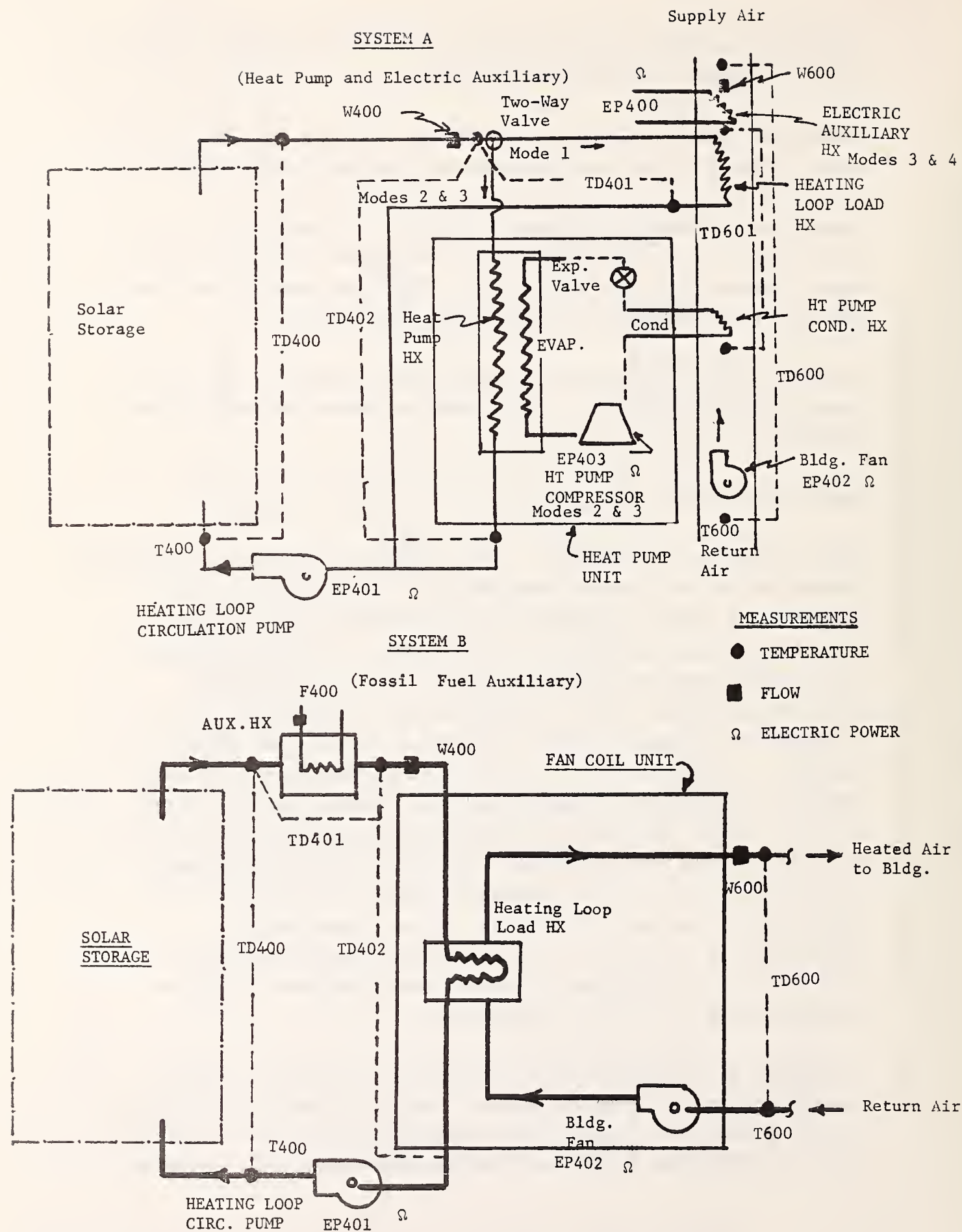
FIGURE 5   SPACE HEATING SUBSYSTEM FLOW SCHEMATICS AND SENSORS

18

CATEGORY	VARIABLE	DESCRIPTION	DEFINING EQUATION
S	Q400	Solar Used for Space Heating	$\int W400 \cdot C400 \cdot TD400 d\tau$
S	Q401	Auxiliary for Space Heating	$\begin{cases} \int W600 \cdot C602(TD600-TD601)d\tau, & \text{SYSTEM A/MODES 3 \& 4} \\ \int W400 \cdot C401 \cdot TD401 d\tau, & \text{SYSTEM B} \end{cases}$
P	Q402	Space Heating Load	$\int W600 \cdot C600 \cdot TD600 d\tau$
S	Q403	Operating Energy	$3413 \int (EP401+EP402)d\tau$
S	Q404	Heat Pump Compressor Energy	$3413 \int EP403 d\tau$, SYSTEM A/MODES 2 & 3
S	Q405	Solar to Heat Pump	$\int W400 \cdot C400 \cdot TD402 d\tau$, SYSTEM A/MODES 2 & 3
S	Q406	Solar to Building Air	$\int W400 \cdot C401 \cdot TD401 d\tau$, SYSTEM A/MODE 1
S	Q407	Heat Pump Load	$\int W600 \cdot C601 \cdot TD601 d\tau$, SYSTEM A/MODES 2 & 3
S	Q408	Heating Loop Load	$\int W400 \cdot C402 \cdot TD402 d\tau$, SYSTEM B
S	Q409	Electric Energy for Aux.	$3413 \int EP400 d\tau$, SYSTEM A/MODES 3 & 4
S	Q410	Fossil Energy For Aux.[1]	$HVF \int F400 d\tau$, SYSTEM B
S	Q411	Total Energy Consumed	$\begin{cases} Q400+Q403 & \text{, SYSTEM A/MODE 1} \\ Q400+Q403+Q404 & \text{, SYSTEM A/MODE 2} \\ Q400+Q403+Q404+Q409 & \text{, SYSTEM A/MODE 3} \\ Q403+Q409 & \text{, SYSTEM A/MODE 4} \\ Q400+Q403+Q410 & \text{, SYSTEM B} \end{cases}$
S	Q412	SHS Fraction of ECSS Elec. Energy	Q400/N110
S	Q413	Elec. Engy. for Solar Space Htg.	$\begin{cases} Q403+Q412 & \text{, SYSTEM A/MODE 1} \\ Q403+Q404+Q412 & \text{, SYSTEM A/MODE 2} \\ Q403+Q404+Q409+Q412 & \text{, SYSTEM A/MODE 3} \\ Q403+Q409 & \text{, SYSTEM A/MODE 4} \\ Q403+Q412 \quad , & \text{, SYSTEM B} \end{cases}$
S	Q414	Elec. Engy. for Conv. Space Htg.[2]	Q402/NHTE
P	Q415	Elec. Energy Saved	Q414-Q413
S	Q416	Fossil Engy. for Conv. Space Htg.[3]	Q402/NHTF, SYSTEM B
P	Q417	Fossil Engy. Saved	Q416-Q410, SYSTEM B
?	N400	Solar Fraction of Heating Load	$\begin{cases} \int(Q405+Q406)d\tau/\int Q402 & \text{, SYSTEM A} \\ \int Q400 d\tau/\int Q402 d\tau & \text{, SYSTEM B} \end{cases}$
S	N401	Solar Fraction of Energy Consumed	$\int Q400 d\tau/\int Q411 d\tau$
S	N402	SHS Coefficient of Performance	$\int Q402 d\tau/\int(Q403+Q404+Q409)d\tau$, SYSTEM A
S	N403	Heat Pump Coefficient of Perf.	$\int Q407 d\tau/\int(Q403+Q404)d\tau$, SYSTEM A/MODES 2 & 3
S	N404	Elec. Aux. Thermal Efficiency	$\int Q401 d\tau/\int Q409 d\tau$, SYSTEM A/MODES 3 & 4
S	N405	Fossil Aux. Thermal Efficiency	$\int Q401 d\tau/\int Q410 d\tau$, SYSTEM B
P	N406	Avg. Bldg. DB Temp.	$(1/TI)\int T600 d\tau$
S	N407	Avg. Bldg. Supply Air DB Temp.	$(1/TI)\int(T600+TD600)d\tau$

(1) HVF = Heating Value of Fuel

(2) NHTE = Thermal Efficiency of Conventional Electric Heating Unit

(3) NHTF = Thermal Efficiency of Conventional Fossil Fuel Heating Unit

FIGURE 5   PRIMARY AND SECONDARY PERFORMANCE FACTORS
FOR SPACE HEATING SUBSYSTEMS

valve directs the flow of solar heated liquid to the heating loop load heat exchanger. If the temperature of the solar heated liquid is insufficient to carry the building load, Mode 2 operation is initiated in which the two-way valve diverts the heating loop flow to the heat pump's evaporator heat exchanger and the heat pump is turned on. This mode uses solar energy indirectly in that the solar heated liquid is used to increase the heat pump's Coefficient of Performance (COP) and thus reduce the consumption of electrical energy required to carry the building heating load. In Mode 3, the heat pump's heating capacity is augmented by the electric resistance heaters in the air duct and in Mode 4 the heat pump and heating loop circulation pump are off and the entire building heating load is carried by the electric resistance heaters.

Figure 5 shows the measurements required for the space heating subsystem. Absolute temperature sensors are located at the heating loop inlet to the solar storage subsystem and at the building return air duct inlet to the heat pump or fan coil unit. Differential temperature sensors are located in the heating loop across the solar storage subsystem, across the heat pump heat exchanger in SYSTEM A and across the heating loop load heat exchanger. A differential temperature sensor is required in the building air loop to sense the dry-bulb temperature difference between the building air supply and return and in SYSTEM A to sense temperature difference across the combined heat pump condensor heat exchanger and the electric auxiliary coil. A liquid mass flow sensor is located in the heating loop and an air mass flow sensor is located in the building air flow circuit. Operating power measurements are required for the heating loop pump, building fan and controls for both systems, and for the heat pump compressor of SYSTEM A. Auxiliary energy consumption, using an electric meter for SYSTEM A and a fuel flow sensor for SYSTEM B are also required.

The performance calculations required for the space heating subsystem are also listed in Figure 5. The primary performance evaluation factors used to characterize the operation of the subsystem are further described in Section 6.

4.4   Space Cooling Subsystem

Figure 6 shows the flow schematic, instrumentation requirements and detailed performance calculations for the space cooling subsystem using a thermal energy actuated absorption chiller as the cooling component. In operation, the solar heated liquid from storage is circulated through the absorption chiller's generator by way of the auxiliary heat exchanger and this provides the required thermal energy source.

PRIORITY	VARIABLE	DESCRIPTION	DEFINING EQUATION
S	Q500	SOLAR USED FOR SPACE COOLING	$\int W400 \cdot C400 \cdot TD400\,d\tau$
S	Q501	AUXILIARY FOR SPACE COOLING	$\int W400 \cdot C401 \cdot TD401\,d\tau$
P	Q502	SPACE COOLING LOAD[1]	$\int[(W600 \cdot C600 \cdot TD600)+(W601 \cdot h_{FG})]\,d\tau$
S	Q503	TOTAL OPERATING ENERGY	$3413 \cdot (EP401+EP402+EP501)\,d\tau$
S	Q504	SCS HEAT REJECTION	$\int W501 \cdot C501 \cdot TD501\,d\tau$
S	Q505	ABS. CHILLER OPER. ENERGY	$3413\int EP501\,d\tau$
S	Q506	ABS. CHILLER THERMAL INPUT	$\int W400 \cdot C402 \cdot TD402\,d\tau$
S	Q507	ABS. CHILLER LOAD	$\int W500 \cdot C500 \cdot Td500\,d\tau$
S	Q508	FOSSIL ENERGY FOR AUXILIARY[2]	$HVF\int F500\,d\tau$
S	Q509	SP. CLG. FRACT. OF SOLAR ELEC. ENGY.	Q500/N110
S	Q510	ELEC. ENGY. FOR SOLAR SP. CLG.	Q503+Q509
S	Q511	ELEC. ENGY. FOR CONV. SP. CLG.[3]	(Q502)/NCLE
P	Q512	ELECTRIC ENERGY SAVED	Q511-Q510
S	Q513	FOSSIL ENGY. FOR CONV. SP. CLG.[4]	Q502/NCLF
P	Q514	FOSSIL ENERGY SAVED	Q513-Q508
S	Q515	TOTAL ENERGY CONSUMED	Q500+Q503+Q508
?	N500	SOLAR FRACTION OF COOLING LOAD	$\int Q500\,d\tau/\int Q506\,d\tau$
S	N501	SOLAR FRACTION OF ENERGY CONSUMED	$\int Q500\,d\tau/\int Q513\,d\tau$
S	N502	SUBSYSTEM COEF. OF PERFORMANCE	$\int Q502\,d\tau/\int Q515\,d\tau$
S	N503	ABS. CHILLER COEF. OF PERFORMANCE	$\int Q507\,d\tau/\int Q506\,d\tau$
S	N504	AUXILIARY THERMAL EFFICIENCY	$\int Q501\,d\tau/\int Q508\,d\tau$
P	N505	AVG. BUILDING DB TEMPERATURE	$(1/TI)\int T600\,d\tau$
S	N506	AVG. DB TEMPERATURE TO BUILDING	$(1/TI)\int(T600+TD600)\,d\tau$

(1) h_{FG} = LATENT HEAT OF VAPORIZATION (BTU/LB)

(2) HVF = FUEL HEATING VALUE (BTU/LB)

(3) NCLE = EFFICIENCY OF CONVENTIONAL COOLING UNIT USING ELECTIRCAL ENERGY

(4) NCLF = EFFICIENCY OF CONVENTIONAL COOLING UNIT USING THERMAL ENERGY
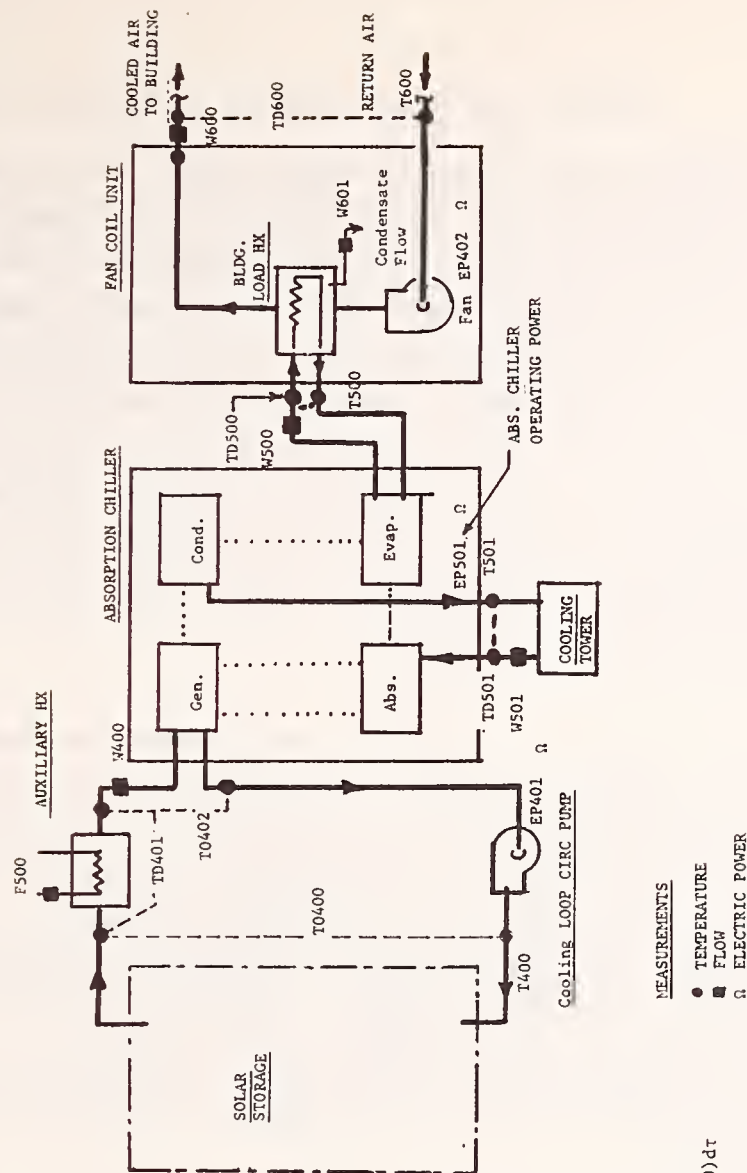
FIGURE 6 SPACE COOLING SUBSYSTEM FLOW SCHEMATIC, SENSORS AND PERFORMANCE CALCULATIONS

MEASUREMENTS
● TEMPERATURE
■ FLOW
Ω ELECTRIC POWER

The absorption chiller's useful thermal output consists of the energy indirectly removed from the building air using an intermediate heat transfer fluid (chilled water or brine) which is pumped through the evaporator. The heat rejection required by the absorption thermodynamic cycle is provided by another intermediate heat transfer fluid (water) which absorbs heat in passing through the absorber and the condensor sections and then rejects this heat to ambient air via a cooling tower. The energy removed from the building air flowing over the load heat exchanger represents the space cooling load. Since most space cooling applications include both sensible cooling and dehumidification processes, it is important to account for the removal of water vapor from the building air in determining the building's cooling load.

Figure 6 shows the measurements required to fully evaluate performance of a solar assisted space cooling subsystem. The temperature, flow and power sensors for the heating loop and fan coil unit are identical to those previously described for the system B configuration space heating subsystem. Additional temperature and flow sensors are required to measure absorption chiller heat rejection and building air dehumidification. Building air dehumidification is determined using a modified rain gauge to determine the rate of condensation at the building load heat exchanger. An additional power sensor is required to measure the operating power of the various pumps, fans and controls used in the absorption chiller.

In measuring wet-bulb temperature (or alternatively measuring relative humidity) it is recognized that the relative high expense and reduced accuracy of the commercially available sensors may not be justified, particularly for the residential portion of the demonstration program. Alternatively, the building cooling load could be defined as the energy added to the chilled water circulating between the absorption chiller and load heat exchanger at the load heat exchanger. This approach does not account for the energy gains in the fan coil unit but does eliminate the requirement for the condensate measurement. Measurement of the alternative building cooling load at the absorption chiller requires coolant mass flow and inlet temperature to the load heat exchanger and temperature difference across the load heat exchanger.

Figure 6 also lists the performance calculations required for the space cooling subsystem and the primary items which characterize the operation of the subsystem and are reported in the overall performance summary. These items are further discussed in Section 6.

22

5.0   PASSIVE SYSTEMS DESCRIPTION AND PERFORMANCE CALCULATIONS

The influence of the building envelope materials and construction, particularly
the area and location of windows, on building heating and cooling loads are
well established. The application of windows, walls, roof sections with sky
lights and roof ponds as part of the architectural design to utilize solar energy
as a significant fraction of the total load is commonly referred to as a passive
solar energy system. Additional requisites for a building design using windows
to qualify and be evaluated as an alternative energy source have been stated
in reference [2] as (1) operable insulating shutters or other devices which,
when drawn or closed, shall cause the window area to keep maximum outward heat
flows below a selected value, and (2) the window areas are shaded to otherwise
protected from the direct solar rays during the cooling season.

Generally the same functional elements such as the collector, storage and energy
conversion subsystems exist in passive systems but physical distinction between these
elements and the building elements is not always possible. Direct measurement
of the thermal energy flows will probably not be possible because of the
dependence on natural heat transport phenomena such as free convection, radiation
and evaporation. Therefore, the heat balance approach previously described for
active systems will have to be greatly modified for passive system evaluation.

In general, the only direct measurements practical will be with temperature
sensors, heat flow meters, scanning radiometers and pyranometers. The performance
evaluation will rely upon measurements of the auxiliary fuel usage and the interior
comfort level. Determination of the energy saved will be obtained from load
calculations for similar buildings without the solar energy system or, when
possible, measured energy consumption in an adjacent similar structure without
a solar energy system.

The following section describes the energy flow, instrumentation requirements
and performance evaluation for two alternate designs assumed for illustrating
the use of passive solar energy for space heating and cooling. The systems
are considered passive because no auxiliary energy is required for the transfer
of thermal energy between the collecting and storage elements and the building
load. Figure 7 illustrates conceptually the two passive solar energy systems
and indicates the required instrumentation for performance evaluation.

One design consists of a water pond with a movable insulation cover that is
thermally integrated into the building structure. The other design consists of
a wall solar collector with a movable insulating device and thermal storage

23
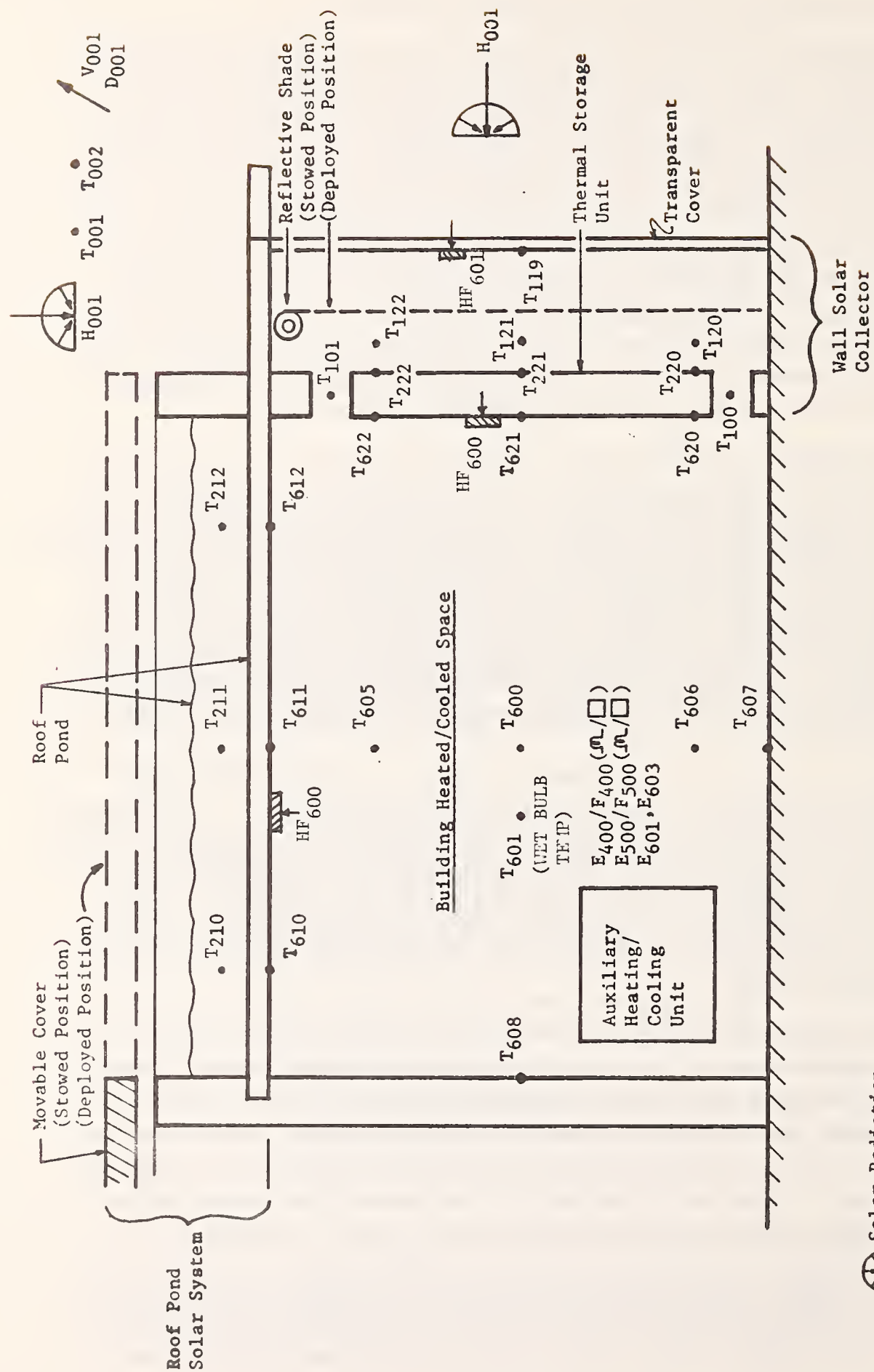
Figure 7 Passive Heating and Cooling System

that is also thermally integrated into the building structure. These two
designs are considered representative of current passive technology but many
other innovative architectural approaches have been built for private use and
their evaluation is in a relatively primitive stage. It is apparent that the
building solar heat gain, thermal resistance, thermal mass and thermal time
constant are the basic parameters governing the building thermal performance.

5.1   Roof Water Ponds

Figure 7 shows the daytime position of the movable insulating cover during the
heating season. In operation, the roof pond is uncovered during the heating
season daytime, thereby enabling solar energy to be stored by raising the internal
energy of the water in the roof pond. At night, the pond is covered to
reduce heat losses and enable the stored energy to be used for space heating by
free convection and radiation from the ceiling. During the cooling season, at
night the roof panel is uncovered and the pond rejects heat by radiation to
the night sky and by evaporation. During the daytime, the roof panel is
covered to prevent absorption of solar energy. Space cooling is provided during
the day because the cool water in the roof panel can absorb the heat that is
released in the space and transferred through the walls and fenestrations.

Roof water ponds can be evaluated in the same manner as conventional solar
collectors. In order to do this, the overall heat transfer coefficient (UA)
must be known as a function of the temperature difference between the roof
average pond water (T_w) and the average building air (T_a). This relationship
can be quantitatively established by heating the roof pond with solar energy
until a maximum temperature for the day is obtained at which time the roof
water pond is covered with the insulated panels. The rate at which the water
temperature decreases times the water mass (m) and specific heat (c_p) gives
the rate of heat transfer to the building, assuming that the heat loss through
the insulated panels is either negligible or can be calculated. Once this
quantitative relationship is established, the useful heat delivered by the water
roof pond to the building can be calculated knowing the value of the aforementioned
temperature difference.

The solar energy collected between time τ_1 and τ_2, Q100 is calculated by:

$$Q100 = m \cdot c_p [T_w(\tau_2) - T_w(\tau_1)] + \int_{\tau_1}^{\tau_2} UA(T_w - T_a) d\tau \qquad (5.1)$$

where UA is the overall heat transfer coefficient between the pond and the ceiling, and $T_W(\tau_2)-T_w(\tau_1)$ is the increase in the average pond temperature during the selected time intervals when the pond is uncovered. From a practical standpoint, daily collector efficiency is the minimum time to obtain reasonable accuracy for performance evaluation. The efficiency can be expressed by:

$$N100 = \int_{\tau_1}^{\tau_2} Q100 \, d\tau / \int_{\tau_1}^{\tau_2} Q001 \, d\tau \qquad (5.2)$$

where the energy collected and the incident solar radiation quantities are summed each day when the pond is uncovered.

The rate at which heat is removed from a building during the summer can be determined in a similar manner. Just before sunrise, the roof water pond is covered with the insulated roof panels. The rate of water temperature increase times the water mass and specific heat product gives the rate at which heat is removed from the building (if the heat transfer through the insulated roof panels is either negligible or can be calculated) as a function of the temperature difference between the water and building air.

It is imperative that the internal air temperature be carefully recorded because performance will depend significantly on the temperature excursions permitted. In addition, it is extremely important that the roof pond water depth also be carefully recorded because it will also affect performance.

The fraction of the annual heating and cooling load furnished by a roof water pond is strongly dependent on the temperature excursions permitted before auxiliary energy is used. Therefore, internal temperature is required for space heating and cooling and relative humidity measurements are needed for the evaluation of space cooling. The electrical power expended for humidity control must be measured also.

Measurements of the fossil or electrical energy used for auxiliary purposes (E400/F400 and E500/F500) are used to determine the total auxiliary energy, Q401 (heating) and Q501 (cooling). The heating or cooling load, Q402 or Q502 respectively, are obtained by adding the solar and auxiliary contributions as follows:

$$Q402 = \int_{\tau_1}^{\tau_2} [UA(T_w-T_a)d\tau + Q401 \qquad (5.3)$$

26

$$Q502 = \int_{\tau_1}^{\tau_2} [UA(T_a - T_w) d\tau + Q501 \qquad (5.4)$$

Because of the building modification to accommodate the roof pond, energy saved calculations will require analytical prediction of the building load for conventional design and construction.

5.2   Wall Collector

The operation of the wall solar collector is shown in Figure 7 during the heating season for sunny days; the insulating device is removed thereby exposing the high thermal capacity wall to solar radiation. At night, the deployed insulating device and transparent cover reduce heat losses to ambient and the heat stored in the wall during the day is transferred by convection and radiation to the space for heating. The wall collector is primarily a heating device so that the useful output during the cooling season is limited to the ventilation capability of the system. To limit solar heat gains during the cooling season, the insulating device must be deployed and the overhanging roof designed to provide shading from direct solar radiation.

For the generalized system schematic in Figure 7 the possible heat flows are the solar input, I001, heat losses from the wall (a function of the wall or window temperatures T119, ambient temperature T001, wind characteristics V001 and D001, and radiation exchange with the exterior surrounding) and the heat delivered or removed from the building heated space.

5.3   Performance Evaluation

Figure 7 shows the sensors utilized for performance evaluation of the passive type solar systems. Although temperature sensors are indicated for the energy storage elements, heat flow meters would also be appropriate. Because of the passive nature of the solar system, air flow measurements are probably impractical and energy transfer and storage must be determined from the measured temperatures and a knowledge of the thermal characteristics of the building. Thus, performance analysis of the passive solar system must rely primarily on transient thermal analysis of the integrated building and solar system, considering the outdoor climatic conditions and the energy release within the building. It should be noted that the exact number and location of the temperature/ heat flow sensors are very dependent on the design of the particular instrumentation deemed necessary for passive system evaluation.

The heat transfer calculations for room temperature predictions are similar to

the building heating/cooling load calculations performed by available computer programs. However, the temperature calculations are more complex because they require exact heat balances considering the room air, surrounding walls and infiltration of the outdoor air. Since the major variable in passive system performance is the hourly room temperature, it is necessary to account for the transient heat conduction and thermal storage of the building and internal mass.

Determination of the temperature and humidity in non-air conditioned rooms responding to randomly fluctuating outdoor climatic conditions can be determined using hourly simulations of heat gain and storage obtained with standard algorithams published by ASHRAE [3].

A computer program employing these algorithms is available [4]. The calculation sequence as depicted in Figure 8, requires detailed data input for the building, weather and operating schedule. Building data includes geometric characterization of the construction and materials used for the exterior envelope, interior partitions, ceilings and floors and their associated thermophysical properties. Weather data is provided in the form of a National Weather Service Tape or provided as measured data including wet and dry bulb temperature, wind, and solar radiation. The operating schedule is used to determine energy release profiles for the appliances and lights and metabolic heat release by the occupants.

Normal solar radiation inputs corrected for local cloud cover, collector tilt angle and shading can be calculated for conventional building construction heat gain or for solar modified construction using roof ponds and window collectors. Routines to calculate the transmission, reflection and absorption for direct and diffuse solar radiation are used to calculate the solar heat gain through fenestrations. The thermal response of the various building structural components and furnishings are calculated using conduction, radiation and convection heat transfer routines to provide the necessary inputs to the room temperature calculation (RMTMP) [4]. This subroutine compares the prescribed room temperature with the calculated temperature, and variances beyond the prescribed limits result in calculation of the heating or cooling loads to satisfy the temperature.
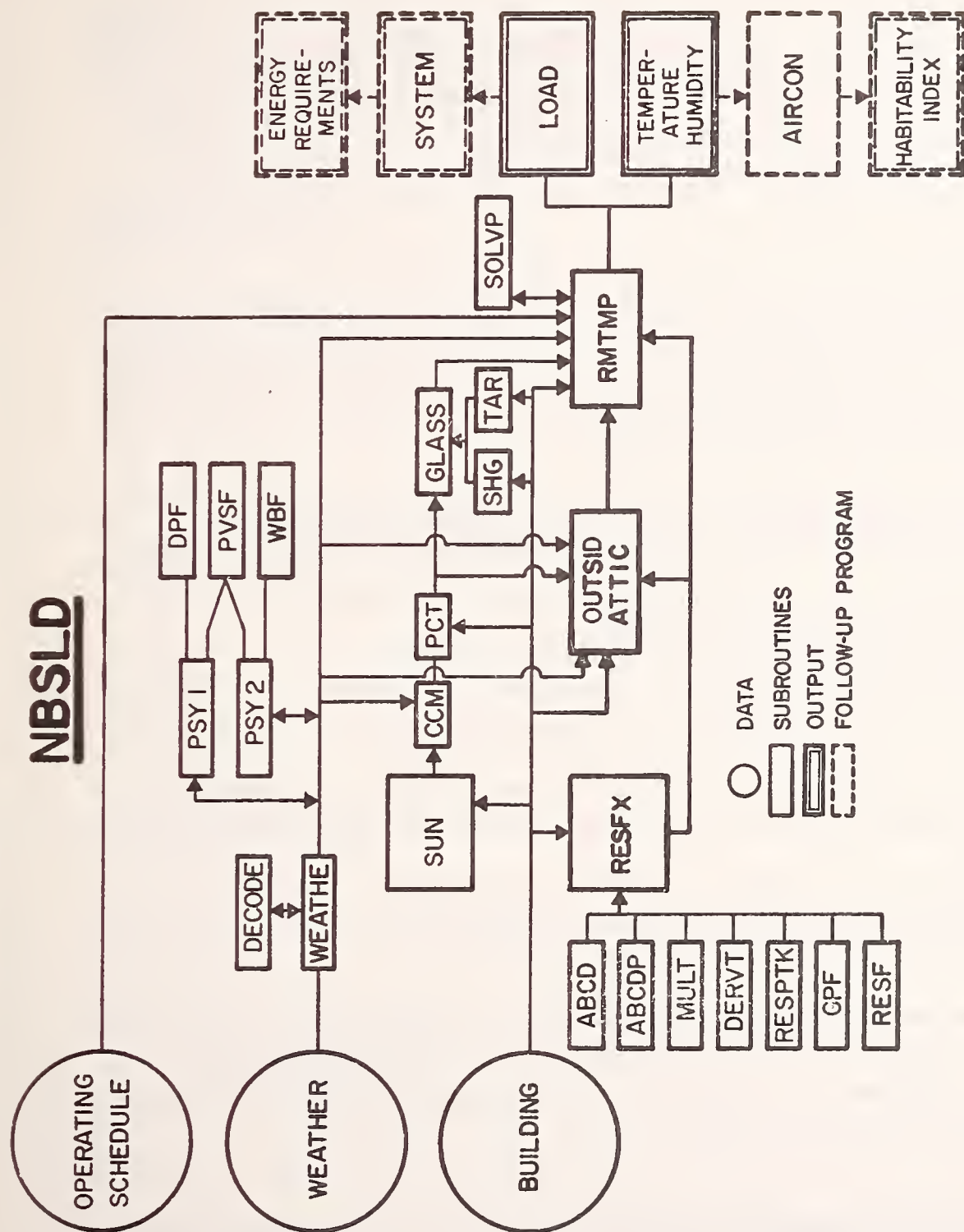
Figure 8   Calculation Sequence for Building Load Program [3]

6. SYSTEMS PERFORMANCE EVALUATION SUMMARY (ACTIVE-SYSTEMS)

As indicated in Figures 3 to 6, numerous calculations are performed for the elements comprising a system, subsystem or for the individual components in the solar assisted heating and cooling system. As previously described, performance evaluation factors are classified into three categories, primary, secondary and special. The primary performance evaluation factors are listed in Table 1 and consist of those evaluation factors that summarize the performance of each subsystem, the solar energy system, the building and climate and the utilization of the solar energy system by the occupant. The secondary performance evaluation factors include the detailed performance of the solar collectors, storage tanks, heat exchangers and other solar energy components as well as the components of the conventional HVAC equipment used such as hot water heaters, furnaces, heat pumps and other energy conversion equipment. Special evaluation factors include those calculations performed using data from certain optional sensors such as the diffuse pyranometer or the collector absorber panel temperature.

This section will describe each term of the primary system performance evaluation summary to clearly define the terminology and calculation method. In addition, some of the more important terms of the secondary and special performance calculations are described.

6.1   Performance Factors – General

Two types of performance factors are indicated in Table 1; a thermal energy quantity defined by the letter "Q", and a performance index defined by the letter "N".

6.1.1   Performance Factors Based on Thermal Energy Quantity

In the evaluation of the net thermal energy flow into or out of a subsystem, the general expression for energy addition to a fluid flowing through a sub-system or component is determined by integrating the measured instantaneous rate of heat addition as follows:

$$Q = \int_{\tau_1}^{\tau_2} \dot{m} c_p \ (T_{out} - T_{in}) d\tau \qquad\qquad (6.1)$$

where $\dot{m}$ is the fluid mass flow rate in LB/HR ,

c_p is the fluid specific heat at constant pressure in BTU/LB °F,

30

$T_{out} - T_{in}$ is the fluid temperature rise in the subsystem or component in °F and

τ_1, τ_2 are the initial and final times of the integration period.

In general, both T_{out} and T_{in} are functions of time, $\dot{m}$ is a function of both time and temperature and c_p is a function of temperature; therefore, evaluation of Equation (6.1) usually involves a numerical integration procedure in which the total time interval is broken down into subintervals that are sufficiently small so that during the subinterval each variable in the integrand can be considered constant.

Ideally continuous data measurement is desired, however, in the actual data acquisition system the sensors are scanned at periodic intervals and the instantaneous measured values are used to evaluate equation (6.1). Changes in the variables between data scans are not determined and errors are introduced into the calculated results. Section 7 describes these errors due to data sampling and presents the results of a study of sampling errors based on data from one of the solar demonstration houses at the Colorado State University [5].

In general, for all thermal energy quantities the smallest integration period desired will be one hour, with additional integration periods to provide cumulative daily, monthly, and seasonal or annual data.

6.1.2   Performance Indices

In the evaluation of a performance index which depends on the ratio of two thermal quantities such as the energy conversion efficiency, the index N is given by:

$$N = \frac{\int_{\tau_1}^{\tau_2} Q_1 \, d\tau}{\int_{\tau_1}^{\tau_2} Q_2 \, d\tau} \qquad (6.2)$$

In this equation Q_1 and Q_2 are hourly thermal energy quantities calculated by Equation (6.1). For meaningful results the integration times must be sufficiently long, not only to preclude division by zero, but to assure that a true average value is obtained. Thus, the performance index calculations involving the ratio of thermal energy quantities may require evaluation on a daily, monthly, or annual basis using hourly values of the thermal energy quantity.

31

Other performance indices such as average temperature are determined by integrating the measured temperature and dividing by the integration period as follows:

$$N = \frac{1}{TI} \int_{\tau_1}^{\tau_2} T_1 \, d\tau \qquad\qquad (6.3)$$

where T_1 is the actual temperature measurement,

τ_1 and τ_2 are the initial and final times of the integration period and $TI = \tau_2 - \tau_1$ represents the total time period over which the average temperature is evaluated.

The minimum integration period varies depending on the particular temperature. For example, outdoor dry bulb temperature would be desired for hourly, daily and monthly periods whereas storage tank ambient temperature might be evaluated on a monthly basis.

6.2   Energy Saved - General

Since the energy sources for both conventional and solar assisted heating and cooling include different energy types such as gas, oil or electrical, it is important to distinguish between at least the fossil sources and the electrical sources. It is conceivable that when a conventional system is replaced with a solar system, the solar system could require more electrical energy to run (due to operating power for the solar pumps, fans or controls) than the conventional system; however, the solar system should significantly reduce the consumption of fossil energy. Due to the difference in energy costs in various parts of the country, the same solar system and same type building in different locations may have wide variance in the cost effectiveness or payback period.

The basic approach to determining the energy saved is to first measure the total electrical energy and the total fossil fuel energy consumed by the solar assisted system to provide a given building energy load at a given occupant utilization level. An assessment of a non-solar system must then be made to determine the type of equipment that would be provided if there were no solar equipment. Since available performance data of energy conversion equipment are usually based on measurements taken at a design condition for steady state equipment operation, the effects of off-design operation and duty cycling on equipment performance must be estimated to improve the accuracy of the predicted energy consumption. Alternatively, equipment performance based on seasonal efficiency rather than design point efficiency should be used.   The electrical energy

32

and fossil energy consumption of the non-solar system must then be calculated
assuming some equipment performance coefficients and operating efficiencies
based on the same building load and occupancy utilization that was measured
for the solar system. The energy saved is then the difference between the
calculated value of energy consumed by the non-solar system and the measured
value of energy consumed by the solar system. In reporting these results,
the assumed non-solar system must be described as well as the assumed performance
characteristics and efficiencies.

6.3   Climatic Primary Performance Factors

6.3.1   Total Solar Energy Incident (Q001,Q002*)

Total incident solar radiation is measured by a sensor mounted in the plane
of the collector array on either a continuously integrated or frequently
sampled basis. Data are recorded at specified intervals for use in the cal-
culation of collector and system efficiencies. For those solar energy systems
having a significant dependence on direct solar radiation (such as concentrating
collectors), diffuse insolation will also be measured independently with a
separate sensor located in the plane of the collector array and the direct
component of incident solar radiation is determined by subtraction of diffuse
from the total incident solar radiation. The total and direct integrated
values of incident solar radiation are calculated by integrating the
instantaneous values as follows:

$$Q001 = \int_{\tau_1}^{\tau_2} I001 \, d\tau \qquad\qquad (6.4)$$

$$Q002* = \int_{\tau_1}^{\tau_2} (I001 - I002) \, d\tau \qquad\qquad (6.5)$$

Where I001 and I002 are the instantaneous values of incident total
solar radiation and diffuse solar radiation respectively, and τ_1, τ_2
are the integrating time intervals.

Q002* is not identified as a primary performance factor in Table 1
however, its importance for certain solar collectors warrants
inclusion as a special measurement for some active and passive solar
energy systems.

6.3.2 Average Ambient Dry Bulb Temperature (N113)

Average ambient dry bulb temperature is a significant parameter in determination
of system performance and comparison of alternate solar energy systems in
different climatic regions. It is obtained by integration of the instantaneous
ambient dry bulb temperatures as follows:

$$N113 = \frac{1}{TI} \int_{\tau_1}^{\tau_2} T001 \, d\tau \qquad (6.6)$$

where T001 is the instantaneous dry bulb temperature, and TI is the
integration period $\tau_2 - \tau_1$.

N113 should be obtained for the hourly, daily and monthly data summaries.

6.4 Energy Collection and Storage Subsystem (ECSS) Primary Performance Factors

The primary performance factors are based on the ECSS shown in Figure 3.

6.4.1 Solar Energy Collected (Q100)

The amount of solar energy collected in a given time period is obtained by
evaluating Equation 6.1 using the appropriate sensors in the ECSS as follows:

$$Q100 = \frac{1}{A_c} \int_{\tau_1}^{\tau_2} W100 \cdot C100 \cdot TD100 \, d\tau \qquad (6.7)$$

Where A_c is the total collector area defined by the outside dimensions
of the collector array, *
W100 = Collector array fluid mass flow rate,
C100 = Specific heat of collector fluid,
TD100 = Fluid temperature increase across the collector array.

Additional data may be required to correct the fluid specific heat for temperature,
concentration, etc.

6.4.2 Total Solar Energy Utilized (Q300, Q400, Q500, Q203)

For the demonstration program, solar energy is used in as many as three applications;
i.e., hot water heating, space heating, and space cooling. For each application,

---

*Proposed Solar collector test procedure [6] rates flat plate collector performance
on transparant frontal area instead of total area, therefore, thermal comparison of
result will require adjustment by appropriate area ratio.

Equation (6.1) is evaluated using the appropriate measurements in the HW loop and in the heating or cooling loop. Since some of the measurements used for the heating and cooling calculations are the same, additional information must be supplied (such as the operating status of the absorption unit) to determine whether the calculation pertains to heating or cooling. The following equations are used to calculate each component for the ECSS using a liquid heat transfer medium (SYSTEM A in Figure 3):

6.4.2.1 Solar Used for Hot Water

$$Q300 = \int_{\tau_1}^{\tau_2} W300 \cdot C301 \cdot TD301 \, d\tau \qquad (6.8)$$

6.4.2.2 Solar Used for Space Heating

$$Q400 = \int_{\tau_1}^{\tau_2} W400 \cdot C400 \cdot TD400 \, d\tau \qquad (6.9)$$

6.4.2.3 Solar Used for Space Cooling

$$Q500 = \int_{\tau_1}^{\tau_2} W400 \cdot C400 \cdot TD400 \, d\tau \qquad (6.10)$$

6.4.2.4 Total Solar Energy Utilized (Liquid Heat Transfer Medium)

The total solar energy utilized is the sum of the solar energy used in each application and is given by:

$$Q203 = Q300 + Q400 + Q500 \qquad (6.11)$$

6.4.2.5 Total Solar Energy Utilized (Air Heat Transfer Medium)

For the ECSS using air as the heat transfer medium (SYSTEM B in Figure 3). the total solar energy utilized is given by:

$$Q203 = \int_{\tau_1}^{\tau_2} W400 \cdot C401 \cdot TD401 \, d\tau \qquad (6.12)$$

6.4.3 ECSS Conversion Efficiency (N111)

The ratio of total solar energy actually utilized to the total solar energy incident on the collector array is termed the solar subsystem conversion

35

efficiency and is a measure of the ability of the ECSS to convert incident solar radiation into useful thermal energy. ECSS conversion efficiency is calculated by:

$$N111 = \int_{\tau_1}^{\tau_2} Q203 \ d\tau / A_c \int_{\tau_1}^{\tau_2} Q001 \ d\tau \qquad (6.13)$$

Because of the solar energy storage time dependence, ECSS conversion efficiency (N111) should be determined only for the monthly. seasonal and annual data summary.

6.5   Hot Water Subsystem (HWS) Primary Performance Factors

6.5.1 Hot Water Load (Q302)

The total thermal energy required for heating HW from the inlet (makeup) to delivery temperature is given by:

$$Q302 = \int_{\tau_1}^{\tau_2} W301 \cdot C301 \cdot (TD301 + TD302) d\tau \qquad (6.14)$$

The HW load (Q302) should be obtained for the hourly, daily, monthly and annual data summary.

6.5.2 Solar Fraction of the HW Load (N300)

The solar fraction of the HW load is calculated by:

$$N300 = \frac{1}{TI} \int_{\tau_1}^{\tau_2} \frac{TD301}{TD301 + TD302} \ d\tau, \ W301{\neq}0 \qquad (6.15)$$

where TD301 and TD302 are the temperature differences across the HW storage tank and auxiliary heat exchangers, respectively, when there is a flow to the HW load (W301≠0).

This parameter should be evaluated on a daily, monthly and annual basis.

6.5.3 HW Electrical Energy Saved (Q311)

The measured electrical energy used by the HW subsystem of Figure 4 is given by:

$$Q309 = Q303 + Q305 + Q308 \qquad (6.16)$$

where Q303 is the energy required to operate the circulation pump, Q305 is the energy input to the auxiliary heater (Q305=0 for a fossil auxiliary), and Q308 is the HWS fraction of the ECSS operating energy.

The calculated electrical energy required to operate a conventional hot water subsystem is given by:

$$Q310 = Q302/NHWE \qquad (6.17)$$

where Q302 is the hot water load previously described, and NHWE is the thermal efficiency of a conventional HW subsystem using electricity as an energy source.

The electrical energy saved is the difference between the calculated electrical energy to operate a conventional system having the same source and delivery temperature and usage rate as the solar energy system and the measured electrical energy required to operate the solar energy system as follows:

$$Q311 = Q310-Q309 \qquad (6.18)$$

If a negative value is obtained for Q311 this implies that the particular solar HWS consumes more electrical energy than the assumed conventional system it is replacing.

6.5.4 HW Fossil Energy Saved (Q313)

The fossil energy used by the solar HWS is calculated in the following manner:

$$Q306 = HVF \int_{\tau_1}^{\tau_2} F300 \ d\tau \qquad (6.19)$$

where HVF is the fuel heating value in BTU/LB and F300 is the measured mass flow rate of fuel to the auxiliary in LB/HR.

The fossil fuel energy required to operate a conventional HWS is calculated from:

$$Q312 = Q302/NHWF \qquad (6.20)$$

where Q302 is the HW load and NHWF is the thermal efficiency of a conventional HW system using fossil fuel as an energy source.

The fossil fuel energy saved is the difference between the calculated fossil energy required to operate a conventional HW system and the measured fossil energy required to operate a solar energy system as follows:

$$Q313 = Q312-Q306 \qquad (6.21)$$

37

6.6   Space Heating Subsystem (SHS) Primary Performance Factors

The primary performance factors are based on the SHS shown in Figure 5.

6.6.1   Space Heating Load (Q402)

The space heating load is the sensible energy added to the air in the building and is given by:

$$Q402 = \int_{\tau_1}^{\tau_2} W600 \cdot C600 \cdot TD600 \ d\tau \qquad (6.22)$$

where   W600 is the building air flow rate,

C600 is the specific heat,

and TD600 is the temperature rise of the air flow across all the heat exchangers in the air handling unit.

The space heating load should be determined for the hourly, monthly and seasonal data summary.

6.6.2   Solar Fraction of Space Heating Load (N400)

The solar fraction of the space heating load for the SHS comprised of a heat pump and electric auxiliary (SYSTEM A) is given by:

$$N400 = \int_{\tau_1}^{\tau_2} (Q406 + Q407) d\tau / \int_{\tau_1}^{\tau_2} Q402 \ d\tau \qquad (6.23)$$

where Q406 is the energy delivered to the heating loop load heat exchanger in mode 1,

and Q407 is the energy delivered to the heat pump evaporator in modes 2 and 3.

The solar fraction of the space heating load for the SHS comprised of the fossil fuel auxiliary (SYSTEM B) is given by:

$$N400 = \int_{\tau_1}^{\tau_2} Q400 \ d\tau / \int_{\tau_1}^{\tau_2} Q402 \ d\tau \qquad (6.24)$$

where Q400 is the energy delivered to the heating loop load heat exchanger,

and Q402 is the space heating load previously described.

This parameter should be determined for the daily, monthly and seasonal data summary.

6.6.3   Space Heating Electrical Energy Saved (Q415)

The electrical energy used by the heat pump system shown as system A in Figure

5 is given by:

$$Q413 = Q403 + Q404 + Q409 + Q412 \qquad (6.25)$$

where Q403 is the energy consumed by the heating loop circulation
pump, building fan and all controls,

O404 is the energy to operate the heat pump compressor,

Q409 is the energy to the electric auxiliary heat exchanger and

Q412 is the SHS fraction of the ECSS operating energy.

The electrical energy consumed by a non-solar heat pump heating system is
given by:

$$Q414 = Q402/NHTE \qquad (6.26)$$

where Q402 is the measured space heating load,

and NHTE is a modified coefficient of performance of the non-solar
heat pump system which as defined in reference [2] includes
electrical energy required to operate the compressor, supply fan,
return fan, outdoor air fan and HVAC control circuit.

The modifications to the equipment COP include the supplemental energy required
for defrosting and auxiliary heating and the reduction in performance due to
cyclic operation at off design conditions. Reference [7] presents data
describing off-design heat pump performance and the discrepancy between manufacturers
performance data and measured performance primarily due to defrosting requirements.

The electrical energy saved is therefore the difference between the calculated
electrical energy required to operate a conventional heating system and the
measured electrical energy required to operate the solar energy system as follows:

$$Q415 = Q414-Q413 \qquad (6.27)$$

6.6.4   Space Heating Fossil Energy Saved (Q417)

The fossil energy saved by an all electric-heating system is obviously zero,
therefore, to illustrate this calculation, the fossil energy used by the alternate
SYSTEM B is given by:

$$Q410 = HVF \int_{\tau_1}^{\tau_2} F400 \, d\tau \qquad (6.28)$$

where   HVF is the heating value of the fuel,

and F400 is the mass flow rate of fuel consumed by the auxiliary.

The fossil-energy consumed by a non-solar heating system must be calculated for
the measured load conditions based on the performance characteristics and/or
component efficiencies of the equipment as follows:

$$Q416 = Q402/NHTF \qquad (6.29)$$

39

where   Q402 is the space heating load and,

NHTF is the assumed thermal efficiency of the equipment.

The fuel energy saved is given by the difference between the calculated fossil energy consumption of the non-solar heating system and the measured fossil energy consumption of the solar energy system as follows:

$$Q417 = Q416-Q410 \tag{6.30}$$

6.7   Space Cooling Subsystem (SCS) Primary Performance Factors

The primary performance factors of the space cooling subsystem are based on the SCS shown schematically in Figure 6.

6.7.1 Space Cooling Load (Q502)

The space cooling load is the total energy, including sensible and latent, removed from the air in the building and is given by:

$$Q502 = \int_{\tau_1}^{\tau_2} [W600 \cdot C600 \cdot TD600 + W601 \cdot h_{FG}]\ d\tau \tag{6.31}$$

where   W600 is the building supply air flow rate,
TD600 is the temperature differential across the fan-coil unit,
W601 is the flow rate of condensed water vapor from the cooling coil,
and h_{FG} is the latent heat of vaporization of the condensate.

Alternatively if air side measurements are not practical, the space cooling load can be approximated from Q507 shown in Figure 6 which is the measured absorption chiller load.

6.7.2 Solar Fraction of Space Cooling Load (N500)

The solar fraction of the space cooling load is given by:

$$N500 = \int_{\tau_1}^{\tau_2} Q500\ d\tau / \int_{\tau_1}^{\tau_2} Q506\ d\tau \tag{6.32}$$

where   Q500 is the solar energy delivered to the SCS,
and Q506 is the total thermal energy delivered to the absorption chiller generator consisting of solar and auxiliary thermal energy.

This parameter should be determined for the daily, monthly and seasonal data summary.

6.7.3 Space Cooling Electrical Energy Saved

The electrical energy used by the solar assisted space cooling subsystem is given by:

$$Q510 = Q503 + Q509 \qquad (6.33)$$

where   Q503 is the cooling subsystem operating energy including power for the heating loop circulation pump, building fan, absorption unit pumps, cooling tower fans and all subsystem controls, and Q509 is the space cooling subsystem fraction of the ECSS electrical energy consumption.

The electrical energy consumed by a non-solar cooling system must be calculated for the measured load conditions, source and sink temperatures using the appropriate conversion efficiency as follows:

$$Q511 = Q502/NCLF \qquad (6.34)$$

where   Q502 is the measured cooling load, and NCLF is the electrical efficiency of the non-solar cooling equipment.

The electrical energy saved is the difference between the calculated electric energy consumption of the conventional cooling system and the measured electric energy consumption of the solar energy system as follows:

$$Q512 = Q511-Q510 \qquad (6.35)$$

6.7.4 Space Cooling Fuel Energy Saved (Q514)

The fossil fuel energy used by the solar space cooling subsystem is given by:

$$Q508 = HVF \int_{\tau_1}^{\tau_2} F500 \ d\tau \qquad (6.36)$$

where   F500 is the fuel mass flow rate to the auxiliary unit, and HVF is the heating value of the fuel.

The fuel energy consumed by a non-solar cooling subsystem must be calculated for the measured load conditions based on the component performance characteristics and/or efficiency as follows:

$$Q513 = Q502/NCLF \qquad\qquad (6.37)$$

where   Q502 is the measured space cooling load,

and NCLF is the thermal efficiency of the non-solar equipment.

The fossil fuel energy saved is given by the difference in the calculated fossil energy consumption of the non-solar cooling system and the measured fossil energy consumption of the solar energy system as follows:

$$Q514 = Q513-Q508 \qquad\qquad (6.38)$$

6.8   Solar Energy System/Building Summary

The following primary performance factors summarize the performance of the overall solar energy system and the building.

6.8.1   <u>Average Building Dry Bulb Air Temperature (N407)</u>

Average building temperature is an occupant utilization parameter that will have a strong influence on system performance for both heating and/or cooling and is therefore useful for comparison of alternate systems. Average dry bulb temperature should be evaluated as follows:

$$N400 = \frac{1}{TI} \int_{\tau_1}^{\tau_2} T600 \ d\tau \qquad\qquad (6.39)$$

where   T600 is the measured building air dry bulb temperature.

This parameter should be determined for the hourly, daily, monthly and seasonal data summary.

6.8.2   <u>Total Auxiliary Energy (Q301, Q302, Q303, Q600)</u>

Auxiliary energy is required for HW, space heating and space cooling whenever the solar system is not capable of meeting the demand. The amount of auxiliary energy required is determined using the same basic approach described in Section 6.4.2 for solar energy utilized and is calculated as follows:

6.8.2.1 Auxiliary Used for HW

$$Q301 = \int_{\tau_1}^{\tau_2} W301 \cdot C302 \cdot TD302 \ d\tau \qquad\qquad (6.40)$$

6.8.2.2 Auxiliary Used for Space Heating

For SYSTEM A of Figure 5, the auxiliary energy used for space heating is given
by:

$$Q401 = \int_{\tau_1}^{\tau_2} W600 \cdot C602 (TD600-TD601) d\tau \qquad (6.41a)$$

For SYSTEM B of Figure 5, the auxiliary energy used for space heating is given
by:

$$Q401 = \int_{\tau_1}^{\tau_2} W400 \cdot C401 \cdot TD401 \, d\tau \qquad (6.41b)$$

6.8.2.3 Auxiliary Used for Space Cooling

$$Q501 = \int_{\tau_1}^{\tau_2} W400 \cdot C401 \cdot TD401 \, d\tau \qquad (6.42)$$

6.8.2.4 Total Auxiliary Energy Utilized

The total auxiliary energy utilized is the sum of the auxiliary energy used for
each application and is given by:

$$Q600 = Q301 + Q401 + Q501 \qquad (6.43)$$

Total auxiliary energy should be determined for hourly, daily, monthly and
seasonal/annual data summary.

6.8.3 Total Operating Energy (Q601)

The total operating energy is the thermal equivalent of the electrical energy
required to run the pumps, fans, compressors and controls but excludes the
electrical energy used for auxiliary heating purposes. The total operating
energy is composed of the individual components as follows:

$$Q601 = Q102 + Q303 + Q403 + Q503 \qquad (6.44)$$

where   Q102 is the solar subsystem operating energy defined in Figure 3,

Q303 is the HW operating energy defined in Figure 4,

Q403 is the space heating operating energy defined in Figure 5,

Q404 is the heat pump compressor energy defined in Figure 5,

Q503 is the space cooling operating energy defined in Figure 6.

43

Total operating energy should be determined for the hourly, daily, monthly and seasonal/annual data summary.

6.8.4   Total Energy Delivered to Building Load (Q602)

The total building energy load is the sum of the HW load, the space heating load and space cooling loads previously defined, and is calculated by:

$$Q602 = Q302 + Q402 + Q502 \qquad (6.45)$$

The total building energy load should be determined for the hourly, daily, monthly, seasonal/annual data summary.

6.8.5   Total Energy Consumed (Q603)

Total energy consumption consists of the total solar, fossil and electric energy consumed by all of the subsystems as follows:

$$Q603 = Q102 + Q307 + Q411 + Q515 \qquad (6.46)$$

where   Q102 is the ECSS operating energy.

Q307 is the HWS total energy consumption defined in Figure 4,

Q411 is the SHS total energy consumption defined in Figure 5,

and Q515 is the SCS total energy consumption defined in Figure 6.

Total energy consumed should be determined for the hourly, daily, monthly and seasonal/annual data summary.

6.8.6   Total Electric Energy Saved (Q604)

The total electric energy saved is given by:

$$Q604 = Q311 + Q415 + Q512 \qquad (6.47)$$

where   Q311, Q415 and Q512 are the electric energies saved for HW, space heating and space cooling, respectively.

6.8.7   Total Fossil Energy Saved (Q605)

The total fuel energy saved is given by:

$$Q605 = Q313 + Q417 + Q514 \qquad (6.48)$$

where   Q313, Q417 and Q514 are the fossil fuel energies saved for HW, space heating and space cooling respectively.

Energy saved should be determined for the hourly, daily, monthly and seasonal/ annual data summary.

6.§.8 Solar Fraction of Building Load (N601)

The solar fraction of the building load is determined by averaging the solar fractions of the individual subsystem loads as follows:

$$N601 = \frac{\int_{\tau_1}^{\tau_2} [N300 \cdot Q302 + N400 \cdot Q402 + N500 \cdot Q502] d\tau}{\int_{\tau_1}^{\tau_2} [Q302 + Q402 + Q502] d\tau} \qquad (6.49)$$

where   N300, N400 and N500 are the solar fractions, respectively, of the HW load, heating load and cooling load,
and Q302, Q402, Q502 are, respectively, the HW load, heating load and cooling load.

6.8.9 System Performance Factor (N602)

The ratio of the total energy delivered to the building load to the total equivalent fossil fuel energy expended is defined to be the system performance factor and is calculated as follows:

$$N602 = \int_{\tau_1}^{\tau_2} Q602 \, d\tau / \int_{\tau_1}^{\tau_2} [Q306 + Q410 + Q508 + \frac{(Q601 + Q305 + Q409)}{NELEC}] d\tau \quad (6.50)$$

where   Q306, Q410 and Q508 are the fossil fuel energies consumed, respectively, for the HW, space heating and space cooling auxiliaries, Q305 and Q409 are the electrical energies consumed respectively for the HW and space heating auxiliaries,

NELEC is the overall thermal efficiency for conversion of fossil energy at the power plant to electrical energy at the building.

The system performance factor should be determined for the daily, monthly and seasonal/annual data summary.

6.9 Secondary Performance Factors and Measurements

In addition to the primary system performance factors described in Section 6.3 to 6.8, certain secondary performance evaluation factors for the ECSS and ECDS are of sufficient importance to warrant further discussion.

6.9.1 Daily Integrated Collector Efficiency (N100)

The ratio of the daily integrated solar energy collected by the array to the daily integrated total solar energy incident on the array is termed the daily integrated collector efficiency and is a measure of the ability of the solar collector to convert daily incident solar radiation into thermal energy available either immediately or for storage and subsequent use thereof to support the building thermal energy load. Daily integrated collector efficiency is calculated by:

$$N100 = \int_{\tau_1}^{\tau_2} Q100 \ d\tau / \int_{\tau_1}^{\tau_2} Q001 \ d\tau \qquad (6.51)$$

where the numerator represents the total thermal energy collected per day for one square foot of collector and the denominator represents the total solar radiation incident on one square foot of collector per day.

6.9.2 Collector Array Instantaneous Performance (N101, N102, N103, N104)

The performance of a flat plate collector operating under steady state conditions can be described by the following equation:

$$\frac{Q_u}{A_c} = F_R \ [(I_T) \ (\tau\alpha)_e - U_L(T_{f,i} - T_a)] \qquad (6.52)$$

where Q_u = rate of useful energy extraction from the collector

A_c = collector area, aperature

F_R = $\dfrac{\text{Actual useful energy collected}}{\text{useful energy collected if the entire collector were at the inlet fluid temperature}}$

I_T = total incident solar radiation

$(\tau\alpha)_e$ = effective transmission absorptance product of collector

U_L = heat transfer loss coefficient for the collector

$T_{f,i}$ = fluid temperature entering collector

T_a = ambient air temperature

Defining the solar collector efficiency as the ratio of useful energy extracted from the collector to the total solar radiation incident, equation (6.52) is rearranged to give collector efficiency as follows:

$$N101 = F_R \ [(\tau\alpha)_e - U_L \ \frac{T_{f,i} - T_a}{I_T}] \qquad (6.53)$$

A plot of equation (6.53) as a function of $(T_{f,i} - T_a)/I_T$ for a range of operating conditions yields a first or second order curve with the y axis intercept equal to $F_R (\tau\,\alpha)_e$ and slope equal to $F_R U_L$.

If an individual collector panel is instrumented the same as the collector array with inlet and exit temperatures and flow rate monitored, or if the entire collector array is co-planer, then by evaluating the two factors $F_R(\tau\alpha)_e$ and $F_R U_L$ over the life of the demonstration, degradation of the array due to changes in the $\tau\alpha$ product or U_L (heat transfer loss coefficient) will be revealed.

Meaningful efficiency measurements are obtained when essentially steady state is achieved for the previous 15 minutes (three data scans, if the scan occurs every five minutes). The following measurements should be constant:

        T001   (ambient dry bulb air temperature)
        T100   (array inlet temperature)
        W100   (array flow rate)
        I001   (total incident solar radiation)

Other constraints for the procedure as obtained from reference (6) are to limit the calculation to times during which the angle between the sun and the collector array normal is less than 30° degrees and the total incident solar radiation is greater than 630 w/m^2 (200BTU/hrft^2). If all the above constraints are satisfied, then data taken at the last data scan are used to calculate the following performance indicies.

6.9.2.1 Instantaneous Collector Array Efficiency (N101)

$$N101 = \frac{W100 \cdot C100 \cdot TD100}{A_c \cdot I001}$$
(6.54)

6.9.2.2 Collector Panel Efficiency Factor (N102)

$$N102 = (T100-T001)/\ I001$$
(6.55)

6.9.2.3 Collector Panel Factors (N103, N104)

The newly calculated values of the parameters N101 and N102 are used together

with previously calculated values of N101 and N102 using the previously described slope/intercept linear curve fit and new values of the collector panel factors N103 and N104 are obtained, where:

$$N103 = F_R (\tau\alpha)_e \qquad (6.56)$$

and,

$$N104 = F_R U_L \qquad (6.57)$$

The above described procedure should be performed at the start of each hour until a data scan occurs which satisfies all specified constraints. For that scan, the calculated values of N101, N102, N103 and N104 are reported in the hourly data summary and no further scans are required for the remainder of the hour. At the start of the next hour the procedure is repeated.

6.9.3   Collector Heat Exchanger Effectiveness (N105)

For the ECSS where the thermal capacitance of the storage container is much greater than the flow capacitance of the collector loop, the collector heat exchanger effectiveness is given by:

$$N105 = \frac{1}{TI} \int_{\tau_1}^{\tau_2} (TD101)/(T101-T200)\, d\tau \qquad (6.58)$$

Evaluation of collector heat exchanger effectiveness can be done on a monthly and annual basis.

6.9.4   HW Heat Exchanger Effectiveness (N106)

The hot water heat exchanger effectiveness is determined as follows:

$$N300 = \frac{1}{TI} \int_{\tau_1}^{\tau_2} (TD300)/(T200 - T300)\, d\tau \qquad (6.59)$$

Due to the requirement for double walled heat exchangers to prevent any possible contamination of potable water with non-potable water, the HW heat exchangers may present a substantial thermal resistance to heat transfer and thereby reduce the amount of solar energy available. Any tendency for fouling of the heat exchangers would be revealed by changes in the calculated values of heat exchanger effectiveness.

6.9.5   Storage Subsystem Efficiency (N108, N109)

The storage subsystem efficiency is defined as the ratio of the sum of the
output of stored thermal energy and the increase in stored thermal energy to
the input of thermal energy to storage as follows:

$$N108 = \frac{\int_{\tau_1}^{\tau_2} (Q201 + Q202)d\tau}{\int_{\tau_1}^{\tau_2} Q200 \, d\tau} \qquad (6.60)$$

where Q201 is the hourly output of thermal energy from the storage
device,

Q202 is the hourly increase in stored energy,

and Q200 is the hourly input of thermal energy to the storage device.

The normal source of thermal energy input to storage is from the solar energy
collectors, however, other thermal energy sources, such as off-peak auxiliary
energy must also be included. Where more than one storage container is used,
individual evaluation is required.

Storage efficiency is related to the subsystem heat losses which may be
either deliberate (such as the dumping of energy to ambient) or non-deliberate
due to air leakage or insulation losses. Heat loss through insulation is related
to the following parameter:

$$N109 = \frac{1}{TI} \int_{\tau_1}^{\tau_2} (T200-T201)d\tau \qquad (6.61)$$

where T200 is the average storage medium temperature, and

T201 is the ambient temperature surrounding the storage container.

Evaluation of these parameters (N108 and N109) should be performed for the
monthly and seasonal/annual data summary.

6.9.6   Average HW Load Temperature (N307)

The average HW delivery temperature to the load is a significant parameter
in the comparison of alternate HW solar systems, in that this temperature
is controlled by the occupants and subsystem performance will depend
on the actual control point setting.

$$N307 = \frac{1}{TI} \int_{\tau_1}^{\tau_2} (T301 + TD301 + TD302)d\tau \qquad (6.62)$$

where   T301 is the make-up water temperature,

TD301 is the temperature difference across the hot water storage,

and TD302 is the temperature difference across the HW auxiliary
heat exchanger.

6.9.7   Average Gallons HW Consumed (N308)

The time of day at which hot water is used and the total daily consumption
are significant parameters in evaluating performance and comparison of
alternate HW solar systems. The average HW consumption in gallons is given
by:

$$N308 = .12 \int_{\tau_1}^{\tau_2} W301 \, d\tau \qquad\qquad (6.63)$$

where   W301 is the measured flow rate in lbs/hr.

The HW consumption should be determined for the hourly, daily, monthly
and annual data summary.

6.9.8   Energy Conversion Equipment Coefficient of Performance

Enegry conversion equipment uses electrical or thermal energy to
raise heat from a low temperature source to a higher temperature sink and
is rated by the ratio of the useful heat transferred to the energy input.
Useful heat transferred consists of heat delivered to the sink in the heating
mode and heat extracted from the source in the cooling mode.

6.9.8.1   Space Heating Equipment COP (N404)

Measurement of the Coefficient of Performance (COP) is desired for energy
conversion equipment such as heat pumps in which the useful thermal energy
delivered to the building is significantly greater than the electrical
energy consumed. Referring to the heat pump system shown as SYSTEM A in
Figure 5, Space Heating COP is calculated from:

$$N404 = \int_{\tau_1}^{\tau_2} Q407 \, d\tau / \int_{\tau_1}^{\tau_2} (Q403 + Q404) d\tau \qquad\qquad (6.64)$$

where   Q407 is the useful thermal energy added to the building
supply air from the heat pump,

Q403 is the electrical energy required to operate the SHS pumps,
fans and controls,

Q404 is the electrical energy required to operate the heat pump
compressor.

This parameter should be determined for the daily, monthly and seasonal
data summary.

6.9.8.2 Space Cooling Equipment COP (N503)

Measurements of the Coefficient of Performance (COP) are desired for thermally
actuated equipment such as the absorption chiller for Figure 6 and for other
equipment such as solar assisted Rankine Cycle equipment or dessicant
dehumidification systems as appropriate.

Referring to the absorption chiller shown in Figure 6, the Coefficient of
Performance is calculated as:

$$N503 = \int_{\tau_1}^{\tau_2} Q507 / \int_{\tau_1}^{\tau_2} Q506 \, d\tau \qquad (6.65)$$

where   Q507 is the useful thermal output of the absorption
chiller as defined in Figure 6,
and Q506 is the thermal energy input to the absorption chiller
as defined in Figure 6.

7.0   UNCERTAINTY ANALYSIS OF SOLAR PERFORMANCE FACTORS

The uncertainty of determining the performance evaluation factors for a part-icular solar energy system/building/climate combination is related to the data requirement accuracy for sensor signal conditioning, data acquisition sampling rate and data processing method. Non-instrumentation variables such as building heating or cooling load, occupancy, conventional heating and air conditioning equipment operation and meteorological parameters must also be considered when comparing the performance of solar energy systems in different buildings or climatic regions.

To establish acceptable tolerances in the performance evaluation factors, the contribution of sensor accuracy and sampling rate error to the total performance factor uncertainty must be derived and set in perspective by comparison with the pertinent non-instrumentation sources of the performance factor uncertainty. The approach, rationale and sensitivity analysis for several performance factors are described in the following sections:

- ° Sensitivity Analysis Methods
- ° Specific Error Analysis
- ° Overall Instumentation Errors
- ° Recommended Sampling Rates and Data Requirement Accuracies

7.1   Sensitivity Analysis Methods

Two methods are in general use for combining precision errors in measuring several variables to estimate the error in a calculated function of those variables. The particular method used depends on whether the component errors are considered to be absolute limits or statistical bounds (such as 3σ limits) the form of the relationship between the variables and the calculated function, and the specification of component errors (percent of reading or absolute in terms of measured units).

7.1.1   Absolute Limits

If the component precision errors are considered to be absolute limits and a functional relationship exists such that

$$T = f(x,y,z) \qquad\qquad\qquad (7.1)$$

If the component errors in x, y, and z are Δx, Δy and Δz respectively, and $f(x,y,z)$ is expanded in a Taylor series; then:

$$f(x + \Delta x, y + \Delta y, z + \Delta z) = f(x,y,z) + \frac{\partial f \Delta x}{\partial x} + \frac{\partial f \Delta y}{\partial y} + \frac{\partial f \Delta z}{\partial z}$$

$$+1/2 \left[\frac{\partial^2 f \Delta x^2}{\partial x^2} + \frac{\partial^2 f}{\partial y^2} \Delta y^2 + \frac{\partial^2 f}{\partial z^2} \Delta z^2 \right] + \ldots \quad (7.2)$$

Neglecting the second order and larger terms because Δx, Δy, Δz are assumed small ($\sim 1\%$), the total measurement error is:

$$\Delta f = \left| \frac{\partial f}{\partial x} \Delta x \right| + \left| \frac{\partial f}{\partial y} \Delta y \right| + \left| \frac{\partial f}{\partial z} \Delta z \right| \quad (7.3)$$

In the general case for a function R (a function of any number of variables) the error can be expressed as:

$$\Delta R = \sum_{i=1}^{n} \left| \frac{\partial R}{\partial X_i} \Delta X_i \right| \quad (7.4)$$

7.1.2   Statistical Bounds

In the absence of a function relating the component error sources, a general equation can be used to find the measurement error. If the measurement is defined by $R(X_1, X_2 \ldots X_n)$, where R is the desired measurement and $\Delta X_1, \ldots \Delta X_n$ are the individual error sources, the following equation can be used:

$$\Delta R = \left[\sum_{i=1}^{n} \left(\frac{\partial R}{\partial X_i} \Delta X_i \right)^2 \right]^{1/2} \quad (7.5)$$

This equation assumes that the errors are random and uncorrelated. The precision errors will be expressed as $\pm \Delta X$. As a probable error in either of the two cases (functional or non-functional relationship), the true value of R will be between $R - \Delta R$ and $R + \Delta R$ for some percentage of all readings. The percentage involved depends upon the error expressions used for the component errors.

7.1.3   Error Analysis - Daily Integrated Collector Array Efficiency

An error analysis of the calculations of daily integrated collector array efficiency is presented to illustrate using both methods discussed in the preceding paragraphs.

From Figure 3, the daily integrated collector array efficiency is calculated as:

$$N100 = \int Q100 d\tau / \int Q001 d\tau \quad = \int W100 \cdot C100 \cdot TD100 \ d\tau / Ac \int I001 d\tau \qquad (7.6)$$

If the component errors are independent of time than the uncertainty in the integrated daily efficiency is the same as the uncertainty in the instantaneous efficiency given by performance factor N101 as:

$$N101 = \frac{W100 \cdot C100 \cdot TD100}{Ac \cdot I001} \qquad (7.7)$$

For purposes of illustration, the following reference conditions and tolerances in each variable are assumed:

$$A_c = 32 \ ft^2 \ \pm 1\% \ \text{(assumption)} \ (\pm .32 \ ft^2), \ \text{collector area}$$

$$W100 = 1 \ GAL/HR \ ft^2 \ x \ 32 \ ft^2 = 269.91 \ lb/hr. \ \pm 2\% \ FS \ (\pm 5.4 \ lb/hr), \ \text{collector flow}$$

$$C100 = 1.0 \ BTU/lb \ °F, \ \text{specific heat (NO TOLERANCE)}$$

$$TD100 = 18 \pm 1.7\% \ (\pm 0.3°F), \ \text{temperature rise through collector}$$

$$I001 = 300 \ BTU/hr \ ft^2 \ \pm 3\% \ (\pm 9 \ BTU/hr \ ft^2), \ \text{incident solar radiation}$$

The nominal array efficiency is determined from equation (7.7) by substitution of the assumed variables at the reference point as:

$$N101 = \frac{(270)\frac{LB}{HR} \ (1.0) \ \frac{BTU}{LB} \ °F \ (18.0) \ °F}{(32 \ )ft^2 \ (300) \ \frac{BTU}{hr \ ft^2}} = .506$$

Equation 7.7 is differentiated with respect to each variable having a non-zero tolerance and each partial derivative is evaluated at the reference condition as follows:

$$\frac{\partial N101}{\partial W101} = \frac{C101 \cdot TD100}{A_c \cdot I001} = \frac{(1.0)(18.)}{(32.)(300.)} = .0019$$

$$\frac{\partial N101}{\partial TD100} = \frac{W100 \cdot C100}{A_c \cdot I001} = \frac{(270.)(1.0)}{(32.)(300.)} = .0281$$

54

$$\frac{\partial N101}{\partial A_c} = -\frac{W100 \cdot C100 \cdot TD100}{A_c^2 \cdot I001} = -\frac{(270)(1.0)(18.0)}{(32)^2(300.)} = -0.0158$$

$$\frac{\partial N101}{\partial I001} = -\frac{W100 \cdot C100 \cdot TD100}{A_c \cdot (I001)^2} = -\frac{(270)(1.0)(18.0)}{(32)(300)^2} = -.0017$$

The error by absolute limits is obtained by substitution of the partial derivatives and tolerances in equation (7-4) as follows:

$$\Delta N101 = |(.0019)(5.4)| + |(.0281)(.03)| + |(-0.0158)(.32)| + |(-.0017)(9.0)|$$
$$\Delta N101 = .0390$$
$$N101 = .506 \pm .039$$

Thus the calculated value of instantaneous efficiency based on absolute error limits indicates an uncertainty of $\pm$ 7.7 percent.

The error by statistical bounds is obtained by substitution of the partial derivatives and tolerances in equation (7.5) as follows:

$$N101 = \left[(.0019 \times 5.4)^2 + (.0281 \times 0.3)^2 + (-0.0158 \times .32)^2 + (-.0017 \times 9.0)^2\right]^{1/2}$$
$$\Delta N101 = .021$$
$$N101 = .506 \pm .021$$

The statistical or rms method indicates about a $\pm$ 4.1 percent uncertainty in the calculation of collector efficiency. As indicated by the sample calculations the absolute limit method gives a larger error value than the statistical method. Because of the randomness of the measurement process for the solar energy systems (i.e., errors among the many different sensors are not correlated), the statistical method is used for the uncertainty and error analysis calculations reported in this document.

7.2   Derivation of the Overall Instrumentation Accuracies

Instrumentation accuracies are caused by sampling errors and by systematic sensor errors due to inaccurate calibration, drift, and non-linearities. To evaluate the effect of sensor and sampling errors on the performance factors, the following information is necessary: the analytical expression for each

performance factor, the range of loads and operating points for the solar energy systems and the sampling period. Application of the error analysis method to determine the uncertainty in solar energy system conversion efficiency is described to illustrate the analysis performed for most of the primary factors.

7.2.1   Temperature Sensor Accuracy

There are several ways of expressing temperature sensor accuracy. If all temperature sensors used to compute energy flows are differential sensors, meaning that a temperature rise or drop, not an absolute temperature is measured then accuracy of measuring a temperature differential is expressed as percent (degrees accuracy in measuring the differential divided by the total differential). If the differential is to be measured using two sensors, then the accuracy is the square root of the sum of the individual accuracies squared divided by the temperature difference or.

$$\text{accuracy} = \sqrt{\sigma_1^2 + \sigma_2^2} \ / \ \Delta T \qquad\qquad (7.8)$$

Thus, a 2% load temperature accuracy requirement and 20°F assumed load temperature difference means that the temperature accuracy should be .4°F for a differential sensor and .3°F for individual sensors. Similarly, a 4% accuracy and 10°F rise across a collector requires a temperature accuracy of .4°F differential or .3°F for individual sensors.

Other combinations of flow and temperature sensors which fulfill instrumentation accuracy requirements can be determined from Figures 9 and 10. These two graphs were computed from the two error equations that constrain flow and temperature sensor errors.

7.2.2   A Description of Sampling Errors

Sampling errors develop when a signal waveform is not sampled quickly enough so that the exact waveform can be reproduced. Because many solar parameters change quite rapidly (e.g., auxiliary fuel flow or insolation), it is not feasible to sample to reproduce the entire waveform. However, it is possible by sampling a large number of times to statistically reproduce the mean of a waveform. For instance, for a monthly measurement period and a 10-minute sample interval, each parameter mean is based on approximately 2,000 samples. It is the statistics of large numbers which governs sample accuracy (provided correlation effects do not arise).

56

$$Q100 = \int W100 \cdot C100 \cdot TD100 \; d\tau$$

$$\text{FROM} \quad \sigma_{Ins} = \sqrt{\sigma_W^2 + \sigma_{TD}^2 + \sigma_I^2 + 2\sigma_S^2}$$

$$\text{WHERE} \; \sigma_I = 3\%, \, \sigma_S = 2\%, \; \text{AND}$$

$$\Delta T = 10°F \, (liq.), \, 40°F \, (air)$$
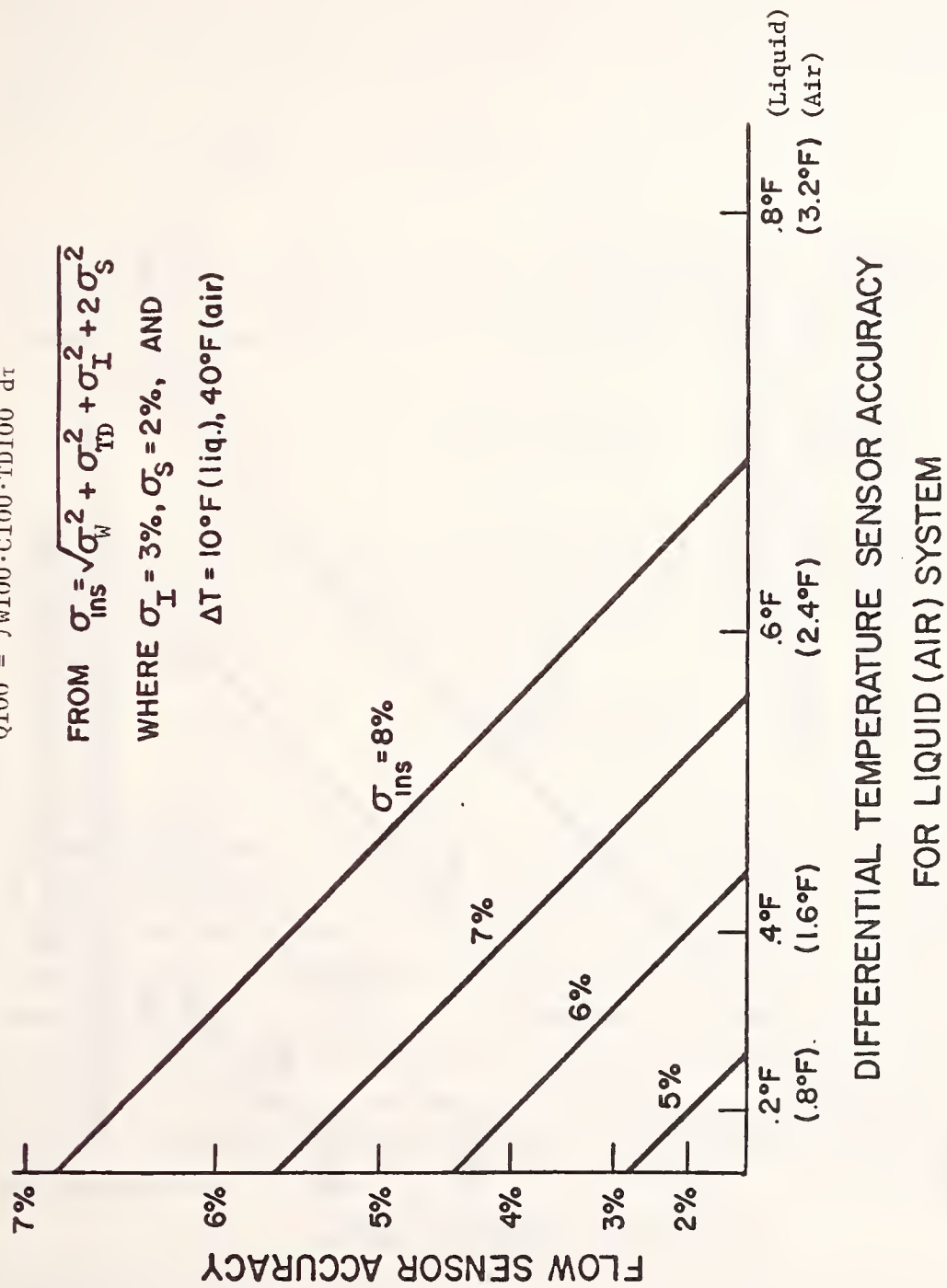
Figure 9   Accuracy in Calculated Solar Energy Collected (Q100)

57
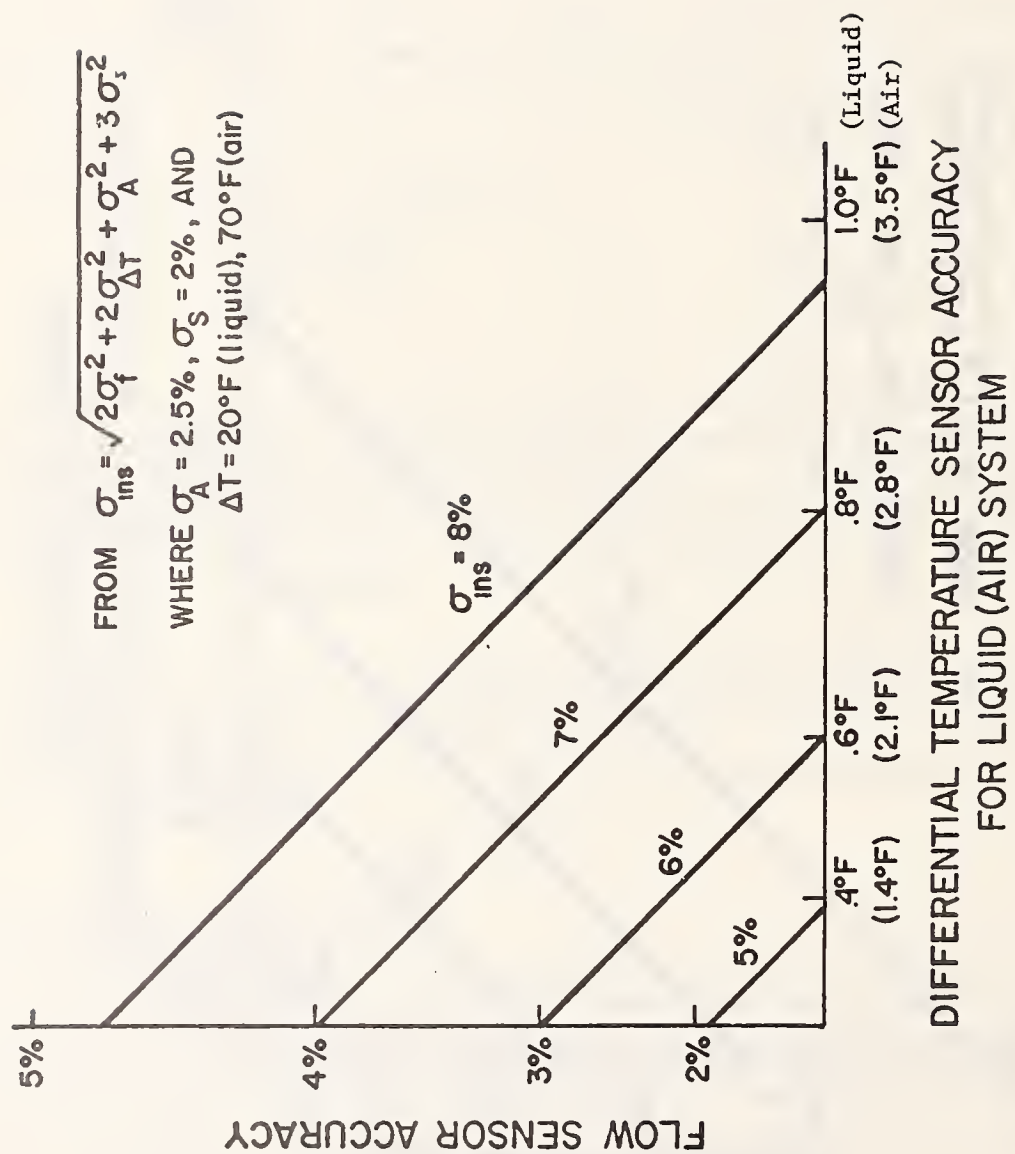
Figure 10 Accuracy in Calculated Solar Used for HW (Q300)

58

In general, lengthening the sampling period (e.g., from one month to one year) by some factor k decreases sampling error by $1/\sqrt{k}$. Similarly, shortening the sampling interval (e.g., from 30 minutes to 5 minutes) decreases sampling error.

The errors due to sampling can be predicted for the three common types of signals. "ON-OFF," "slowly varying," and "rapidly varying." Error in measuring "ON-OFF" signals is a function of the total number of samples N and the duty cycle, d

$$\sigma = \sqrt{\frac{1-d}{Nd}} \qquad \text{(ON-OFF)} \qquad (7.9)$$

For "slowly varying" signals (signals that cycle much fewer than once in 2π samples) error is a function of the number of samples, N, and the mean percent change of the signal during one sample interval, a:

$$\sigma < \frac{a}{\sqrt{N(1-a)}} \qquad \text{(slowly varying)} \qquad (7.10)$$

For "rapidly varying" signals (signals that cycle much faster than once every 2π samples), error is a function of the number of samples, N, and the ratio of the varying to steady signal component, b:

$$\sigma < \frac{b}{\sqrt{N}\,(1-b)} \qquad \text{(rapidly varying)} \qquad (7.11)$$

Decreasing the sample interval by a factor of k results in an error decrease of approximately $1/k$ for "ON-OFF", $1/k\sqrt{k}$ for "slowly varying" and $1/\sqrt{k}$ for "rapidly varying." Examples of "ON-OFF", slowly varying, and rapidly varying signals might be auxiliary input to load, storage temperature, and insolation, respectively, for a 2 minute to 60 minute sampling interval. Actual standard deviations for different sampling rates and periods have been computed for insolation, collector output, auxiliary output, etc., using Colorado State House No. 1 data [5]. Typical data for insolation values integrated from measurements made at different intervals are listed in Tables 2 a and 2 b.

Assuming the 2 minute sampling rate represents the most accurate value obtained, the actual sampling error results are listed in Table 3 and scaled to different sampling intervals and periods. There is wide variation in the monitoring interval required by the different parameters. For example, the analysis indicates insolation need only be monitored once every 15 minutes to maintain a weekly variance below 1%, but auxiliary sampling with a non-integrating sensor must be made.

59

Table 2a CSU Sampled Data Using Different Sampling Intervals (Summer 1975)

Parameter Insolation [5]

Date	2	5	Minutes 10	20	30	60
6/21	1132.9	1130.0	1118.9	1128.3	1124.2	1160.7
7/9	1111.3	1119.0	1089.9	1100.4	1035.5	995.4
7/13	1768.2	1776.2	1772.6	1763.9	1759.3	1765.7
7/17	1255.3	1266.6	1270.9	1273.0	1242.9	1227.0
7/21	1248.0	1271.6	1254.3	1241.1	1153.9	1072.2
7/23	1263.4	1246.8	1253.1	1204.3	1259.7	1271.7
7/25	1815.2	1811.4	1809.0	1799.1	1792.0	1767.3
7/27	1850.4	1846.6	1840.5	1827.7	1815.1	1779.6
7/29	1564.5	1558.1	1534.4	1515.9	1633.1	1513.0
7/31	1205.6	1207.8	1245.6	1229.3	1219.8	1233.3
S.D per day		0.8%	1.3%	2.0%	3.3%	5.3%

Table 2b Parameter Insolation   (Winter 1974-75)

Date	2	5	Minutes 10	20	30	60
12/21	455.0	449.1	446.4	455.2	466.6	465.9
12/23	165.9	159.5	158.0	152.2	159.7	143.7
12/25	1478.9	1476.0	1472.7	1457.4	1445.9	1396.3
12/27	1238.6	1235.8	1235.1	1228.9	1251.7	1270.1
12/29	948.0	937.8	933.3	916.6	896.7	846.5
12/31	1108.1	1102.0	1086.0	1034.4	1045.6	976.0
1/4	1248.4	1242.6	1246.7	1246.2	1205.9	1224.6
1/6	1395.4	1388.1	1380.4	1345.3	1327.4	1228.9
1/15	730.9	741.1	725.0	735.6	778.2	755.0
1/17	1022.4	1017.6	1015.6	1112.4	111.3	1173.3
S.D. per day		0.7%	1.1%	4.3%	5.1%	9.6%

TABLE 3

RANGE OF MEASURED DAILY VARIANCE WITH DATA EXTRAPOLATED
FOR WEEKLY, MONTHLY, AND YEARLY PERIODS.

SAMPLING FREQUENCY (MIN)	INSOLATION				
	5	10	20	30	60
Daily	.7 - .8	1.1-1.3	2.0-4.3	3.3-5.1	5.2-9.6
Weekly	.3	.4 - .5	.8 - 1.6	1.2-2.0	2.0-3.6
Monthly	.1	.2	.4 - .7	.6 - .9	1.0-1.7
Yearly	.1	.1	.1 - .2	.2 - .3	.3 - .5

SAMPLING FREQUENCY (MIN)	COLLECTOR OUTPUT				
	5	10	20	30	60
Daily	3.3-4.6	5.3-11.1	13.9-20.1	18.2-21.5	19.7-23.8
Weekly	1.2-1.7	2.0-4.0	5.2-7.5	7.0-8.0	7.5-9.0
Monthly	.6 - .8	.9-2.0	2.5-3.7	3.3-3.9	3.6-4.3
Yearly	.2	.3 - .6	.7-1.0	.9-1.1	1.0-1.3

SAMPLING FREQUENCY (MIN)	AUXILIARY TO LOAD				
	5	10	20	30	60
Daily	6.7-23.6	6.3-30.9	10.2-43.3	15.8-66.5	23.3-111.8
Weekly	2.5-9.0	2.5-11.5	4.0-16.5	6.0-25.0	9.0-42.0
Monthly	1.2-4.3	1.1-5.6	1.8-8.0	2.8-12.0	4.2-20.0
Yearly	.7	.7	1.1	1.7	2.6

Using the CSU data and the suggested sampling accuracies from Section 7.2.2, sampling rates for various sensors are determined as listed in Table 5.

Data Requirements	Weekly Summations	Monthly Summations	Yearly Summations
	(minutes)	(minutes)	(minutes)
load flow	<5	5	30
collector flow and			
temperature	5	10	60
auxiliary input	<5	5	60
insolation*	30	60	60

*Based on insolation at Colorado State University, Fort Collins, Col. 1974-74.

Table 4   Sampling Rates as a Function of Time Interval for Several Data Requirements Types

Sensors requiring sampling rates greater than once every five minutes can be continuously integrated and then sampled. It is recognized that the data utilized is for a specific system, load and climatic conditions and will only provide estimates of sample rates for other combinations of these factors. For example, insolation sample rates are a function of the weather variability and a rate of 3 minutes is used in the Washington, D.C. area to obtain an uncertainty of about 1% [8]. A sampling rate of 5 minutes or less is recommended for both insolation and auxiliary energy related measurements.

7.2.3   Solar Energy Conversion Efficiency (N111)

The conversion efficiency of a heating and HW solar energy system is determined by dividing the solar energy delivered to the load by the available insolation.

Instrumentation uncertainty (σ_{INS}) is given by:

$$\sigma_{INS}^2 = \left(\sigma_{W_1}^2 + \sigma_{TD_1}^2 + \sigma_{S_1}^2\right)\left(\frac{Q300}{Q300 + Q400}\right)^2 + \left(\sigma_{W_2}^2 + \sigma_{TD_2}^2 + \sigma_{S_2}^2\right)\left(\frac{Q400}{Q300 + Q400}\right)^2 + \sigma_I^2 + \sigma_{S001}^2 \tag{7.12}$$

where σ_W and σ_{TD} are uncertainties in solar-to-load flow and temperature difference sensors, σ_S is the sampling uncertainty, Q300 and Q400 is solar energy to hot water and heating respectively, σ_I is insolation sensor uncertainty, and σ_{S001} is the insolation sampling uncertainty.

62

Assuming conditions such that Q300>>Q400, the instrumentation accuracy is:

$$\sigma_{INS}^2 = \sigma_{W_1}^2 + \sigma_{TD_1}^2 + \sigma_{S_1}^2 + \sigma_I^2 + \sigma_{S001}^2 \qquad (7.13)$$

The sensor accuracy and sampling rate accuracy necessary to achieve a 6% instrumentation uncertainty is determined as described in the following sections.

7.2.4   Sensor Accuracy

The two worst case RMS instrumentation error equations that determine necessary sensor accuracies for system and collector array efficiencies respectively are

$$\sigma_{INS}^2 = \sigma_{W301}^2 + \sigma_{TD301}^2 + \sigma_{I001}^2 + \sigma_{S300}^2 + \sigma_{S001}^2 \qquad (7.14)$$

$$\sigma_{INS}^2 = \sigma_{W100}^2 + \sigma_{TD100}^2 + \sigma_{I001}^2 + \sigma_{S100}^2 + \sigma_{S001}^2 \qquad (7.15)$$

where

$\sigma_{W301} = \sigma_{W100}$ = flow sensor accuracies

σ_{TD301} = load temperature sensor accuracy (20°F differential)

σ_{TD100} = array temperature sensor accuracy (10°F differential)

σ_{I001} = insolation sensor accuracy

σ_{S300} = sampling error for solar or auxiliary to load

σ_{S001} = sampling error for insolation

σ_{S100} = sampling error for collector output

On the basis of performance a reasonable strategy for initial selection of sensor accuracy and sampling rate is to balance the error terms of the error equations. For example, using the instrument error equation for system conversion efficiency and a 6% instrument error criterion, the error terms would be balanced according to:

$$\frac{6\%}{\sqrt{5}} \simeq 2.7\% \simeq \sigma_{W301} \simeq \sigma_{TD301} \simeq \sigma_{I001} \simeq \sigma_{S300} \simeq \sigma_{S001} \qquad (7.16)$$

63

Using this term balancing strategy, sensor and sampling accuracies are selected and iteratively refined to reasonable values using tradeoff charts shown in Figures 9 and 10. The results for the projected sensor accuracy and sampling requirements are as follows:

Sensor	Sensor Accuracy	Sampling Accuracy
load flow	$+ 2\%$	$\pm 2\%$
load temp.	$\pm 2\%$	—
collector flow	$\pm 2\%(\text{liq})\pm 3\%(\text{air})$	$\pm 2\%$
collector temp.	$\pm 4\%(\text{liq})\pm 3\%(\text{air})$	—
insolation	$\pm 3\%$	$\pm 2\%$
auxiliary input	$\pm 2.5\%$	$\pm 2\%$

7.3   SUMMARY

The final instrumentation accuracy and performance factor uncertainty will depend upon economic tradeoffs of sensor cost, installation and maintenance.

Using the instrument error equations and selecting a desired instrumentation uncertainty of 6% as being reasonable and achievable, the values of sensor accuracy and sampling rate were assigned to the various measurements as shown in Table 5.

64

TYPE	DESIGN	DATA REQUIREMENT	RANGE	ACCURACY	MEASUREMENT FREQUENCY
Climatic	I001	Total Radiation	0-350	$\pm$ 3% Btu/ft^2-hr FS	5 min or less
	I002	Diffuse Radiation	0-100	$\pm$ 6% Btu/ft^2-hr FS	5 min
	T001	Outdoor DB Temperature	-20 to 120	$\pm$ 2°F	Avg/hr
	V001	Wind Velocity	0 to 100	$\pm$ 3 mph	Avg/hr
	D001	Wind Direction	0 to 360	$\pm$ 20°F	Avg/hr
	T002	Outdoor Wet Bulb Temp	32 to 90	$\pm$ 2°F	Avg/hr
Collector and Transport Subsystem	T100	Collector Inlet Temp	40 to 220	$\pm$ 0.5°F (L) $\pm$ 1°F (A)	5 min
	TD100	Collector Temp Diff	-10 to +50	$\pm$ 0.3°F (L) $\pm$ 1.2°F (A)	5 min
	T101	Storage Inlet Temp	60 to 230	$\pm$ 0.5°F (L) $\pm$ 2°F (A)	5 min
	TD101	Storage Temp Diff	0 to 100	$\pm$ 0.3°F (L) $\pm$ 2.5°F (A)	5 min
	T102	Collector Absorber Temp	30 to 450	$\pm$ 3°F	Daily at noon
	W100	Collector Flow Rate	varies	$\pm$ 2% (L) $\pm$ 3% (A) FS	5 min
	PD100	Collector Press Diff	varies	$\pm$ 2% FS	Daily at noon
Storage Subsystem	T200	Storage Media Ave Temp	60 to 230	$\pm$ 2°F	hr,
	T201	Storage Ambient Temp	-20 to 120	$\pm$ 3°F	hr,
	PD101	Storage Press Diff (Air)	0 to 4"H$_2$O	$\pm$ 2% FS	hr,
Hot Water Subsystem	T301	Makeup Water Temp	30 to 90	$\pm$ 0.5°F	Avg/hr.
	T300	HX Inlet Temp	40 to 160	$\pm$ 0.5°F	5 min
	TD300	HX Temp Diff	0 to 50	$\pm$ 0.3°F	5 min
	TD301	Storage Temp Diff	0 to 75	$\pm$ 0.3°F	5 min
	TD302	Auxiliary Temp Diff	0 to 100	$\pm$ 0.3°F	5 min or less
	W300	Circulation Flow Rate	varies	$\pm$ 2% FS	5 min
	W301	Load Flow Rate	varies	$\pm$ 3% FS	5 min
Heating Subsystem	T400	Load Return Temp	70 to 180	$\pm$ 0.5°F (L) $\pm$ 2°F (A)	5 min
	TD400	Storage Temp Diff	0 to 50	$\pm$ 0.3°F (L) $\pm$ 2°F (A)	5 min
	TD401	Auxiliary Temp Diff	0 to 100	$\pm$ 0.3°F (L) $\pm$ 2°F (A)	5 min
	W400	Circulation Flow Rate	varies	$\pm$ 2% (L) $\pm$ 3% (A) FS	5 min
	TD402	HTG Load Temp Diff	0 to 100	$\pm$ 0.3°F (L)	5 min
Cooling Subsystem	T500	Load HX Inlet Temp	40 to 60	$\pm$ 0.5°F	5 min
	TD500	Load HX Temp Diff	0 to 75	$\pm$ 0.3°F	5 min or less
	T501	Cooling Tower Inlet Temp	40 to 120	$\pm$ 0.5°F	5 min
	TD501	Cooling Tower Temp Diff	0 to 20	$\pm$ 0.3°F	5 min or less
	W500	Load HX Flow Rate	varies	$\pm$ 2% FS	5 min or less
	W501	Cooling Tower Flow Rate	varies	$\pm$ 2% FS	5 min or less
Operating Power & Auxiliary Energy	EP101	Collector Circ Pump Power	ΔKW varies	$\pm$ 5% FS	5 min
	EP301	HW Circ Pump Power	ΔKW varies	$\pm$ 5% FS	5 min
	EP401	HTG Loop Circ Pump Power	ΔKW varies	$\pm$ 5% FS	5 min
	EP402	Bldg Fan Power	ΔKW varies	$\pm$ 5% FS	5 min
	EP403	Heat Pump Compress Power	ΔKW varies	$\pm$ 2% FS	5 min or less
	EP501	Absorp Chiller Oper Power	ΔKW varies	$\pm$ 2% FS	5 min or less
	EP300	HW Elec Aux Power	ΔKW varies	$\pm$ 2% FS	5 min or less
	EP400	HTG Elec Aux Power	ΔKW varies	$\pm$ 2% FS	5 min or less
	F300	HW Aux Fuel Flow	varies	$\pm$ 2% FS	5 min or less
	F400	HTG Aux Fuel Flow	varies	$\pm$ 2% FS	5 min or less
	F500	Cooling Aux Fuel Flow	varies	$\pm$ 2% FS	5 min or less
Building/System	T600	Bldg Return Air DB Temp	50 to 90	$\pm$ 2°F	5 min
	TD600	Supply/return Air Temp Diff	0 to 80	$\pm$ 2°F	5 min
	T601	Bldg Return air WB Temp	20 to 80	$\pm$ 2°F	5 min
	T602	Bldg Supply Air WB Temp	20 to 80	$\pm$ 2°F	5 min
	W600	Building Air Flow Rate	varies	$\pm$ 2% FS	5 min
	W601	Condensate Flow	varies	$\pm$ 5%	5 min
	HF600	Heat Flow Meter	0.25 to 30°F ΔT	$\pm$ 5%	5 min
	TD601	HT Pump Cond & Load HX Temp Diff	0 to 80	$\pm$ 2°F	5 min

Table 5 INSTRUMENTATION RANGE, ACCURACY AND MEASUREMENT FREQUENCY

8.0   APPLICATION OF PERFORMANCE FACTORS

The performance factor data generated during the Demonstration Program will provide the basis to directly determine parameters such as energy saved, thermal efficiency and energy contributions to the various functional loads. However, to fulfill the program national goals the data will also be applied to determine correlations between building types, climates and heating and cooling system designs, to verify design methods and to establish reasonable performance goals.

Although exact system or subsystem comparisons must await the selection of specific solar system/building/climate combinations, examples of the format and general use of performance factors are presented as illustrations of how the data can be utilized.

8.1   Solar Energy System Thermal Performance

The technical selection of a solar system is based primarily on the thermal performance in terms of energy collected on monthly or annual/seasonal periods. Data such as shown in Figure 11 presents the amount of energy utilized for auxiliary energy as well as for the heating and cooling functions and the total energy supplied for a single site. Individual comparisons of solar energy systems (in similar climates) and collector areas can be made using this type of chart. For systems with varying collector size, the energy quantity can be expressed per unit collector area. Comparisons are made for each unique type of solar system to include air, liquid, active and passive. The data should be tabulated for monthly, seasonal and annual time periods to cover the following functional areas as appropriate.

Functions:
A. Hot Water
B. Space Heating
C. Space Cooling
D. Space Heating and Space Cooling
E. Space Heating and Hot Water
F. Space Heating and Cooling and Hot Water
G. Space Cooling and Hot Water

8.2   Solar Energy System Thermal Effectiveness

The effectiveness of a solar energy system to meet the total functional loads on a cumulative basis for each building type can be illustrated for a single site as shown in Figure 12. Comparison of the effectiveness of similar solar system types
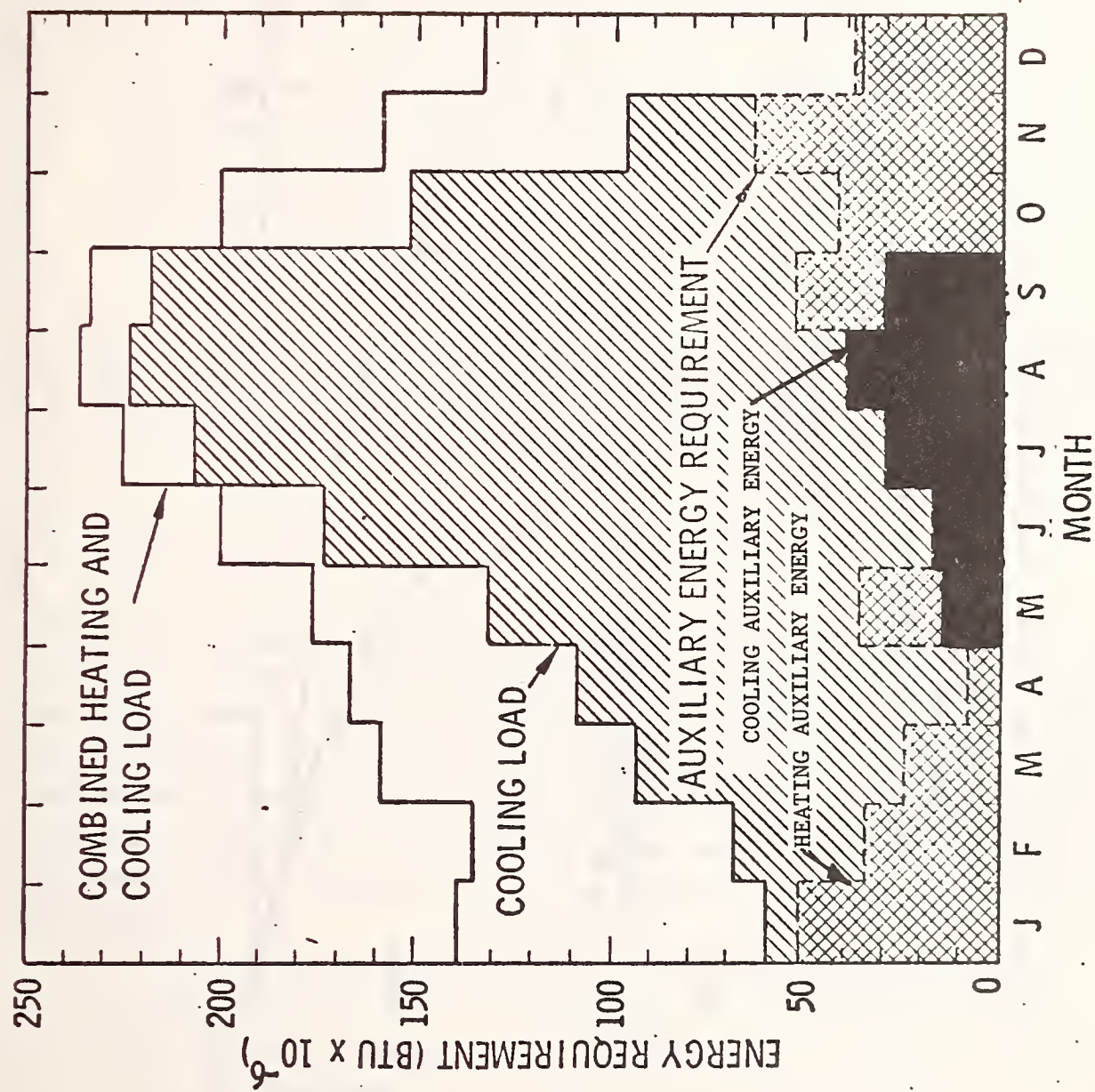
66

Figure 11 Monthly Heating and Cooling Loads and Auxiliary Energy Requirement
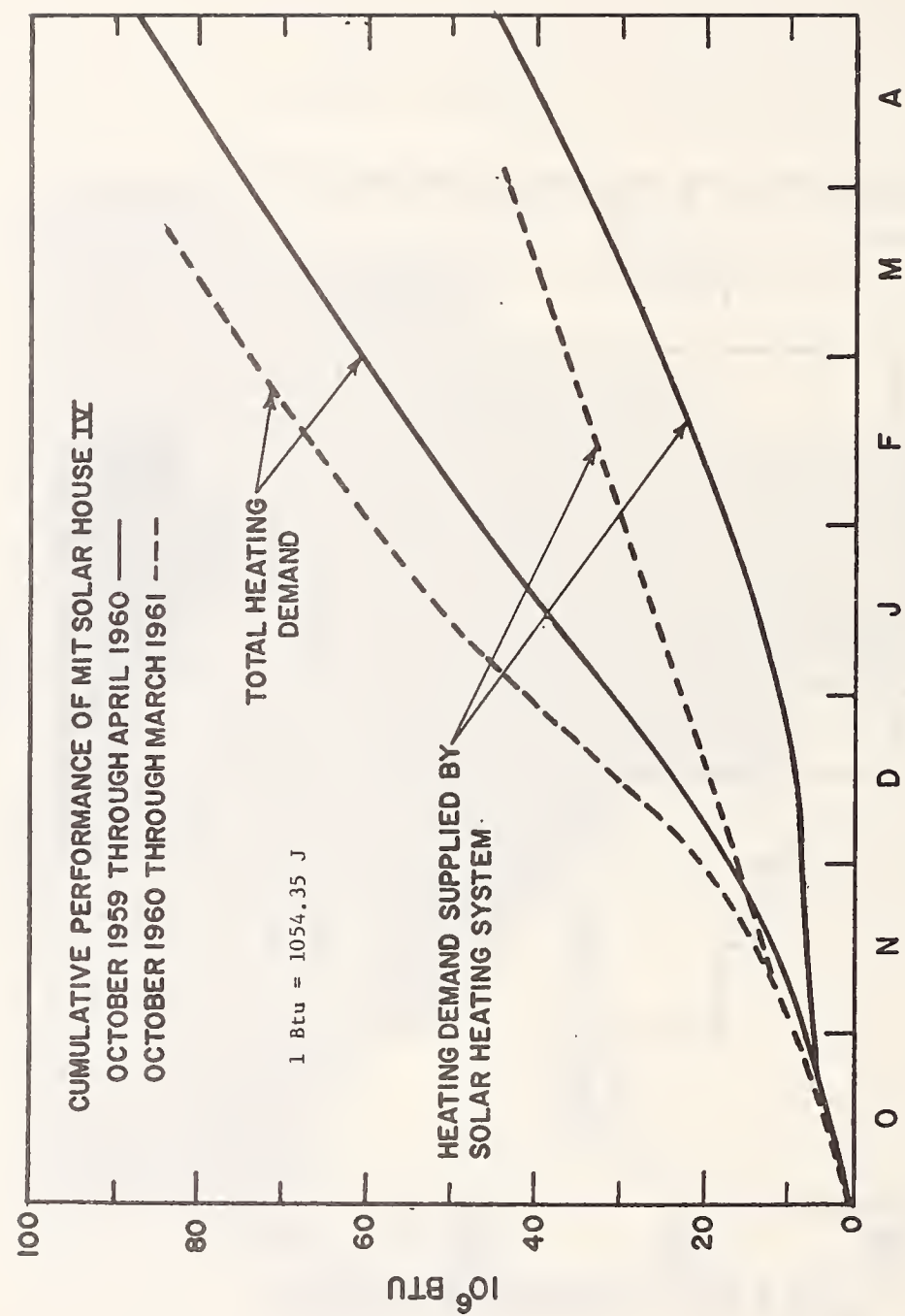
Figure 12 Cumulative Energy Use for the MIT Solar House IV during Two Winter Heating Seasons [9]

and climates on a seasonal basis is done by normalizing the building size and load per degree day of heating or cooling and presenting the data in tabular form for monthly, seasonal and annual time periods.

8.3   Analytical Predictions

The design of solar systems is currently based on analytical models and calculated performances. The demonstration program will provide the measured data for comparison with prediction of the following performance factors:

(1) Energy Delivered to Load (HW, heating, cooling, total)
(2) Solar Fraction of Load (HW, heating, cooling, total)
(3) Solar Energy Conversion Efficiency
(4) Energy Saved (Electric and Fossil)
(5) Collector Array Efficiency

Comparisons can be made on an individual site basis as illustrated in Figures 11 and 12 or tabular data for many sites can be used to determine standard deviations as a function of climate and building characteristics for monthly and annual periods.

8.4   Solar Collector Array

The greatest technical innovations are needed in the development of collectors, therefore, comprehensive characterization, measurement, and comparison of operating performance data for the many collector varieties will be necessary. Because of the influence of site integration and operating mode, comparison of preinstallation performance data for individual panels and the array performance, as illustrated in Figure 13, is desirable using instantaneous and daily, monthly and annual efficiencies. Other comparisons based upon design or material properties are listed as follows:

    A. Flat Plate
        1. Absorber Coating
            a. Flat Black
            b. Selective

        2. Covers
            a. Number
            b. Material Type

69

FLAT PLATE COLLECTOR
DOUBLE-GLAZED, 0.3 cm TEMPERED GLASS
ALUMINUM ROLL-BOND ABSORBER
COATED WITH FLAT-BLACK PAINT
7.6 cm GLASS FIBER BACK INSULATION

——— PUBLISHED DATA (PPG INDUSTRIES)
SOUTH FACING, 45° TILT

⊙ EXPERIMENTAL DATA, NBS TEST HOUSE
SOUTH FACING, 55° TILT

$\dfrac{\bar{t}_f - t_a}{I}$, $\dfrac{°F\ Hr\ Ft^2}{BTU}$
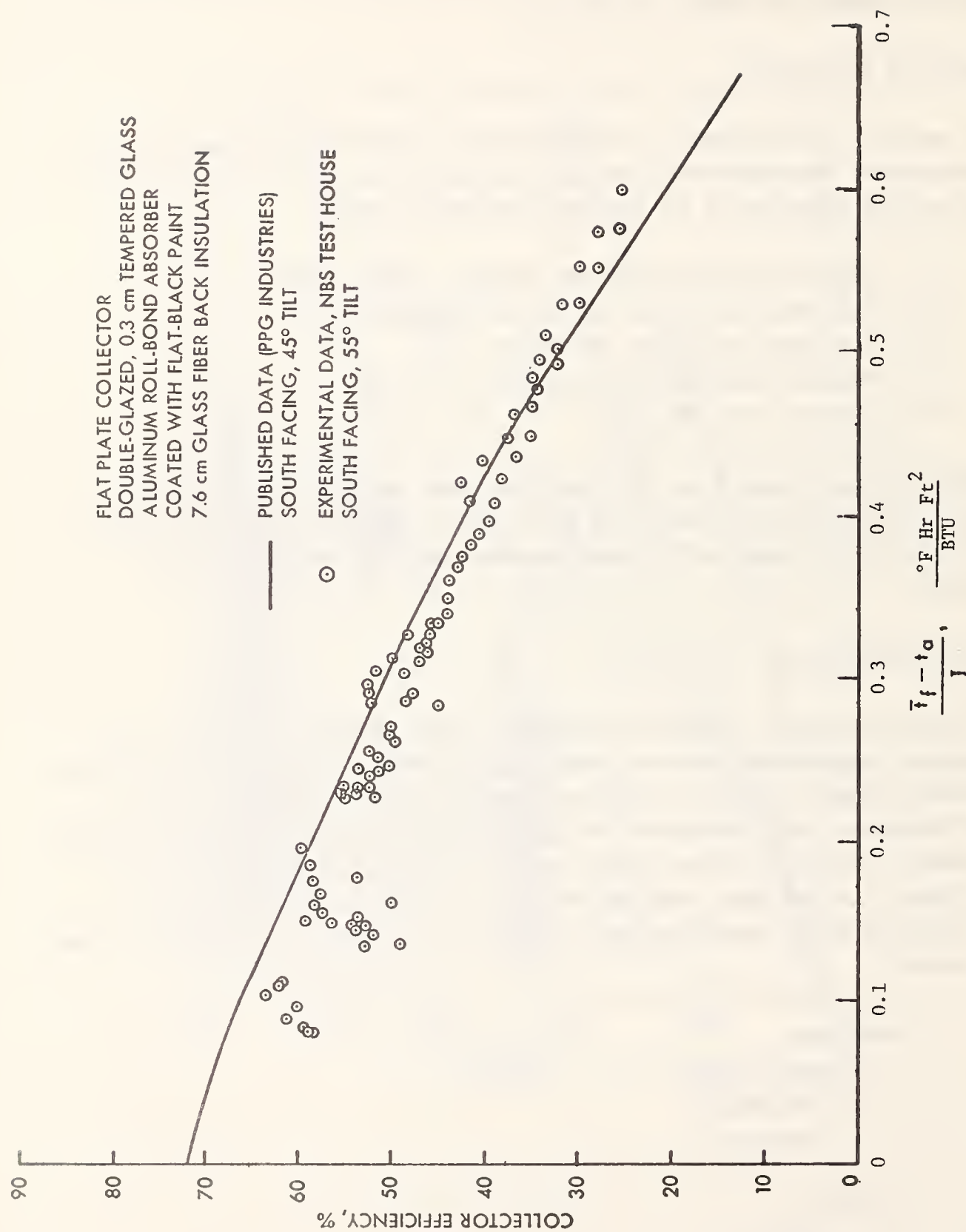
COLLECTOR EFFICIENCY, %

Figure 13 Comparison of Collector Panel and System Collector Array Performance [10]

B. Concentrator

    1. Cylindrical

    2. Tubular

    3. Trapezoidal

    4. Other

8.5   Component Predicted Performance

It is not the intent of the test and evaluation program to develop components
but the influence of the operating mode and environment will be determined on
major subsystems or components as listed below:

A. Collector Array

B. Storage

C. Energy Transport

D. Energy Conversion Equipment

An example of the comparisons in collector performance between predicted and
experiment are shown in Table 6 for the three key heat transfer areas: (a) solar
absorptance-transmittance product $(\alpha\tau)_e$; (b) heat removal efficiency factor
(F_R); and (c) heat loss coefficient (U_L). These values are obtained by
reducing the collector performance data during selected periods of quasi-steady
state to plot in the slope-intercept form.

An example of the use of the slope-intercept plot to illustrate collector
material degradation is shown in Figure 14. Tabular values of $\alpha\tau$ and U_L for
similar materials as a function of climatic exposure will reveal the differences
related to environmental conditions.

8.6   Climatic Data

Climatic data measured during the program will be reported for hourly, monthly and
annual data as follows:

A. Total solar radiation at collector tilt angle

B. Direct solar radiation at collector tilt angle for selected sites

C. Ambient dry bulb temperature

D. Ambient wet bulb temperature at selected sites

E. Wind direction and velocity at selected sites

These data will be tabulated and plots indicating variations over the continental
United States will be available.

71

COLLECTOR CONFIGURATION	EXPERIMENTAL RESULT				ANALYTIC PREDICTION			
	INTERCEPT	$\alpha\tau_e$	F_R	U_L	INTERCEPT	$\alpha\tau_e$	F_R	U_L
Selective absorber, two glass covers (baseline collector)	0.74	0.80	0.93	0.63	0.74	0.77	0.96	0.46
Nonselective absorber, two glass covers	0.80	0.83	0.96	0.98	0.74	0.77	0.96	0.71
Selective absorber, one glass cover	0.82	0.87	0.94	0.84	0.79	0.83	0.95	0.61
Nonselective absorber one glass cover	0.89	0.89	1.0	1.3	0.78	0.83	0.94	1.03

Table 6 Comparison of Collector Performance Coefficients Derived from Testing and Analysis [11]
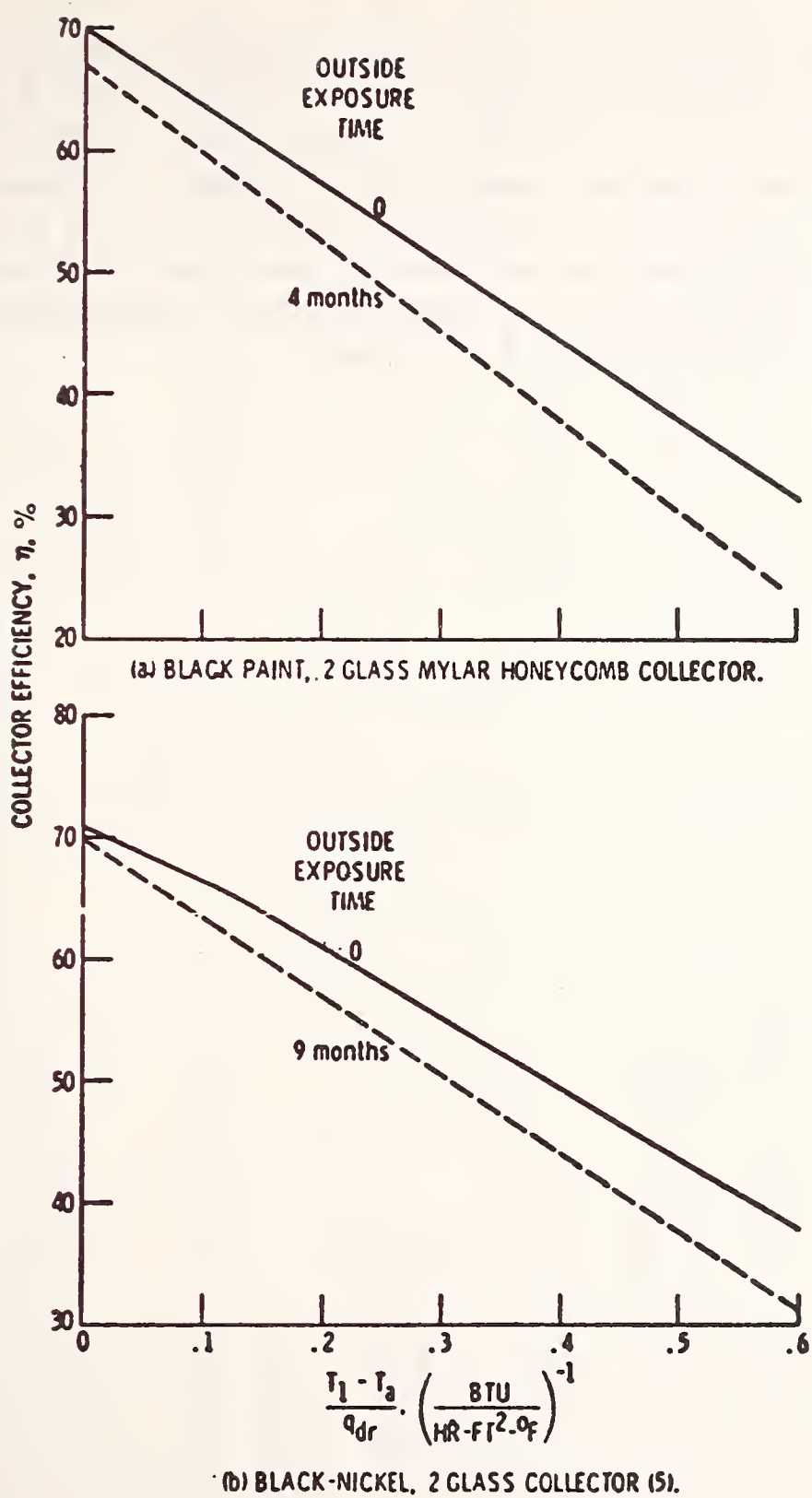
72

Figure 14   Illustrations of Detecting Collector Degradation From
Thermal Performance Measurements.

73

8.7   Recommendations

Table 7 lists a number of data correlations and evaluations possible with the available measurements and calculated performance factors. Due to the large number of building types solar energy systems and climatic regions, it is obvious that computerized data reduction will be necessary to perform the necessary evaluation. It is therefore recommended that additional study of the data format and computerized data reduction requirements be under taken to more efficiently implement the various correlations studies planned and to assure availability of the results to the potential users on a timely basis.

PERFORMANCE FACTORS   EVALUATION AREA

PERFORMANCE FACTORS	EVALUATION AREA
Q100, Q300, Q400, Q500, Q600	1. Solar system type versus thermal performance in similar climate and function.
Q300, Q400, Q500, Q600, Q301, Q401, Q501, Q602, Q603	II. Solar system effectiveness in meeting total demand for various buildings as a function of climate.
N601, N602, Q001, Q100, Q601, N100, N113	III. Correlation between analytical and measured thermal performance for various climates and applications
Q311, Q313, Q415, Q417, Q512, Q514, Q604, Q605	IV. Fossil and electric energy saving as a function of climate and building type.
Q001, Q100, Q300, Q400, Q500, N100, N101, N102, N113	V. Correlation between collector type and climate (same function).
Q001, N200, N201, N103, N101, N102, N104, N300, N400, N500	VI. Correlation between component measured and predicted performance (same climate and function).
Q001, Q002, T001, T002, V001, D001	VII. Inputs to the Data Bank

TABLE 7 Application of Specific Performance Factors to Evaluation Areas

75

9.0   Conclusions

The quantity and type of measurements described reflect a level of instrumentation
that will provide a capability for full evaluation of each solar energy system
and for each building, partial evaluation of most components performance and
measurement of local climatic data.

To reduce instrumentation costs, an assessment of the significance of the per-
formance factors should be made for each proposed demonstration unit. The four
factors considered essential for the performance of solar energy systems are:

   °   conventional energy saved by the solar energy system
   °   solar fraction of total load
   °   solar energy system conversion efficiency
   °   solar energy collected per unit collector area.

The primary tool used to determine the data requirements and the selection of
instrumentation is the analytical heat balances. Sufficient heat balance cal-
culations are required to equate the total energy input to the total energy output
for the subsystem or component plus an acceptable heat loss to provide an energy
balance closure of about ten percent. Errors greater than approximately ten percent
for active systems and fifteen percent for passive systems will not permit useful
comparison between different systems. Error analysis of most performance evaluation
factors for active solar energy systems have shown that the experimental data can be
obtained with accuracy of about $\pm$ 5 percent using commercially available sensors.

10.0   REFERENCES

1. National Plan for Solar Heating and Cooling (Residential and Commercial Applications)
    ERDA-23A, October 1975.

2. ASHRAE Standard 90-75, "Energy Conservation in New Building Design," 1975. Available
    American Society of Heating and Refrigerating and Air Conditioning Engineers, Inc.,
    345 East 47th Street, New York, N.Y.   10017

3. "Procedures for Determining Heating and Cooling Loads for Computerized Energy
    Calculations", The Task Group on Energy Requirements for Heating and Cooling, ASHRAE,
    345 East 47th Street, New York, 1971.

4. T. Kusuda, "NBSLD, Computer Program for Heating and Cooling Loads in Buildings", NBS
    Report NBSIR 74-574, November 1974.

5. Personal Communication, Dr. Dan S. Ward, Colorado State University, Ft. Collins,
    Colorado; and Study on "Instrumentation Type, Range, Accuracy, and Measurement
    Frequency Required to Monitor and Evaluate the Thermal Effectiveness of Solar Heating
    and Cooling and Hot Water Systems", NBS Purchase Order No. 608692, March 1976.

6. ASHRAE Standard 93-P "Method of Testing for Rating Solar Collectors Based on Thermal
    Performance", August 1976 (Available ibid ASHRAE).

7. G. E. Kelly, "Potential of Air-to-Air Heat Pumps for Energy Conservation in
    Residential Buildings", NATO Advanced Study Institutes, Series E: Applied Science
    No. 15, Noordoff-leyden, 1976 (Available from National Bureau of Standards, Washington,
    D C 20234)

8. Personal Communication, Dr. William H. Klein, Radiation Biology Laboratory,
    Smithsonian Institution, Rockville, Maryland, January 1976.

9. Engebretson, C. D. , The Use of Solar Energy for Space Heating, M. I. T. Solar
    House IV, "Proceedings of the United Nations Conference on New Sources of Energy",
    Rome, August 21-31, 1961, Vol. 5 III e.2 pp. 159-172.

10. J. E. Hill, T. E. Richtmyer and J. Jenkins, "Initial Test Results for a Solar Cooled
    Townhouse in the Mid-Atlantic Region", National Bureau of Standards, Washington, D C
    20234, Presented at ASHRAE Semi-Annual Meeting, June 1976.

11. J. W. Ramsey, J. T. Borzoni and T. H. Holland, "Development of Flat-Plate Solar
    Collectors for the Heating and Cooling of Buildings, "NASA CR-134804, June 1975.

U.S. DEPT. OF COMM. BIBLIOGRAPHIC DATA SHEET	1. PUBLICATION OR REPORT NO. NBSIR 76-1137	2. Gov't Accession No.	3. Recipient's Accession No.
4. TITLE AND SUBTITLE Thermal Data Requirements and Performance Evaluation Procedures for the National Solar Heating and Cooling Demonstration Program			5. Publication Date
			6. Performing Organization Code
7. AUTHOR(S) E. Streed, M. McCabe, D. Waksman, J. Hebrank, T. Richtmyer			8. Performing Organ. Report No.
9. PERFORMING ORGANIZATION NAME AND ADDRESS NATIONAL BUREAU OF STANDARDS DEPARTMENT OF COMMERCE WASHINGTON, D.C. 20234			10. Project/Task/Work Unit No. 4606500 and 4606505
			11. Contract/Grant No. ERDA - 49(1) - 3800
12. Sponsoring Organization Name and Complete Address (Street, City, State, ZIP) Energy Research & Development Admin. Dept. of Housing and Division of Solar Energy Urban Development Washington, DC 20545 Division of Energy Washington, DC 20410			13. Type of Report & Period Covered Interim
			14. Sponsoring Agency Code

15. SUPPLEMENTARY NOTES

16. ABSTRACT *(A 200-word or less factual summary of most significant information. If document includes a significant bibliography or literature survey, mention it here.)*

This report presents the results of a study to determine the data requirements and performance evaluation factors to be used in the National Solar Heating and Cooling Demonstration Program. Solar energy systems used for heating hot water, space heating, and space cooling have been considered and specific measurements and analytical procedures have been recommended to determine the thermal effectiveness for daily, monthly, seasonal, or annual operating periods. The sensor accuracy and sampling rate effects on measurement uncertainty for several performance factors is presented. Application of the individual performance factors for the comparison of subsystem and system thermal performance as a function of building type and climatic region is discussed.

17. KEY WORDS *(six to twelve entries; alphabetical order; capitalize only the first letter of the first key word unless a proper name; separated by semicolons)*

Data requirements; measurement uncertainty; solar energy systems evaluation; thermal performance.

18. AVAILABILITY ☒ Unlimited	19. SECURITY CLASS (THIS REPORT)	21. NO. OF PAGES
☐ For Official Distribution. Do Not Release to NTIS	UNCLASSIFIED	85
☐ Order From Sup. of Doc., U.S. Government Printing Office Washington, D.C. 20402, <u>SD Cat. No. C13</u>	20. SECURITY CLASS (THIS PAGE)	22. Price
☒ Order From National Technical Information Service (NTIS) Springfield, Virginia 22151	UNCLASSIFIED	$5.00